Engineering and Urology Society

34th Annual Meeting

Sunday May 5th, 2019

Chicago, IL

http://engineering-urology.org/

The Engineering and Urology Society holds its 34th Annual Meeting: "Found in Translation", on Sunday, May 5th in Chicago. The mission of the Engineering and Urology Society, a subsection of the Endourological Society, is to promote the development and application of new technology in urology through facilitating collaboration between engineers, physicists, and urologists.

Jaime Landman, M.D. and Zhamshid Okhunov, M.D. (meeting co-chairs) from the University of California, Irvine have organized a unique opportunity to better understand advanced contemporary urologic technologies and the process of successful technology development as presented by world class urologist and biotechnology industry leaders. Lectures on the thulium fiber laser, MRI fusion imaging, aquablation, applications of novel simulation technologies and role of artificial intelligence and machine learning in Urology will be presented. Expert lectures will be delivered on next generation approaches for urologic tissue repair and regeneration in lower urinary tract disease. Two **keynote lectures** will be presented: Dr. Ralph Clayman will review the role of immersive virtual reality as a disruptive technology in management of stones, renal masses and transplant surgery, and Dr. Peter Chang, co-director of the UCI Center for AI and Machine Learning, will review the role of AI and machine learning in urology today and in the future. Finally, for the first time in the history of the meeting, **a CEO Roundtable**, including 5 globally prominent CEO/Chair leaders (Dr. Arie Belldegrun, Dr. Ralph Clayman, Dr. Fred Moll, Mr. Abel Ang and Mr. Kurt Azabarzin) who have each had a major role in transforming urology via translational engineering, will share their experiences overcoming challenges in translation and delivering products from bench to bedside.

Two **poster sessions** in the afternoon provide researchers with the opportunity to present their work and update the attendees on the progress on the field and latest innovations. The review of the abstracts for the poster sessions was performed online by a group of 34 reviewers from around the world. Each paper received between 12 and 16 reviews. We would like to thank the reviewers, listed at the end of this program book, for their essential contribution to the quality of the meeting and their constructive comments that they made for the research.

Based on the review scores, the Society presents **Awards** to two abstracts. These are listed at the end of this program book, together with the Top 10 abstracts, and Best Reviewer Awards. The authors of all awarded abstracts are invited to submit full length articles to the Journal of Endourology on the respective topics. We gratefully thank all reviewers for their hard work, objective scoring, and contribution to the success of the meeting. We thank Dr. George Nagamatsu the founder and first president of the society, and Dr. Jack Vitenson the first Society Treasurer for setting up the foundations based upon which we meet.

Please visit the website http://engineering-urology.org for a complete version of this program including the abstracts presented.

We welcome all urologists, engineers, scientists from industry and academia to join us for this cross-disciplinary experience. "Alone we can do so little; together we can do so much."

Jaime Landman
Zhamshid Okhunov
Dan Stoianovici

Boston Scientific – Urology

Boston Scientific is a leading developer of less-invasive medical technologies. Products for the Urology/Women's Health division include devices for the diagnosis and treatment of kidney stones, BPH, female urinary incontinence, and pelvic floor reconstruction. Please visit our exhibit to learn about our newest technologies and our commitment to physician education.

Cook Medical

Cook Medical has been a leading supplier of medical devices for urologists for over 35 years. Offering interventional and Biodesign® technologies that support diagnostic and therapeutic procedures in adult and pediatric urology, Cook has placed particular emphasis on stone management as well as both male and female pelvic health.

PROGRAM

Engineering & Urology Society
Found in Translation
Sunday, May 5th, 2019
Marriott Marquis Chicago

7:00am	**Registration**
7:50am – 8:00am	**Welcome**
	Jaime Landman, MD; *Professor of Urology and Radiology* *Chairman, Department of Urology* *University of California Irvine*
	Zhamshid Okhunov, MD *Endourology Fellow,* *Department of Urology* *University of California Irvine*
8:00am – 9:30am	**The Disruptors and Translational Success**
8:00am – 8:15am	Lasers in Urology: The Role of Thulium Fiber Lasers *Speaker*: *Gregory Altshuler, PhD; President, IPG Medical Corporation*
8:15am – 8:30am	MRI Fusion Imaging: Past, Present and Future *Speaker*: *Peter Pinto, MD; Professor of Urology, National Cancer Institute*
8:30am – 8:45am	Aquablation: A Transformative Ablation *Speaker*: *Nikolai Aljuri, PhD; President and CEO, PROCEPT BioRobotics*
8:45am – 9:00am	State of the Art Robotics *Speaker: Mihir Desai, MD; Professor of Urology, Department of Urology* *University of Southern California, Keck School of Medicine*
9:00am – 9:15am	Simulation in Urology: Where We Are And Where Are We Going *Speaker: Robert Sweet, MD; Professor of Urology,* *University of Washington, Seattle*
9:15am – 9:30am	iVR: A Disruptive Technology *Speaker: Ralph Clayman, MD; Professor of Urology,* *Dean Emeritus, Department of Urology, University of California, Irvine*
9:30am – 10:00am	**Artificial Intelligence and M achine Learning**
9:30am – 10:00am	Artificial Intelligence & Machine Learning in Urology: Present and Future *Speaker: Peter Chang, MD; Director, Center of Artificial Intelligence in* *Diagnostic Medicine, University of California, Irvine*

PROGRAM

10:00am – 10:30am	**Next Generation Approaches for Urologic Tissue Repair and Regeneration**
10:00am – 10:15am	Surgical and Pharmacological Breakthroughs in the Management Of Obstructive Bladder Disease *Speaker: Joshua Mauney, MD; Assistant Professor of Surgery, Department of Urology, Harvard Medical School*
10:15am – 10:30am	Surgical and Biomaterial Advances for Regeneration of the Lower Urinary Tract *Speaker: Trinity Bivalacqua, MD; R. Christian B. Evensen Professor, Director of Urologic Oncology* *James Buchanan Brady Urologic Institute, Johns Hopkins University*
10:30am – 10:45am	**Awards Presentation** *Dan Stoianovici* Intraoperative Guidance for Robotic Partial Nephrectomy Using Surface-Based Registration: Initial Model Assessment Improving Prostate Cancer Margin Prediction with Machine Learning
10:45am – 12:00pm	**CEO/Chair Roundtable: The Real Transformers Overcoming Challenges in Translation** Kurt Azabarzin *Vice President of R&D, CONMED Corporation* Abel Ang *Group Chief Executive Officer, Accuron MedTech* Fred Moll *Chairman and Chief Executive Officer, Auris Health, Inc.* Ralph Clayman, MD *Professor of Urology, Dean Emeritus, Department of Urology* *University of California, Irvine* Arie Belldegrun, MD *Professor of Urology, University of California, Los Angeles* *Chairman, UroGen Pharma, Inc.*
1:00pm – 2:00pm	**Poster Session 1 (Great Lakes Ballroom B)** Salvatore Micali, Zhamshid Okhunov, Bogdan Geavlete
2:30pm – 3:30pm	**Poster Session 2 (Great Lakes Ballroom B)** Tareq Aro, Dylan Isaacson, Esteban Emiliani

PROGRAM

POSTER SESSION 1
1:00 PM – 2:00 PM

Moderators: Salvatore Micali, Zhamshid Okhunov, Bogdan Geavlete

No	Title	Presenting Author
1	REDUCED CORE TARGETED (RCT) BIOPSY: COMBINING MULTIPARAMETRIC MAGNETIC RESONANCE IMAGING - TRANSRECTAL ULTRASOUND FUSION TARGETED BIOPSY WITH LATERALLY-DIRECTED SEXTANT BIOPSIES - AN ALTERNATIVE TEMPLATE FOR PROSTATE FUSION BIOPSY	Alireza Aminsharifi
2	SALVAGE PROSTATE CRYOABLATION FOR THE MANAGEMENT OF LOCAL RECURRENCE AFTER PRIMARY CRYOTHERAPY: A RETROSPECTIVE ANALYSIS OF FUNCTIONAL AND INTERMEDIATE-TERM ONCOLOGICAL OUTCOMES ASSOCIATED WITH A SECOND FREEZE	Alireza Aminsharifi
3	ELECTRICAL FIELD STIMULATION OF DISTAL URETERAL TISSUE DEMONSTRATES A ROLE FOR TAMSULOSIN, GLI PROTEINS AND ERYTHROPOIETIN IN URETERAL CONTRACTILITY	Kymora Scotland
4	INTRA-PRACTICE UROLOGIST-LEVEL VARIATION IN FUSION BIOPSY OUTCOMES	Jaya M. Telang
5	EVALUATION OF THE EFFECT OF IMMERSIVE VIRTUAL REALITY ON RESIDENT, SURGEON AND PATIENT ANATOMIC UNDERSTANDING IN THE SETTING OF LAPAROSCOPIC PARTIAL NEPHRECTOMY	Egor Parkhomenko
6	PROCEDURE SPECIFIC DISPOSABLE UROLOGICAL RIGID ENDOSCOPES APPROACHING REALITY	Joseph DiTrolio
7	**TOP 10 ABSTRACT** IMAGING THE DEVELOPING HUMAN UROGENITAL SYSTEM WITH LIGHT SHEET FLUORESCENCE MICROSCOPY	Dylan Isaacson
8	RENAL THREE-DIMENTIONAL RECONSTRUCTION TO PLAN ROBOTIC-ASSISTED LAPAROSCOPIC PARTIAL NEPHRECTOMY: OUR PRELIMINARY EXPERIENCE	Salvatore Micali
9	EX VIVO FLUORESCENCE CONFOCAL MICROSCOPY IN THE ASSESSMENT OF UROTHELIAL CARCINOMA GRADING IN BLADDER AND URETER: OUR PRELIMINARY EXPERIENCE	Ahmed Eissa
10	**TOP 10 ABSTRACT** ROBOTIC 3D ULTRASOUND-GUIDED TARGETING FOR PERCUTANEOUS RENAL ACCESS	Tareq Aro

11	**TOP 10 ABSTRACT** DIGITAL STONE MEASUREMENT IN URETEROSCOPIC STONE PROCEDURES: A WORKFLOW FEASIBILITY STUDY	Tareq Aro
12	CAN INTRA-VESICLE ULTRASOUND SURFACE MAPPING REPLACE CYSTOSCOPY? NOVEL TECHNIQUE AND PROOF OF CONCEPT	Tareq Aro
13	THE 3D BIOPSY SYSTEM: A NOVEL APPROACH UTILIZING NEW MEDICAL DEVICES TO IMPROVE THE DIAGNOSTIC ACCURACY AND LOCALIZATION OF DISCREATE CANCEROUS LESIONS WITHIN THE PROSTATE GLAND	Nelson N. Stone
14	IN VIVO PORCINE EVALUATION OF A NOVEL SELF-CONTAINED BLADDER IRRIGATION SYSTEM (MULTIPHZE)	Pengbo Jiang
15	**BEST ABSTRACT AWARD** INTRAOPERATIVE GUIDANCE FOR ROBOTIC PARTIAL NEPHRECTOMY USING SURFACE-BASED REGISTRATION: INITIAL MODEL ASSESSMENT	Bryn Pitt
16	MEASUREMENT AND CALCULATION OF LATERAL TRAPPING STRENGTH OF ULTRASOUND FOCUSED BEAMS FOR THE MANIPULATION OF KIDNEY STONES	Mohamed A. Ghanem
17	DEVELOPMENT OF HYDROGEL-BASED, FULL PROCEDURAL SIMULATION TRAINING PHANTOMS FOR UROLOGICAL SURGERY	Michael P. Wilson
18	SINGLE-PORT TRANSVESICAL ROBOTIC SIMPLE PROSTATECTOMY: EARLY CLINICAL CASES USING THE SP ROBOT PLATFORM	Guilherme V. Sawczyn
19	ADJUSTABLE LOOP FOR TRANSURETHRAL RESECTION	Steven Monda
20	PRECISE FOCAL THERAPY OF THE PROSTATE USING PHOTODYNAMIC APPROACH	Ilias Skalkidis
21	DYNAMICS OF FOLEY CATHETER INSERTION: A CADAVER STUDY	Amer Safdari
22	REAL-TIME WOUND AREA TRACKING AND 3D-MORPHOLOGICAL EDGE DETECTION	Yimin M. Zhao
23	EXTRAPERITONEAL SINGLE PORT ROBOTIC RADICAL PROSTATECTOMY: CLINICAL EXPERIENCE WITH THE FIRST 10 CASES	Rair Valero
24	**TOP 10 ABSTRACT** DEVELOPMENT OF AN OFFICE BASED LASER ABLATION SYSTEM FOR PROSTATE CANCER	Josh Shubert

25	ROBOTIC RECTOVESICAL FISTULA REPAIR AFTER ROBOTIC ASSISTED RADICAL PROSTATECTOMY FOR PROSTATE CANCER	Surcel C.

POSTER SESSION 2
2:30 PM – 3:30 PM

Moderators: Tareq Aro, Dylan Isaacson, Esteban Emiliani

No	**Title**	**Presenting Author**
26	TECHNOLOGICAL ADVANCEMENTS IN LARGE PROSTATE ENDOSCOPIC SURGERY PUT TO THE TEST OF TIME - AN EVIDENCE-BASED, LONG-TERM, PROSPECTIVE, RANDOMIZED-CONTROLLED CLINICAL COMPARISON BETWEEN BIPOLAR PLASMA VAPORIZATION, RESECTION AND ENUCLEATION VERSUS OPEN PROSTATECTOMY	Bogdan Geavlete
27	THE LONG-TERM IMPACT OF NBI TECHNOLOGICAL ADVANCEMENT IN NON-MUSCLE INVASIVE BLADDER CANCER ONCOLOGIC OUTCOME – A FIVE YEARS' PROSPECTIVE, RANDOMIZED-CONTROLLED CLINICAL ANALYSIS ASSESSING THE OPTICALLY ENHANCED DIAGNOSTIC ACCURACY BY COMPARISON TO STANDARD WHITE LIGHT VISUALIZATION	Bogdan Geavlete
28	IN VITRO EVALUATION OF STONE FRAGMENT EVACUATION: URETEROSCOPY SUCKS	Garen Abedi
29	**TOP 10 ABSTRACT** REAL-TIME HIGH RESOLUTION DIAGNOSTIC IMAGING FOR PROSTATIC TISSUE WITH EX VIVO FLUORESCENCE CONFOCAL MICROSCOPY: OUR PRELIMINARY EXPERIENCE	Ahmed Eissa
30	MULTI-TUMOR SILICONE PARTIAL NEPHRECTOMY MODELS FOR ROBOTIC-ASSISTED LAPAROSCOPIC PARTIAL NEPHRECTOMY TRAINING	Charles H. Schlaepfer
31	NOVEL RENAL COLLECTING SYSTEM MODEL FOR PROCEDURAL TRAINING UNDER ULTRASOUND GUIDANCE	Tareq Aro
32	"OPERATOR DUTY-CYCLE": ANALYSIS OF LASER ACTIVATION PATTERNS DURING HOLMIUM LITHOTRIPSY	Ali H. Aldoukhi
33	IMAGE CORRECTION FOR RIGID CYSTOSCOPY	Sunghwan Lim
34	THE DEVELOPMENT OF AN AUTOMATED, SELF-SUSTAINING KIDNEY CANCER REGISTRY FROM ELECTRONIC HEALTH RECORDS	Niranjan J. Sathianathen

35	MOSES TECHNOLOGY IN MINIPERC: IN PURSUIT OF TOTAL STONE CLEARANCE.	Gopal Ramdas Tak
36	**BEST ABSTRACT AWARD** IMPROVING PROSTATE CANCER MARGIN PREDICTION WITH MACHINE LEARNING	Alan Priester
37	**TOP 10 ABSTRACT** A PRECLINICAL TRANSRECTAL BOILING HISTOTRIPSY SYSTEM FOR PROSTATE ABLATION	George R. Schade
38	**TOP 10 ABSTRACT** IMAGE GRADIENT AT KIDNEY-TUMOR BOUNDARIES AS A PREDICTOR OF COMPLEXITY IN NEPHRON SPARING SURGERY	Nicholas Heller
39	EFFICIENCY OF HOLMIUM LASER LITHOTRIPSY USING A STONE STABILIZATION SUCTION DEVICE	Matthew S. Lee
40	NEURAL-NETWORK BASED ACOUSTIC MONITORING OF CAVITATION IN LITHOTRIPSY	Kazuki Maeda
41	COMPUTER GENERATED TUMOR VOLUME, SURFACE AREA AND IRREGULARITY AS PREDICTORS OF PATHOLOGICAL OUTCOMES IN RENAL CELL CARCINOMA	Arveen Kalapara
42	EFFECTS OF HUMAN URINE AND ARTIFICIAL URINE ON URETERAL STENT MECHANICAL PROPERTIES	Bradley C. Hansen
43	ROBOTIC-ASSISTED EXTRAPERITONEAL DUAL KIDNEY TRANSPLANTATION USING THE SP® SURGICAL SYSTEM IN A PRE-CLINICAL MODEL	Mohamed Eltemamy
44	URINE CONDUCTIVITY FOR USE IN AMBULATORY URODYNAMICS	Benjamin Abelson
45	PROSPECTIVE COHORT STUDY COMPARING THE DIAGNOSTIC YIELD AND SAFETY OF OFFICE-BASED TRANSPERINEAL VS. TRANSRECTAL PROSTATE BIOPSY	Alexa R. Meyer
46	EARLY CLINICAL OUTCOMES IN THE USE OF THE DA VINCI SINGLE PORT SURGICAL SYSTEM IN PROSTATECTOMY PATIENTS	Michael Zhang
47	MRI CHANGES AFTER IN-OFFICE FOCAL CRYOABLATION OF PROSTATE CANCER: A PILOT STUDY	Steve R. Zhou
48	**TOP 10 ABSTRACT** OUT OF THE RECTUM: FREE-HAND FULLY TRANSPERINEAL FUSION-GUIDED PROSTATE BIOPSY	Reza Seifabadi
49	A NOVEL MICROFLUIDIC DEVICE FOR ISOLATION OF EXTRACELLULAR VESICLES	Richard C. Zieren

ABSTRACTS

ABSTRACT 1

REDUCED CORE TARGETED (RCT) BIOPSY: COMBINING MULTIPARAMETRIC MAGNETIC RESONANCE IMAGING - TRANSRECTAL ULTRASOUND FUSION TARGETED BIOPSY WITH LATERALLY-DIRECTED SEXTANT BIOPSIES - AN ALTERNATIVE TEMPLATE FOR PROSTATE FUSION BIOPSY

Alireza Aminsharifi[1,2], Rajan T. Gupta[1,2,3], Efrat Tsivian[1], Sitharthan Sekar[3], Christina Sze[1], Thomas J. Polascik[1,2]

[1]Division of Urologic Surgery, [2]Duke Cancer Institute and
[3]Department of Radiology Duke University Medical Center, Durham, North Carolina

Introduction: To introduce and assess the efficacy of a reduced core targeted (RCT) biopsy template (image-targeted + laterally directed *sextant* biopsy) to detect clinically-significant cancer in patients with elevated PSA and a previous negative biopsy or on active surveillance. The performance and added value of either targeted alone vs random sextant vs combined biopsy template was appraised.

Methods: Data from 113 patients with a suspicious lesion on mpMRI and previous history of extended 10-12 core standard biopsy who subsequently had a RCT-biopsy were analyzed. These patients had at least one prior negative standard 10-12 core biopsy (n=70) or were on active surveillance (n=43). At least two samples were taken from each mpMRI lesion as a targeted biopsy together with the classic laterally-directed sextant biopsy.

Results: In patients having previous negative biopsy (n=70), the RCT biopsy detected any cancer versus clinically-significant cancer in 62.9% versus 32.9%, respectively. Targeted biopsy diagnosed more clinically-significant cancers than sextant biopsy (31.4% versus 25.7%, p<0.01). In this cohort, the use of targeted fusion biopsy upgraded the biopsy grade group (GrGp) in 15 (21.4%) patients compared to sextant biopsy. In patients on active surveillance, the RCT biopsy identified any cancer versus clinically-significant cancer for detection rates of 74.4% versus 39.5%, respectively. Fusion targeted biopsy diagnosed more clinically-significant cancers than sextant biopsy did (37.2% versus 18.6%, p=0.002). The use of targeted biopsy upgraded the biopsy GrGp in 12 (27.9%) patients.

Conclusion: As a preliminary study, among men with MRI suspicious lesions and previous negative prostate biopsy or those under active surveillance, an image-targeted plus sextant biopsy platform can be associated with increased efficiency of detecting clinically-significant prostate cancer with fewer random cores. Future large series are needed to validate the clinical implication of this reduced core template in comparison with targeted fusion biopsy plus standard 12-core schema.

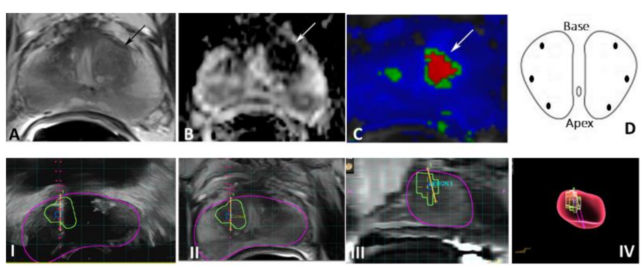

Figure 1. **Upper panel: (A)** Axial T2-weighted (T2W) image reveals ill-defined decreased T2 signal at the level of the left anterior transition zone of the mid-gland (arrow). **(B)** Diffusion-weighted imaging (DWI) and axial apparent diffusion coefficient (ADC) map demonstrate markedly restricted diffusion in this region (arrow). **(C)** Colored perfusion map created using post-processing software from dynamic contrast-enhanced (DCE) - MRI acquisition demonstrates suspicious perfusion kinetics for prostate cancer (arrow), corresponding to the findings seen on T2W and DWI. Lesion was scored PI-RADS 4 and patient elected RCT biopsy (mpMRI/TRUS fusion plus laterally directed sextant biopsy - schematic shown in **(D)**) revealing Gleason 3 + 5 = 8 prostate cancer (60% pattern 3, 35% pattern 4 and 5% pattern 5, GrGp 4) involving 30 mm of aggregate length and 70% of biopsy tissue. **Lower panel:** Screen capture from mpMRI/TRUS fusion biopsy of the lesion in the left anterior transition zone showing the needle within the lesion (outlined in green) with the center of the lesion denoted by the small blue circle on both the real-time TRUS image (I) and fused mpMRI image (II). Also, included are sagittal reformatted images from mpMRI (III) and three dimensional model of the prostate and the lesion with the biopsy cores within the lesion (IV). Based on the biopsy results and mpMRI findings, patient was deemed a poor active surveillance candidate and elected radical prostatectomy revealing Gleason 4 + 3 = 7 (GrGp 3) prostate cancer.

ABSTRACT 2

SALVAGE PROSTATE CRYOABLATION FOR THE MANAGEMENT OF LOCAL RECURRENCE AFTER PRIMARY CRYOTHERAPY: A RETROSPECTIVE ANALYSIS OF FUNCTIONAL AND INTERMEDIATE-TERM ONCOLOGICAL OUTCOMES ASSOCIATED WITH A SECOND FREEZE

Alireza Aminsharifi[1], Ghalib Jibara[1], Efrat Tsivian[1], Matvey Tsivian[1],Ahmed Elshafei[2,3] , Thomas J. Polascik[1]

[1]Division of Urologic Surgery, Duke Cancer Institute, Durham, North Carolina, [2]Urology Department, Cleveland Clinic, Cleveland, OH, [3]Urology Department, Medical School, Cairo University, Egypt

Introduction: To examine the outcomes of salvage prostate cryoablation for managing patients with biopsy-proven local recurrence after primary cryotherapy.

Methods: The records of 108 patients treated with salvage prostate cryoablation for biopsy-proven local recurrence after primary cryotherapy were retrospectively reviewed. Oncological outcome was defined by the rate of biochemical recurrence (BCR) after salvage ablation using the Phoenix criteria. Major complications after a second cryoablation procedure along with one-year functional outcomes in terms of continence and potency were also analyzed.

Results: 108 men (mean age 69.3 ± 7.1 years) with mean prostate-specific antigen level 7.08 ±7.4 ng/mL were treated with whole gland or focal (n=17, 15.7%) salvage cryoablation following failed primary cryosurgery. 58 of 108 patients (53.7%) had received either androgen deprivation therapy (ADT) (n= 35, 32.4%) or radiotherapy (n=23, 21.3%) before salvage ablation. The 2-year and 5-year BCR rates after salvage therapy were 28.2% and 48.3%, respectively (Figure 1). At univariate analysis, a higher preoperative Gleason score and D'Amico risk category ($p < 0.0001$) as well as a higher preoperative PSA density >0.15 ng/mL/cc ($p=0.02$) were significantly associated with the risk of BCR. At multivariable analysis, the only significant factor associated with risk of BCR after the second ablation was a higher D'Amico risk category ($p=0.008$).
Persistent urinary incontinence (1-4 pads/day) in 8 (7.4%), temporary urinary retention in 4 (3.7%) and rectourethral fistula in 4 (3.7%) patients were reported one year after the second cryoablation. During the same period, 13.8% of patients were able to have either spontaneous or medication-augmented erections sufficient for intercourse.

Conclusion: This series, to our knowledge, represents the largest cohort of patients receiving two consecutive cryoablation treatments. Local failure after primary prostate cryoablation can be salvaged by a second cryosurgery with acceptable intermediate-term disease control. Patients should be counseled regarding the side effect profile associated with a second cryoablation.

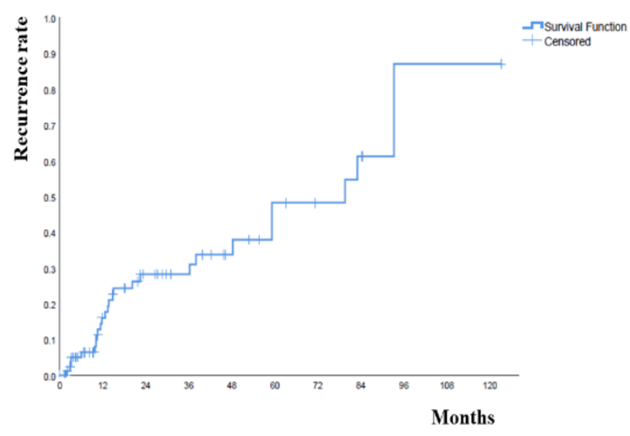

Figure 1: Kaplan-Meier curve demonstrating biochemical recurrence rates after salvage prostate cryoablation in a cohort of 108 patients with local failure after primary cryotherapy.

ABSTRACT 3

ELECTRICAL FIELD STIMULATION OF DISTAL URETERAL TISSUE DEMONSTRATES A ROLE FOR TAMSULOSIN, GLI PROTEINS AND ERYTHROPOIETIN IN URETERAL CONTRACTILITY

Kymora Scotland[1], Lu Wang[2], Ben Chew[1], Chun Seow[2] and Dirk Lange[1]

[1]Department of UrologicSciences, University of British Columbia
[2]Heart Lung Institute, University of British Columbia

Introduction: Ureteral contractility is a poorly understood process. Contractions have been demonstrated to occur in the smooth muscle layers of the ureter (PMC3897663). Previous work suggests the involvement of gli family proteins (PMID:28188758) and erythropoietin (EPO) in regulating mammalian ureteral smooth muscle contraction (PMID:25200805). We sought to devise a method by which the effects of these proteins on distal human ureteral tissue contractility could be investigated.

Methods: IRB approval was obtained to procure portions of extraneous distal ureteral tissue from living donor renal transplants. Ureteral tissue contractility was assessed in an electrical field stimulation (EFS) device designed specifically for the evaluation of smooth muscle contraction. Tissue was defatted and prepared in approximately 1mm thick rings mounted vertically in a tissue bath with one end fixed to a stationary hook and the other to a servo-controlled lever of a length-force transducer. The tissue bath contained Krebs buffer solution at 37°C that was bubbled with a 95% O_2-5% CO_2mixture. The muscle preparation was equilibrated for one hour. Muscle was then activated by EFS. A uniform electric current was achieved using a 60-Hz AC stimulator with platinum electrodes. An isometric contraction was elicited after each stretch. Contractile force was recorded with each stimulation with and without the presence of a gli inhibitor (GANT61) or EPO. Each ureteral specimen was subsequently fixed and studied by immunohistochemistry to determine gli, EPO and alpha adrenergic receptor expression.

Results: EFS successfully elicited contractions in the ureteral tissue. Administering tamsulosin decreased ureteral contractile force. Inhibiting Gli signaling decreased contractility as early as 60 minutes post-administration. EPO decreased ureteral contractile forces within 5 minutes compared to untreated controls. Staining revealed differential gli1 protein and α-adrenergic receptor expression in ureteral smooth muscle and epithelial tissue with EPO receptor expression confined to the epithelial layer.

Conclusion: Distal ureteral contractile forces are decreased by inhibitors of gli family proteins and the α-adrenergic receptor. EPO was shown to act within a short time frame, suggesting ion channel involvement instead of changes in gene expression. Continuing work will elucidate the role of these proteins in coordinating ureteral contractions. This has implications for the use of pharmacologic methods to address ureteral contractility and dysfunctional peristalsis during stone passage, ureteroscopy, in transplant patients and potentially to reduce symptoms from ureteral stents.

ABSTRACT 4

INTRA-PRACTICE UROLOGIST-LEVEL VARIATION IN FUSION BIOPSY OUTCOMES

Jaya M. Telang[1], Ji Qi[1], Anna M. Johnson[1], Rabia S. Martin[1], Matthew S. Davenport[2], Prasad R. Shankar[2], Nicole E. Curci[2], Chandy S. Ellimoottil[1], Jeffrey S. Montgomery[1], John T. Wei[1], Simpa S. Salami[1], James E. Montie[1], David C. Miller[1], Arvin K. George[1],

[1]Michigan Medicine – Department of Urology, Ann Arbor, MI
[2]Michigan Medicine – Department of Radiology, Ann Arbor, MI

Introduction: Level 1 evidence supports use of MR and fusion biopsy (FBx) in the prostate cancer diagnostic pathway. The success of nascent FBx programs depends on multiple factors including MR image quality, MR interpretation, MR-ultrasound image registration, and FBx technique. Using a cohort of experienced urologists, we aimed to define expected provider-level variation in cancer detection rate (CDR) and FBx upgrading at a large academic center.

Methods: We identified all men in the prospective Michigan Urological Surgery Improvement Collaborative (MUSIC) registry who underwent multiparametric prostate MRI (mpMRI) and FBx at Michigan Medicine from 8/2017-9/2018. mpMRI was performed at a single site on a 3T magnet (Philips Ingenia, Siemens Vida); all studies met PIRADSv2 criteria for technical requirements. Each MR interpretation was performed by one of 13 radiologists in the cohort (2-12 years' experience). Patient, imaging, and pathology characteristics were reviewed and stratified by urology provider. Bivariate and multivariable logistic regression analyses were performed to assess variation in cancer detection rate (CDR) at urology provider level, controlling for patient age, PSA, race, family history, clinical stage, and PIRADS score. High grade (HG) cancer was defined as grade group (GG)≥2. Upgrading was defined as any increase in GG by biopsy type (standard cores vs. targeted cores) within the same patient.

Results: We identified 333 patients in the MUSIC registry who had FBx. Provider-level performance demonstrated no significant variation among providers in any domain on multivariate analysis (Figure 1). Though upgrading by standard cores for all providers was higher than expected (13.3%-25.3%), upgrading to HG cancer on standard cores was low (expected <15%, observed 2.2%-12.7%), reflecting an increased detection of GG1 on standard biopsy.

Conclusion: Amongst trained FBx providers within a single center with consistent mpMRI image quality and interpretation, minimal variation in CDR or upgrading rates exists. Greater study power will validate these early findings and provide insight into similar domains across radiology providers.

Outcome	MUSIC Benchmark*	Urologist A n=104	Urologist B n=45	Urologist C n=94	Urologist D n=90	p-value**
Overall CDR	>55%	78.85%	60%	72.34%	67.78%	
Target CDR	>45%	67.31%	51.11%	57.45%	57.78%	
Standard CDR	>50%	70.19%	53.33%	59.57%	57.78%	
HG by Target Cores CDR	>35%	45.45%	46.34%	40%	42.86%	
UG by Target Cores	>15%	26.92%	17.78%	25.53%	18.89%	
UG by Standard Cores	<15%	21.15%	13.33%	25.53%	18.89%	
HG UG by Target Cores	>20%	16.35%	13.33%	13.83%	11.11%	
HG UG by Standard Cores	<15%	8.65%	2.22%	12.77%	5.56%	

Benchmark met / Within 10% of benchmark / Greater than 10% from benchmark

*MUSIC benchmarks determined by radiology/urology consensus based on published literature
**Multivariate analysis controlling for age, PSA, prostate volume, race, family history, clinical stage, and PIRADS score.

Figure 1: Comparison of MUSIC Fusion Biopsy Scorecard domains by Urology biopsy provider

ABSTRACT 5

EVALUATION OF THE EFFECT OF IMMERSIVE VIRTUAL REALITY ON RESIDENT, SURGEON AND PATIENT ANATOMIC UNDERSTANDING IN THE SETTING OF LAPAROSCOPIC PARTIAL NEPHRECTOMY

Egor Parkhomenko[1], Mitchell O'Leary[1], Francis Jefferson[1], Shoaib Safiullah[2], Ryan James[3], Logan Grimaud[1], Roshan M. Patel[1], Kamaljot S. Kaler[1], Edward Uchio[1], Ralph V. Clayman[1], and Jaime Landman[1].

[1]Department of Urology, University of California, Irvine, Orange, CA
[2]Department of Urology, University of Missouri, Columbia, MO
[3]Department of Biomedical Informatics and Medical Education, University of Washington, Seattle, WA

Introduction: Upwards of 2500 black and white two-dimensional (2D) images are obtained during typical computed tomography (CT) or magnetic-resonance (MR) imaging of a renal mass; these images are then reviewed by surgeons in order to assess the optimal surgical approach for performing a partial nephrectomy (PN). In contrast, immersive virtual reality (iVR) combines all 2500 images into a single, technicolor 3D headset display that enables the surgeon to interact with the anatomy in an immersive environment. Herein, we evaluated the efficacy of iVR for surgical planning and patient education prior to PN.

Methods: 3D anatomical maps were created from CT/MRI data using *3D Slicer* and Bosc, a VR system (Pyrus Medical). iVR models (n=17) were reviewed by 3 experienced surgeons with a head-mounted display (Oculus Rift, Facebook Inc.). Surgeon preoperative anatomical understanding was assessed with a questionnaire after reviewing only CT images and again after the iVR experience (0=poor; 10=excellent). A postoperative survey assessed the anatomical accuracy of iVR and any changes in the operative approach based on the iVR experience. A Likert-type survey assessed surgeons' and patients' iVR experience (1=strongly disagree to 5=strongly agree).

Results: iVR significantly improved surgeons' understanding of the location, size, shape/orientation of the tumor, the optimal surgical approach, and the pertinent anatomy ($p < 0.01$) (Table 1). All 3 surgeons strongly agreed that iVR is a valuable planning tool (4.9/5), that they would recommend iVR to a colleague (4.9/5), and that they would use iVR to teach residents (4.9/5). Reviewing iVR changed the surgeons' operative approach in 11/17 of cases (65%). Moreover, patients agreed that iVR reduced their preoperative anxiety (4.23/5).

Conclusion: iVR improved surgeons' anatomical understanding, reduced patients' anxiety, and accurately represented the encountered anatomy. Preoperative review of an iVR model altered the surgical approach in two-thirds of cases.

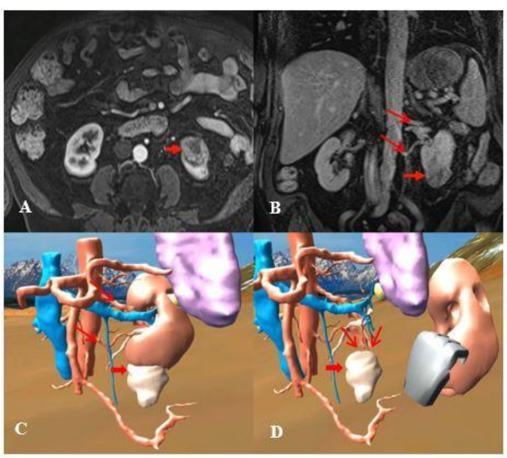

Figure 1: A) Transverse view of a MRI scan depicting a lower pole renal mass. Red arrow indicates medial border of the tumor. **B)** Coronal view of same MRI scan depicting two renal arteries. Thin red arrows highlight the two renal arteries. **C)** iVR model depicting the renal anatomy and associated vasculature. Thin red arrows highlight the two renal arteries seen in B. **D)** iVR model. Hand (white) seen removing renal parenchyma to reveal two, tumor-feeding renal arteries. Thin red arrows indicate feeding arteries.

Table 1: Surgeon and Patient iVR Assessment Questionnaire Scores

Surgeons' image understanding (0 = poor; 10 = excellent)			
	CT (n = 17)	VR (n = 17)	p-value
Location of Renal Mass	7.00	9.76	**<0.001**
Size of renal mass	7.35	9.76	**<0.001**
Shape & Orientation of the Renal Mass	6.29	9.76	**<0.001**
Optimal Surgical Approach	6.82	9.82	**<0.001**
Arterial Vasculature Relative	6.47	9.76	**<0.001**
Venous Vasculature	6.23	9.88	**<0.001**
Collecting System	5.47	9.71	**<0.001**
Hilar Anatomy	5.76	9.59	**<0.001**
Ureter Location	6.71	9.76	**<0.001**
Surgeon Pre-Operative Assessment (n = 17) (1 = strongly disagree, 5 = strongly agree)			
iVR Improved Understanding & Confidence for the Surgery	5.00 (4-5)		-
Valuable Surgical Planning Tool	4.94 (4-5)		-
Use iVR for Future Surgery	4.94 (4-5)		-
Recommend iVR to Colleagues	4.94 (4-5)		-
Use iVR to Teach Residents	4.94 (4-5)		-
Surgeon Post-Operative Assessment (n = 17) (1 = strongly disagree, 5 = strongly agree)			
iVR Helped Navigate Anatomy	4.71 (2-5)		-
iVR Correlated with Hilar Anatomy	4.64 (1-5)		-
iVR Correlated with Collecting System	4.76 (4-5)		-
iVR Correlated with Vasculature	4.76 (1-5)		-
iVR Correlated with Mass Location & Size	4.88 (4-5)		-
iVR Altered the Operative Approach	64.7% (n=11/17)		-
Patient Immersive Virtual Reality Model Pre-Operative Assessment (n = 13) (1 = strongly disagree, 5 = strongly agree)			
	Pre-iVR	**Post-iVR**	**p-value**
Understanding of the Renal Mass Location	4.46	5.00	**0.007**
Understanding of the Renal Mass Size	4.46	5.00	**0.019**
iVR Improved Understanding of Why PN is Needed	5.00		-
Feel Less Concerned About Surgery After Viewing iVR model	4.23 (2-5)		-

ABSTRACT 6

PROCEDURE SPECIFIC DISPOSABLE UROLOGICAL RIGID ENDOSCOPES APPROACHING REALITY

DiTrolio, J.V., M.D.[1], La Salle, M.D., M.D.[2.] Deolankar, J.[1], Komaravolu, S.[1]

[1]Rutgers/New Jersey Medical School, Newark, NJ
[2]St. Barnabas Medical Center, Livingston, NJ

Introduction: Purpose-oriented disposable cost effective endoscopes have been a dream and challenge for the past decade. With electronic chip development decreasing in cost and size, urological endoscopes are rapidly approaching reality. Benefits would be to reduce labor-intense storage, purchase, reprocessing, and sterilization. Avoidance of expensive endoscopic video tower, along with transportable bedside implementation makes this the time to consider disposable endoscopes as a reality.

Methods: ProSurg Neo Cystoscopes ™ were evaluated for procedure-specific use. Employing a 400x400 video chip at the tip in a family of rigid cystoscopes 12-15 OD with a 5-8 Fr working channel. In-handle LED light source delivered by fiber optics to the working end, and utilizing a laptop/tablet power source and video monitor, in conjunction with the video link module, giving the capability to visualize, transmit or memorialize the surgical event. These were evaluated for ease of use, functionality, quality of image, and cost effectiveness in the office or bedside setting.

Results: The ProSurg Neo Cystoscope ™ family of products was able to deliver purpose-oriented equipment in the $150-200 range. They were used effectively in cystoscopic evaluation, stent placement/removal; and transurethral vaporization of both bladder tumors and benign prostatic hypertrophy. Disposable cystoscopes were specifically designed for single-use in association with a standard laptop computer/tablet, providing power source and visualization. Video image was outstanding with no need to sterilize, clean, or repair the cystoscopes. Cost, when compared to standard cystoscopies was equal without the upfront cost of purchase and the additional expense of a video support tower.

Conclusion: Disposable scopes have passed the tipping point and are now a reality with improved stellar imaging, minus the cost of a video tower, reprocessing, or repair costs, which are most likely caused by handling, cleaning, or sterilization. The future has arrived and it is not out of the range of reality to purchase a ureteral stent, with guidewire, pusher, and introductory cystoscope all in one package, or a PVP laser fiber, with continuous-flow cystoscope included at a favorable price. Further innovations will only improve the equipment.

ABSTRACT 7 **TOP 10 ABSTRACT**

IMAGING THE DEVELOPING HUMAN UROGENITAL SYSTEM WITH LIGHT SHEET FLUORESCENCE MICROSCOPY

Dylan Isaacson*[1], MD, MPH; Dylan McCreedy[2,], PhD; Meredith Calvert[3], PhD; Joel Shen[4], BS; Adriane Sinclair[5], PhD ; Mei Cao[5], BA; Yi Li[5], MD; Todd McDevitt[6,8], PhD; Gerald Cunha[5], PhD; and Laurence Baskin[5,7], MD

[1]Department of Urology, Northwestern University Feinberg School of Medicine, Chicago, IL
[2]Department of Biology, Texas A&M University, College Station, TX
[3]Histology and Light Microscopy Core, J. David Gladstone Institutes, San Francisco, CA
[4]CytomX Therapeutics, Inc. South San Francisco, CA.
[5]Department of Urology, University of California, San Francisco, San Francisco, CA
[6]Department of Bioengineering and Therapeutic Sciences, J. David Gladstone Institutes, San Francisco, CA
[7]Division of Pediatric Urology, University of California San Francisco Benioff Children's Hospital, San Francisco, California
[8]Institute of Cardiovascular Disease, J. David Gladstone Institutes, San Francisco, CA

Introduction: Light sheet fluorescence microscopy (LSFM) is a recently-developed technique that uses thin planes of light to optically section whole-mount cleared and immunolabeled biologic specimens, enabling rapid 3D imaging of external and internal structures at subcellular resolution. Our group has newly applied LSFM to identify products of differential gene expression throughout the entire developing human fetal urogenital system [1, 2, 3].

Methods: Fifty-one deidentified human fetal urogenital organs were fixed in 4% paraformaldehyde and cleared using a modified Passive CLARITY Technique (PACT) [4]. Cleared specimens were immersed in primary and secondary antibodies, embedded in low-melting point agarose and allowed to equilibrate in Histodenz™ (Sigma-Aldrich, St. Louis, MO, USA) refractive index-matching solution. Optical sections were acquired using a Lightsheet Z.1 device (Carl Zeiss AG, Oberkochen, Germany). Sections were 3D reconstructed and processed into video and still images in Imaris (Bitplane AG, Zurich, Switzerland)

Results: Sections were acquired and reconstructed in under two minutes per specimen. Every major developing human fetal urogenital organ was successfully imaged, including the kidneys/adrenal glands, bladder/ureters, prostate, Müllerian ducts/ovaries, Wolffian ducts/testes, the penis and the clitoris. Figure 1 demonstrates a 12-week human fetal bladder/prostate stained for Alpha-SMA (purple, expressed in smooth muscle) and S100 (green, nerves). The interlaced muscle fibers of the bladder are visible and contrast with the circumferential fibers of the ureter and prostate. Nerve fibers are visible running lateral to the prostate, ureterovesical junction and bladder. Figure 2 shows a 14-week human fetal testis stained with E-cadherin (green, epithelia) and anti-Müllerian hormone (AMH, Sertoli cells). E-cadherin highlights the epithelium of the head and body of the epididymis and proximal ductus deferens. AMH highlights developing fetal seminiferous tubules.

Conclusion: We have successfully applied LSFM to image human fetal organs throughout the urinary and genital systems. This work enables a new generation of study to elucidate normal development and the genetic basis of congenital urogenital anomalies.

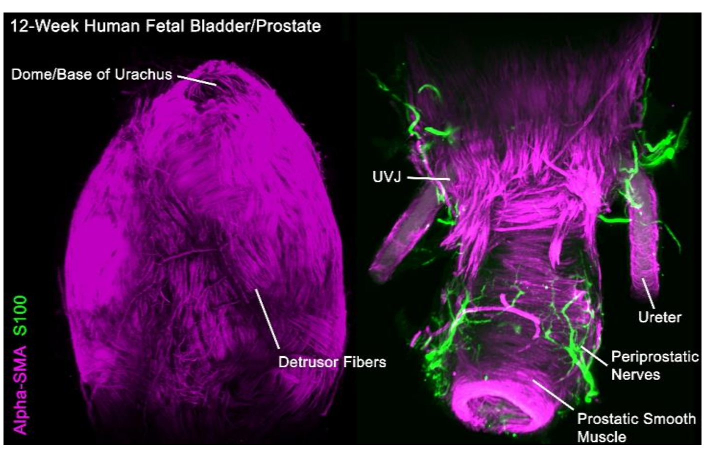

Figure 1: 12-week human fetal bladder/prostate stained with Alpha-SMA (purple, smooth muscle) and S100 (green, nerves)

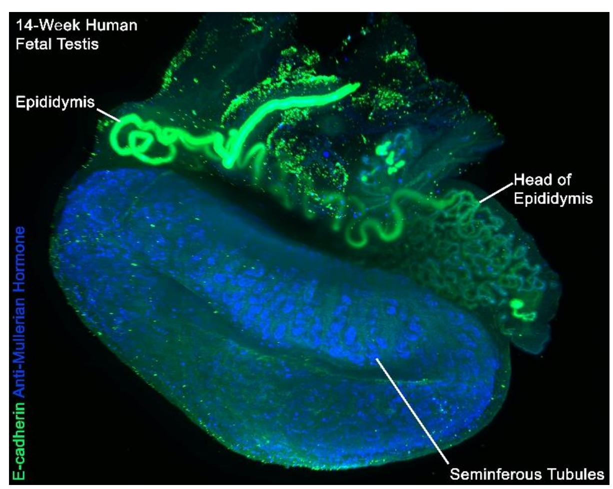

Figure 2: 14-week human fetal testis stained with E-cadherin (green, epithelia) and AMH (blue, Sertoli cells)

ABSTRACT 8

RENAL THREE-DIMENTIONAL RECONSTRUCTION TO PLAN ROBOTIC-ASSISTED LAPAROSCOPIC PARTIAL NEPHRECTOMY: OUR PRELIMINARY EXPERIENCE

Inzillo R.[1], Puliatti S.[1], Dourado Meneses A.[3], Eissa A.[1,2] , Zoeir A.[1,2] , Del Prete C[1], Sighinolfi M.C.[1] , Rocco B.[1], Micali S.[1]

[1]Dept. of Urology, University of Modena and Reggio Emilia, Italy,
[2]Dept. of Urology, Faculty of Medicine, Tanta University, Egypt
[3]Dep.t of Urology, Hospital São Marcos. Teresina. Brazil.

Introduction: There is an increasing interest in the use of three-dimensional reconstruction images based on CT-angiography scan for the pre and intra- operative planning of partial nephrectomy in the recent years. Different softwares have been tested to create reconstructions for laparoscopic and robot-assisted partial nephrectomy. In our department, we started to perform robot-assisted partial nephrectomies with the help of the DOCDO reconstruction software (www.docdo.com.br), which allows a pre-operative planning based on the anatomy and the vascularisation of the kidney. We prepared a short questionnaire about the reliability of the software that the surgeon had to fill after the surgery.

Methods: The CT scans of five consecutive patients who underwent robotic partial nephrectomy were subject to 3D reconstruction using the DOCDO software. The 3D reconstruction could be “manipulated” by the surgeon before and during the surgery, in order to identify the hilum (including the renal vessels), ureter, collecting system and the renal mass, all shown in different colors during reconstruction. The images can be uploaded on a computer, tablet or smartphone and be easily accessible. The surgeries were performed by a single surgeon using a trans-peritoneal approach. The survey consisted of three initial questions about the easiness for the surgeon in identifying and reaching the renal vessels and their branches using the DOCDO images, the ease of use of the software, and the intention to benefit from the reconstruction in the next cases. A second aspect that we wanted to analyze with the survey was the correspondence and the reliability of the reconstructions related to the RENAL nephrometry score. Five questions in this section were strictly related to the five prameters of the RENAL score (Radius, Exophytic/Endophytic, Nearness to the collecting system or sinus, Anterior/posterior, Location relative to polar lines). The surgeon had to give a score from one to five for each of the questions.

Results: The surgeries were carried out without intra-operative or post-operative complications. Regarding the survey, the surgeon gave a maximum score to all the questions proposed, describing the 3D reconstruction programme as “ intuitive, efficient and reliable”.

Conclusion: The results of this preliminary experience demonstrates that DOCDO 3D reconstruction software is a promising and easily interpretable tool that may facilitate the robot-assisted partial nephrectomy; however, further studies are required to confirm these results.

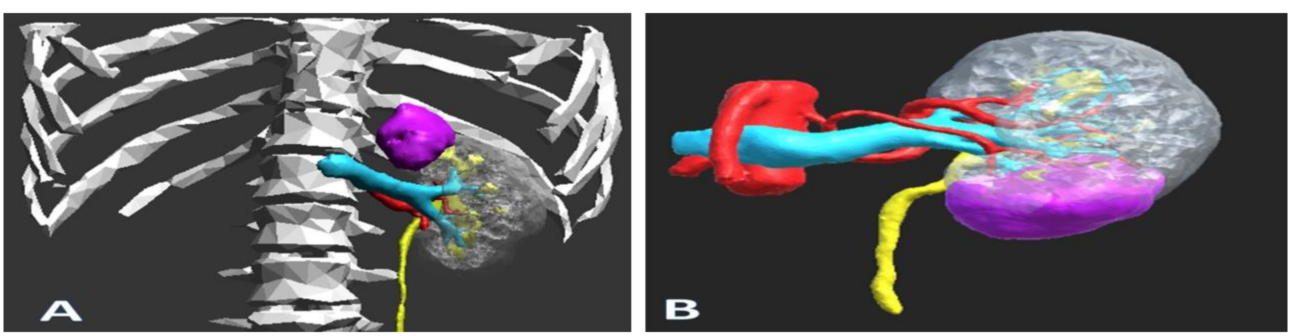

Figure: (A) a 3D reconstructed image of upper pole renal mass (B) a 3D reconstructed image of a lower pole renal mass in both images the tumor is seen in violet color, the ureter in yellow, the veins in light blue and the arterires in red.

ABSTRACT 9

EX VIVO FLUORESCENCE CONFOCAL MICROSCOPY IN THE ASSESSMENT OF UROTHELIAL CARCINOMA GRADING IN BLADDER AND URETER: OUR PRELIMINARY EXPERIENCE

Eissa A.[1,2], Puliatti S.[1], Bevilacqua L.[1], Sighinolfi M.C.[1] , Bertoni L.[3] , Reggiani Bonetti L.[4] , Zoeir A.[1,2], Patel V.[5], Micali S.[1], Rocco B.[1]

[1]Dept. of Urology, University of Modena and Reggio Emilia, Italy, [2]Dept. of Urology, Faculty of Medicine, Tanta University, Egypt, ,[3]Dept. of Surgical, Medical, Dental and Morphological Sciences with Interest transplant, Oncological and Regenerative Medicine, University of Modena and Reggio Emilia, Italy, [4]Dept. of Pathology, University of Modena and Reggio Emilia, Modena, Italy. [5]Dept. of Urology, Global Robotics Institute, Florida Hospital-Celebration Health Celebration, Florida, USA.

Introduction: Fluorescence Confocal Microscopy (FCM) is a novel technology that provides optical microscopic images of freshly excised tissue. It may provide potential advantages over the currently available "real time" pathological examination modalities (frozen section and confocal laser microscopy) including fast acquisition of images, maintenance of specimen integrity for further analysis, and Hematoxylin & Eosin like digital images that are easy to interpret and can be sent online for analysis [PMID24030744].

Methods: The FCM VivaScope® 2500M-G4 (Mavig GmbH, Munich, Germany; Caliber I.D.; Rochester NY, USA) is an optical technology that depends on two different types of lasers (785 nm, and 488 nm) to provide optical microscopic images of freshly excised tissues based on two different modalities; the reflectance mode (different refractive indices of subcellular structures) and the fluorescence mode (using fluorescent agents to increase the contrast within the epithelium-stroma). The FCM is characterized by vertical resolution of 4 µm, maximum penetration depth of 200 µm, total scan area of 25 x 25 mm, and 550X magnification power. Furthermore, the microscope is equipped with a 38X water immersion objective with numerical aperture of 0.85 [http://www.vivascope.de].

We hypothesized that FCM can be used for ex-vivo "real-time" diagnosis of high grade/low grade urothelial carcinoma in bladder and ureter. We present our preliminary experiences in the first four patients. We prospectively collected data from 4 urothelial cancer patients (3 bladder, 1 ureter). Six specimens were collected (5 bladder, 1 ureter) during TURBT and flexible-URS.

Results: All the digital FCM images were ready in less than 5 minutes. In the ureteral specimen, there was accordance between the FCM images grade and the histopathological grade (High grade). The bed of resection was ablated after FCM examination by Holmium laser. The patient was then scheduled for nephroureterectomy. Concerning the bladder specimens, we found accordance between the grading of FCM images and the final histopathology all the specimens of bladder urothelial carcinoma (100%). Furthermore, three specimens obtained from two patients were found to be high grade, while the remaining two specimens from one patient were low

Conclusion: FCM is a promising technology for real time histopathological examination according to our initial results. The images are processed in less than 5 minutes. This technology may provide potential advantages in selecting patients eligible for conservative treatment in ureteral urothelial carcinoma and those eligible for intra-vesical chemo and immunotherapy in bladder cancer. However, further studies are required to confirm the results.

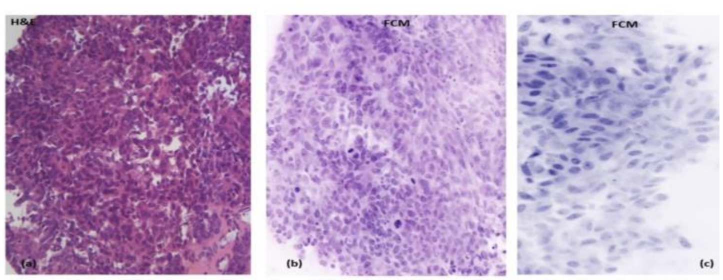

Figure: (a) show the H&E image of the ureter; (b)The digital image of the ureteral specimen showing high grade tumor; (c) FCM image of the bladder showing low grade tumor

ABSTRACT 10 **TOP 10 ABSTRACT**

ROBOTIC 3D ULTRASOUND-GUIDED TARGETING FOR PERCUTANEOUS RENAL ACCESS

Tareq Aro[1,2], Sunghwan Lim[1], Doru Petrisor[1], Dan Stoianovici[1,2]

[1]Robotics Laboratory, [2]Department of Urology, Johns Hopkins University

Introduction: Percutaneous NephroLithotomy (PCNL) access to the kidney is commonly performed under X-Ray fluoroscopy guidance. With this 2D image, several trial and error puncture attempts are often required. Moreover, these expose the patient and personnel to ionizing radiation. Alternatively, PCNL access can be achieved under ultrasound guidance, without radiation exposure and with similar success rate in expert hands. However, this requires substantial training, skill, and involves a harder learning curve. We developed a simple, easy to operate, ultrasound-guided robotic system for acquiring percutaneous renal access. This has the potential to eliminate the trial and error attempts for gaining accurate access, reduce variability among urologists and the required level of skill.

Methods: A 3 degree of freedom (DoF) robot [1, Abs. 42] was used to manipulate an ultrasound probe (EUP-B512, Hitachi Inc.). A needle-guide was designed to fit the system as a part of the probe adapter. The robot enables a 3D ultrasound imaging by acquiring image-position pairs during a scan procedure. A 3D volume image is then reconstructed based on the pairs. Dedicated image acquisition software, navigation, and robot control software was developed in C/C++ with open source libraries such as OpenCV [2] and VTK [3]. A novel ultrasound compatible gelatin model was produced at the lab; an online available CT scan was used to replicate the exact anatomy of the left collecting system and its relation to the patient's skin surface using 3DSlicer software [4], CREO (PTC, Needham, MA) was used to assemble a containment box and a shaft. The collecting system was printed with a special dissolvable filament that was later dissolved using D-Limonene. The mockup was created with 300 bloom gelatin:glycerin:sorbitol:water (300:300:200:2500 in gr) at 55°C.

A scan of the mockup shows the 3D volume image (Fig. 1c). A desired calyx is chosen, manual repositioning of the robot is performed before a second scan and targeting. A desired trajectory to the target is achieved by selecting a possible trajectory among the infinitely many trajectories on the constant cone surface that is shaped by the robot kinematics restriction and has a peak point on the target (Fig. 1b). An 18Ga percutaneous access needle (Naviguide, Boston Scientific Inc.) was inserted manually through the guide to the depth of the calyx, which was observed during real-time ultrasound.

Results: Two of the calyces were successfully reached from a desired starting point with the needle using the robotic guidance after the second scan. One calyx required another repositioning and scanning in order to achieve a preferable trajectory before needle insertion.

Conclusion: Using the robotic system may prove to have several clinical advantages: the reconstruct provided with a single scan can help urologists understand the 3D anatomy and orientation of a patient's collecting system; with minimal practice a junior or senior urologist can possibly access the collecting system percutaneously using only ultrasound imaging. Future tests and clinical trial are needed to test the safety and feasibility of the system.

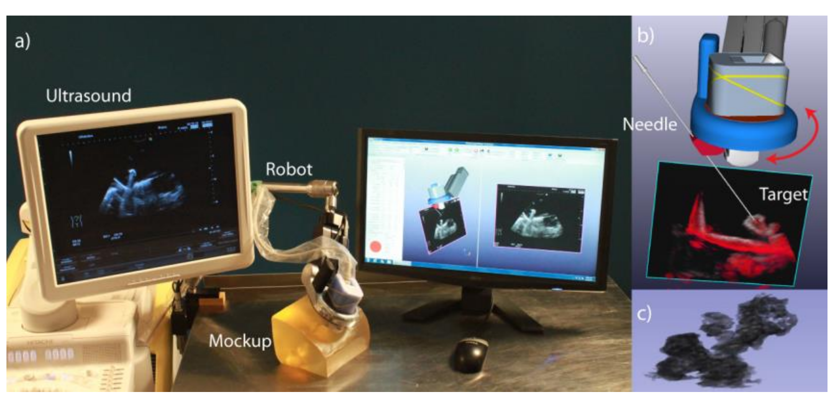

Figure 1: a) Experiment setup. b) Virtual environment showing the robot arm, needle trajectory and desired target, red arrow shows cone rotation direction. c) automatically rendered volume image of the collecting system after the robotic ultrasound scan

ABSTRACT 11 **TOP 10 ABSTRACT**

DIGITAL STONE MEASUREMENT IN URETEROSCOPIC STONE PROCEDURES: A WORKFLOW FEASIBILITY STUDY

Kevin Koo[2], Tareq Aro[1,2], Sunghwan Lim[1,2], Doru Petrisor[1,2], Dan Stoianovici[1,2], Brian R. Matlaga[2]

[1]Robotics Laboratory, [2]Department of Urology, Johns Hopkins University

Introduction: Accurately estimating stone fragment size is an important task during ureteroscopic stone management. We previously reported an ex vivo validation of a novel software that can measure small stone fragments [EUS2018 Abs.4, PMCID: 29084456]. Here we present the feasibility of integrating the software into the operating room workflow (AUA2019 PD08).

Methods: The scale of ureteroscopic image, $s[mm/pixel]$, can be estimated from the tip position of the endoscopic instrument, $t[pixel]$, which is measured from the right edge of the image. A linear relationship exists between those two parameters, such that $s = wt + b$, where w and b are constant numbers. Once the image scale s is determined, the size of the object in ureteroscopic image can be measured.

In the experiment, mock stones were used to mimic a variety of stone sizes and fragmentations. Using a commercial model of the kidney and ureter, we performed two versions of a timed basketing task. In the conventional version, the ureteroscope was navigated from the ureteropelvic junction (UPJ) to the stone in a superior pole calyx. Then, the stone was retrieved with the basket back to the UPJ. In the measurement version, real-time measurement of the stone was performed using the software, followed by retrieval to the UPJ. Differences in task completion time and fragment characteristics were compared.

Results: A total of 20 stone fragments (Fig. 1) were selected with different combinations of internal characteristics: size (mean 7.1 mm, range 3.2–10.3 mm), 3-dimensional shape (50% pyramidal, 30% ovoid, 20% cuboid), surface contour (50% smooth, 50% rough), and planar symmetry (60% asymmetric, 40% symmetric). In the conventional version, mean completion time was 16.5s (range 10.1–33.6s), compared with a mean completion time of 38.8s (range 27.2–60.0s) in the measurement version. The additional time required to perform real-time measurement averaged 22.2s (range 8.8–42.6s).

Conclusion: Integrating software for real-time stone measurement during ureteroscopy is feasible and has a modest effect on the time required for stone manipulation. These findings support in vivo trials to enhance clinical decision-making in ureteroscopic stone management.

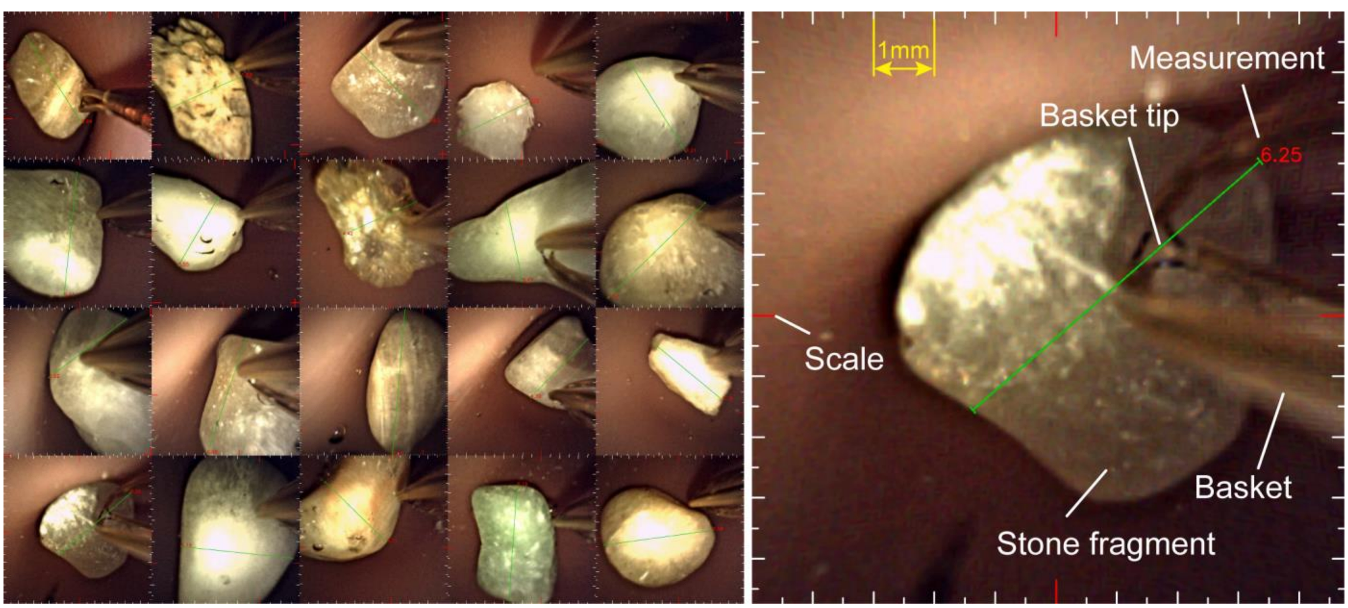

Figure 1: Left: Ureteroscopic images of 20 stone fragments, Right: Measurement of stone fragment no.16

ABSTRACT 12

CAN INTRA-VESICLE ULTRASOUND SURFACE MAPPING REPLACE CYSTOSCOPY? NOVEL TECHNIQUE AND PROOF OF CONCEPT

Tareq Aro[1,2], Sunghwan Lim[1], Doru Petrisor[1], Dan Stoianovici[1,2]

[1]Robotics Laboratory, [2]Department of Urology, Johns Hopkins University

Introduction: Cystoscopy remains the only acceptable method for demonstrating bladder urothelial carcinoma lesions, various imaging modalities remain unreliable for the diagnosis or follow-up. Intra-vesicle imaging with a saline filled bladder may provide better resolution. No such modality is used to date, even though small and miniature ultrasound transducers exist and are used in other medical fields. Using a robot system to handle the ultrasound probe and surface rendering software, we demonstrate the feasibility of a novel technique for future intra-vesicle surface mapping of the bladder.

Methods: We used a linear transrectal ultrasound transducer (Hitachi EUP-U533L) connected to a special robot system, developed at Johns Hopkins Urology Robotics Laboratory, capable of performing a 360 degree controlled rotation. The robot enables a 3D US imaging by acquiring image-position pairs during the scan procedure. A 3D volume image is then reconstructed based on the pairs. Dedicated image acquisition software, navigation, and robot control software was developed in C/C++ with open source libraries such as OpenCV *[1]* and VTK *[2]*. A cylindrical construct with an internal diameter of 10 cm was used to create a mockup using bloom Gel powder, various shapes of gel protrusions representing tumors with sizes 3-50 mm were glued to the interior using molten gel. The volume scan of the mockup submerged in water was transferred into the 3DSlicer *[3]*, surface mapping was created using segmentation tool. Surface images were examined to determine if all protrusions were identified and if artifacts existed. The software shows both the 3D constructed surface and the original US images so that any area on the surface image can be automatically traced to the original US for an operator to decide if it is a rendering artifact or an actual protrusion.

Results: Surface 3D reconstruction is shown for half a cylinder at a time for ease of interpretation; a full 360^0 surface image is available when needed. After examining the final rendered reconstruct (Fig. 1), all the protrusions were clearly visible on the surface images, small artifact areas were dismissed as non-tumors when looking at the original ultrasound images in the software as explained.

Conclusion: Intra-vesical scanning of a water filled bladder with a special robotic system and surface mapping software may be able to replace / augment cystoscopy in the future. The miniature ultrasound technology already exists and needs adaptation for urologic use. Future trials with new specialized ultrasound probes are necessary.

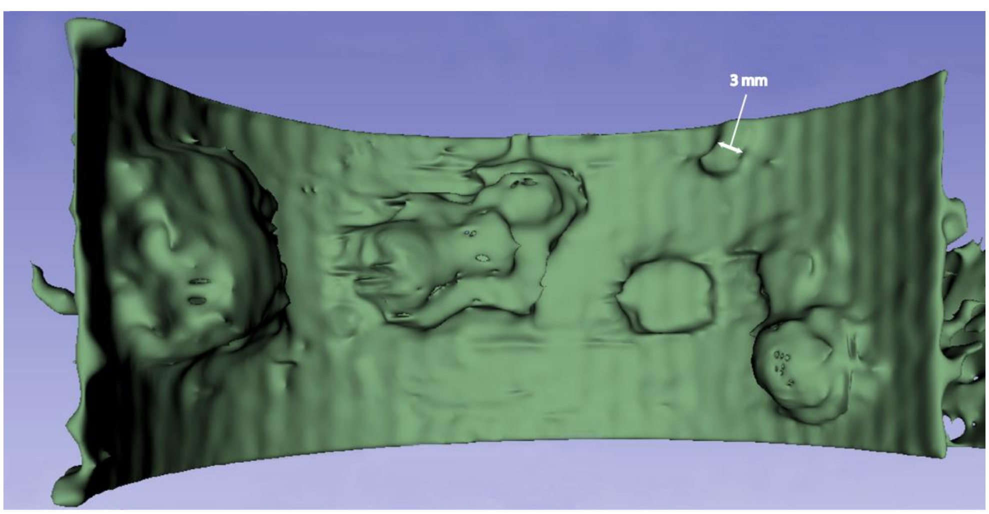

Figure 1: surface mapping of 180^0 scan of the cylindrical surface showing multiple protrusions as small as 3mm

ABSTRACT 13

THE 3DBIOPSY SYSTEM, A NOVEL APPROACH UTILIZING NEW MEDICAL DEVICES, TO IMPROVE THE DIAGNOSTIC ACCURACY AND LOCALIZATION OF DISCREATE CANCEROUS LESIONS WITHIN THE PROSTATE GLAND

Nelson N. Stone[1], Paul Arangua[2], E. David Crawford[2]

[1] The Icahn School of Medicine at Mount Sinai, New York, New York and 3DBiopsy, Inc., Aurora, CO.
[2] The University of Colorado Health Sciences Center, Aurora, CO.

Introduction: The inaccuracy of contemporary prostate biopsy persists despite the popularity of MRI-guided approaches. A novel biopsy platform, which enables accurate sampling and characterization of the entire prostate may prove to be more effective for focal therapy planning and targeting.

Methods: 3DBiopsy is developing a novel system with an adjustable length needle (2-6 cm) and corresponding variable actuator, sophisticated targeting software with or without MRI co-registration, and a bar-coded integrated pathology sample processing system (IPS) that maintains the integrity of the longer cores and enables the exact spatial location of all tumors.

Results: A transperineal mapping prostate biopsy was performed on a prostate phantom with MRI lesions (SIM^{TM}) utilizing the Company's proprietary 15-G biopsy needle. The needle was designed with ridges along its notch to prevent tissue bunching and a trocar tip that markedly reduced deflection. Compared to the Bard, the 3DB needle had decreased deflection from 0.9 to 0.2 mm ($p<0.001$) and 1.9^{0} to 0.2^{0} ($p<0.001$). The annotated MRI was co-registered to the real-time ultrasound (US) images utilizing the 3DBiopsy Digital Image Guided Software (Figure 1, 3DIGS). The 3DIGS created a biopsy plan of 5mm intervals capable of detecting lesions as small as 0.1cc and included the regions of interest (Figure 2). The 15-G needle was inserted through a proprietary 15-G template attached to a standard brachytherapy stepper at position #1. The software indicated the length of the specimen required which was set on the actuator (between 2-6cm). Upon needle insertion, the virtual needle was aligned to it in the axial and sagittal planes (Figure 3). The needle was retracted to the apex, fired and removed. Simulated pathology results and lesion locations were uploaded to the 3DIG in preparation for focal therapy planning (Figure 4). Tissue specimens were taken from RP specimens using the 3DB Actuator (Figure 5) and placed in the IPS (Figures 6-7).

Conclusion: The 3DIGS is simple to use and requires no expensive hardware components. The software is housed in a PC cart system which is plug and play into most US systems. The 15-G biopsy needles can obtain tissue lengths from 2-6 cm, collecting more than 90% without fragmentation or bunching.

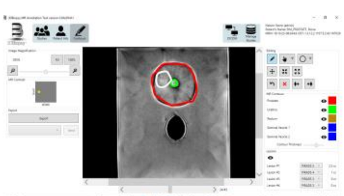
Figure 1: MRI Annotation


Figure 2: 3DIGS Mapping

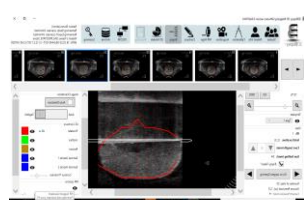
Figure 3: Sagittal Biopsy Image

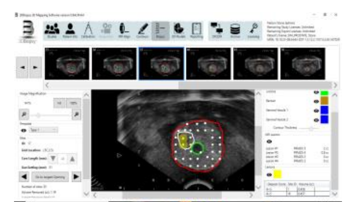
Figure 4: 2 lesion representations


Figure 5: Adjustable Actuator

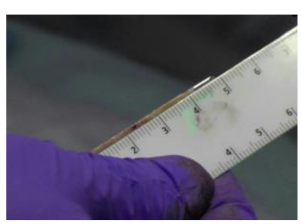
Figure 6: 4.1cm RP biopsy


Figure 7: Biopsy in IPS

ABSTRACT 14

IN VIVO PORCINE EVALUATION OF A NOVEL SELF-CONTAINED BLADDER IRRIGATION SYSTEM (MULTIPHZE™)

Pengbo Jiang[1], Roshan M. Patel[1], Shlomi Tapiero[1], Jaime Landman[1], Ralph V. Clayman[1]

[1]Department of Urology – University of California, Irvine

Introduction: Current standard bladder irrigation (SBI) methods are tedious and pose a biohazard risk due to spillage of blood and urine on the patient, environment, and provider. The Multiphze™ enclosed irrigation system (Multiphze LLC) (MIS), a newly developed self-contained system, was designed to eliminate spillage while improving the efficiency of clot evacuation.

Methods: While under inhalation anesthesia, two female, juvenile pigs were each injected with 100mg IV fluorescein. Via cardiac puncture, 60cc of blood was withdrawn and then instilled into the pig's bladder via a 24Fr 3-way catheter. After 10 minutes, 3 urologists (i.e. chief resident, endourology fellow, and junior faculty), with prior experience using the standard Piston Irrigation Tray (Bard Medical) each performed bladder irrigation with 4L of sterile water; each operator performed a trial with the standard technique as well as with the Multiphze™ system. Time of each irrigation cycle and clarity of drainage fluid using a spectrophotometer were recorded after each liter of irrigation. Total areas of spillage on the procedural field and on the operator were identified with a Wood's lamp and then quantified.

Results: The mean irrigation time for the 4 liters of water with MIS and SBE were 17.9 and 23.1 min (p = 0.035), respectively. The mean clarity measurements at the end of each trial were similar for both MIS and SBI: 82.7% and 82.9%, respectively. Wood's lamp illumination revealed 98% reduction of spillage with MIS compared to SBI: mean spillage area of 19.8 cm^2 and 1001.3 cm^2, respectively (p = 0.034). Despite users having no experience with the novel system, the MIS was intuitive to use, and all operators had reduction in irrigation time (range 2 to 9 minutes).

Conclusion: The newly developed Multiphze™ irrigation system reduced the time to successfully clear a clot filled bladder by 22% in a porcine model. Furthermore, the enclosed system demonstrated a reduction in spillage of the spent irrigant.

	Standard	Multiphze	
Time to irrigate 1 L (min.)	5.8 [4.1-7.4]	4.5 [3.7-5.5]	$p < 0.001$
Time to irrigate 4 L (min.)	23.1 [18.5-26.2]	17.9 [16.4-19.1]	$p = 0.035$

Table 1. Mean irrigation times among all operators

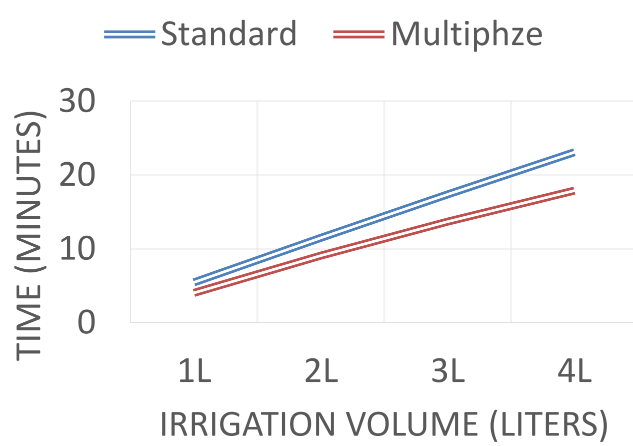

Figure 1: Time comparison over irrigation cycle

ABSTRACT 15 **BEST ABSTRACT AWARD**

INTRAOPERATIVE GUIDANCE FOR ROBOTIC PARTIAL NEPHRECTOMY USING SURFACE-BASED REGISTRATION: INITIAL MODEL ASSESSMENT

E. B. Pitt[1], J. M. Ferguson[1], N. L. Kavoussi[2], E. J. Barth[1], R. J. Webster III[1], S. D. Herrell[2]

[1]Department of Mechanical Engineering, Vanderbilt University, Nashville, TN
[2]Department of Urologic Surgery, Vanderbilt University Medical Center, Nashville, TN

Introduction: While robotic partial nephrectomy can improve long-term outcomes when treating renal cell carcinoma [1], it remains underutilized because of its technical challenges [2]. Effective image guidance has the potential to increase utilization of partial nephrectomy by reducing challenges associated with locating critical subsurface anatomy. We have created a new image guidance system for the da Vinci Surgical System for this purpose. We present a preliminary phantom experiment to evaluate accuracy of our image guidance system and demonstrate its utility in localization of subsurface features.

Methods: A silicone kidney phantom made based on patient imaging was cast with a spherical exophytic tumor model. Prior to experiments, the kidney was attached to a rigid platform containing optical tracking markers. The phantom was imaged with CT, and the kidney and tumor were segmented. In the operating room, a layer of synthetic fat was placed over the area of the phantom containing the tumor. Our image guidance interface was displayed through the da Vinci's surgeon console, alongside the endoscopic camera view. Surgeons used the image guidance system to collect surface data by lightly tracing over the exposed kidney surface with the da Vinci's instruments (Fig. 1-A). Using this data, our system computed a globally optimal surface registration [3] to the segmented kidney image. After registration, surgeons used image guidance to place the tip of an optically tracked needle probe through the layer of fat, into the tumor model (Fig. 1-B). An optical tracking system provided probe position data and post-operative evaluation of registration accuracy.

Results: Using the image guidance system, surgeons easily identified the surgical target. After needle insertion, the fat layer was lifted for visual assessment of needle placement accuracy (Fig. 1-C). Figure 1-D shows the surface-based registration of the kidney overlaid with the ground-truth image location (measured by optical tracking). The distance between the centroid of the tumor model in the registered image and the ground-truth image serves as a preliminary measure of target registration error for our method (1.9 mm).

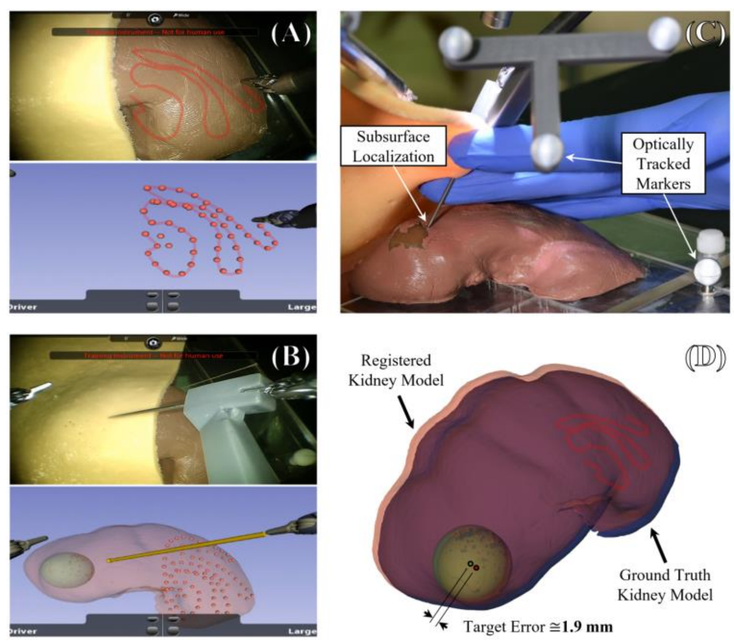

Figure 1: A. Kidney surface data collection. B. Needle insertion task with image guidance. C. Fat lifted to view results of needle insertion. D. Registration result vs. tracked ground truth phantom.

Conclusion: These preliminary results suggest that a surface-based registration technique enabled by lightly tracing da Vinci instruments over a portion of the kidney surface is sufficiently accurate for intraoperative image-to-anatomy registration using the da Vinci Surgical System. Additionally, the success of the needle placement task demonstrates the utility of image guidance for locating subsurface features during surgery. The lack of additional hardware makes touch-based registration an attractive option for fast implementation and adoption in the operating room. Full quantitative analysis of the image guidance system, including *ex vivo* and i*n vivo* experiments, is ongoing.

ABSTRACT 16

MEASUREMENT AND CALCULATION OF LATERAL TRAPPING STRENGTH OF ULTRASOUND FOCUSED BEAMS FOR THE MANIPULATION OF KIDNEY STONES

Mohamed A. Ghanem[1], Adam D. Maxwell[1,2], Vera A. Khokhlova[1,3], Oleg A. Sapozhnikov[1,3], Michael R Bailey[1,2]
[1] Center for Industrial and Medical Ultrasound, Applied Physics Laboratory, University of Washington, Seattle, WA
[2] Department of Urology, University of Washington School of Medicine, Seattle, WA
[3]Physics Faculty, Moscow State University, Moscow Russian Federation

Introduction: Acoustic waves can apply a force to objects. The acoustic radiation force allows the synthesis of acoustic traps that can manipulate objects in multiple directions. Several studies have been published on theoretical models of the acoustic radiation forces, although the majority of the theoretical and experimental work to demonstrating and quantifying the forces or manipulation was focused on small particles. In this work, we focus on the measurements of the lateral radiation forces on objects similar to and larger than the acoustic wavelength and compare the results against theory, with the goal of applying these traps to noninvasively and controllably manipulate urinary tract stones.

Methods: A 256-element ultrasound focused array was used to synthesize three different trapping beam shapes. Vortex beams and two other beams having similar annular pressure distribution in the focal plane were synthesized by specifying the phase and amplitude of each element. Spherical targets made from glass, ceramic and brass with different sizes were placed on a transparent acoustic plate normal to the acoustic propagation axis that was rigidly attached to the array. Each sphere was trapped in the beam as the plate rotated with the array until it fell due to gravity. The measured angle was recorded and compared against the theoretical angle then the lateral trapping forces were nondimensionalized with respect to the bead weight for a specific beam power. To demonstrate controllable noncontact manipulation, beads up to 5 mm were moved in a complex 2D pattern on the plate.

Results: The measured and calculated angles agreed within 10%. The maximum lateral force occurred when the target diameter was equal to the beam width, while objects up to 40% larger than the beam width. The maximum lateral force measured was 280 mg at spatial peak pulse averaged intensity (I_{SPPA}) of 90 W/cm^2 and spatial peak temporal averaged intensity (I_{SPTA}) of 45 W/cm^2. This lateral force was sufficient to lift a 6 mm 6 mm COM stone in water. In addition, beads were successfully moved in a 3-leaf clover pattern, with <10%. Error between the programmed and actual paths of the manipulated beads.

Conclusion: The work demonstrates the ability to steer and manipulate dense objects at power levels that are unlikely to cause injury to tissues *in vivo*. Although spatial peak pulse average intensity and spatial peak temporal averaged intensity are not the only measures of safety, for reference, the diagnostic ultrasound limits for I_{SPPA} and I_{SPTA} are 190 W/cm^2 and 0.72 W/cm^2. Such technology may potentially be used in the relief of urinary stone obstruction or in the facilitation of of clearance of stones or fragments. Work support by NIH through NIDDK P01 DK043881 and K01 DK104854.

ABSTRACT 17

DEVELOPMENT OF HYDROGEL-BASED, FULL PROCEDURAL SIMULATION TRAINING PHANTOMS FOR UROLOGICAL SURGERY

Michael P. Wilson[1], PhD, Jonathan J. Stone[1], MD, Nelson N. Stone[2], MD
[1]Simulated Inanimate Models LLC
[2]3D Biopsy, Inc.

Introduction: Physical phantoms are key components of medical education, including training for urological surgery. Currently, available phantoms exhibit numerous shortcomings: biomechanical behavior and imaging capabilities are unrealistic, and very few options exist for the simulation of complete operative procedures. Furthermore, expensive prices discourage widespread training use. We sought to engineer novel physical training phantoms for various urological surgical procedures.

Methods: 3D-printing and injection molding were used to engineer two physical phantoms: 1) a prostate phantom to simulate imaging, biopsy and treatment of prostate cancer, and 2) a complete genitourinary (GU) system including penis with urethra, prostate, bladder, ureters and kidneys. The GU model was designed for simulation of transurethral resection of prostate and bladder tumors (TURP and TURBT), ureteral catheterization, and ureteral and renal lithotripsy. Medical-grade ultrasound, MRI, and CT imaging was used to validate radiologic appearance. Clinicians that used the phantoms were surveyed with questions regarding the biomechanical and imaging realism of the phantoms and training value.

Results: We constructed a hydrogel prostate phantom containing a 45.2 cc prostate that includes internal simulated malignant lesions. We successfully identified chemical mixtures that generated realistic imaging properties, and prostate phantom imaging compatibility was validated for brachytherapy (Figure 1A-B) and targeted biopsy (Figure 1C-D). We constructed several iterations of the prostate phantoms, incorporating firsthand feedback from clinicians to improve prostate size, shape, imaging characteristics, usability features, and various anatomical elements. Survey results found that 100% of participants agreed the prostate phantom had realistic ultrasound imaging, is easy to use, is an ideal teaching tool and improves technical skills. We constructed a prototype complete GU system (Figure 1E-F) and were able to simulate a TURBT, TURP (Figure 1G-K), and ureteroscopy (Figure 1L-M).

Conclusion: We have engineered two phantoms to enable efficient training for full urological surgical procedures. Future work will focus on enhancing the realism and usability of our phantoms, as well as conducting further clinical validation in order to deliver a superior training experience.

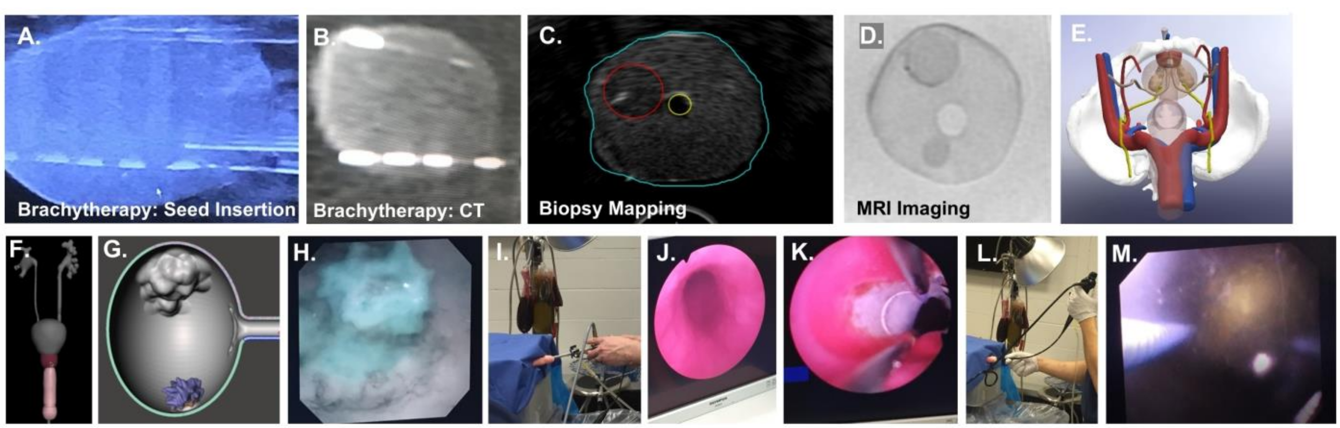

Figure 1: Versatile Phantom Training Capabilities. A. Sagittal ultrasound showing seed placement for brachytherapy simulation. B. Sagittal CT scan showing seed placement for post-procedure validation following brachytherapy simulation. C. Biopsy mapping of simulated malignant lesion (red circle) in transverse ultrasound using 3D Biopsy software for transperineal biopsy simulation. D. T2 Axial MRI image showing two malignant lesions within prostate. E-F. CAD drawings of GU phantom, including urethra, prostate, bladder, and ureters in proper orientation. G. CAD drawing of bladder with two tumors present for resection. H. Endocscopic view of bladder tumor. I. Resectoscope placement on GU phantom. J. Endoscopic view of penile urethra. K. TURP performed on GU phantom. L. Ureteroscope placement. M. Uretoscopy on GU phantom with stent and stone visible.

ABSTRACT 18

SINGLE-PORT TRANSVESICAL ROBOTIC SIMPLE PROSTATECTOMY: EARLY CLINICAL CASES USING THE SP ROBOT PLATFORM

Guilherme V.Sawczyn[1] ,Rair Valero[1], Juan Garisto[1], Jihad Kaouk[1]

[1] Glickman Urological and Kidney institute, Cleveland Clinic, Cleveland, OH, USA

Introduction: We present our initial clinical experience with single-port robotic simple prostatectomy using a new purpose built da Vinci SP® Robot Platform. We compared the perioperative outcomes of transvesical (SP-TvSP) and transperitoneal (SP- TpSP) simple prostatectomy using this novel platform.

Methods: SP-TvSP: With the patient positioned flat and supine on the operative table, a 30 mm infra-umbilical incision is made after percutaneous needle identification of the bladder dome, and a GelPOINT Mini advanced access platform (Applied Medical, Rancho Santa Margarita, CA) is inserted directly into the bladder. A 25 mm multichannel robot port and a 12-mm accessory laparoscopic port are placed through GelPOINT and the da Vinci SP® Surgical System (Intuitive Surgical, Sunnyvale, CA) is docked. The bladder is insufflated with CO2 at 12 mmHg pneumovesicum pressure.
SP-TpSP: With the patient positioned in lithotomy Trendelenburg position, a 30 mm supra-umbilical incision is made and GelPOINT port is inserted into the peritoneal space. Pneumo insufflation is then established at 12 mmHg. The bladder is bivalved and the protate adenoma is enuculated and hemostasis is achieved. A mucosal advancement flap is sutured to the urethra to cover the resected area.

Results: All surgeries were completed by robotic laparoscopic approach, no drains were inserted and there were no short-term complications. Following results are on table 1. All patients were continent and had a good urine flow post operatively with no post void residual volume.

Conclusion: Simple prostatectomy using the Vinci SP® platform is feasible and could be an alternative for the well-established open simple prostatectomy. Previous publication [1] and our early clinical experience suggest that the SP platform is feasible for the transvesical approach that allow for a small cystotomy incision, avoids Trendelenburg positioning and avoids entering the peritoneal cavity. Further, larger sample and long-term studies are needed to corroborate our findings.

Table 1

	n	Prostate Size (average)	Estimated blood loss	Extra-Portals	Total operative time (average minutes)	Lenght of inpatient stay (days)	Pain Scale at Discharge	Post-operative urethral catheter (days)
Transperitoneal approach	2	246g	225 ml	1 (50%)	186	1	3,5	11
Transvesical approach	2	105g	50 ml	0	173	1	2,5	10

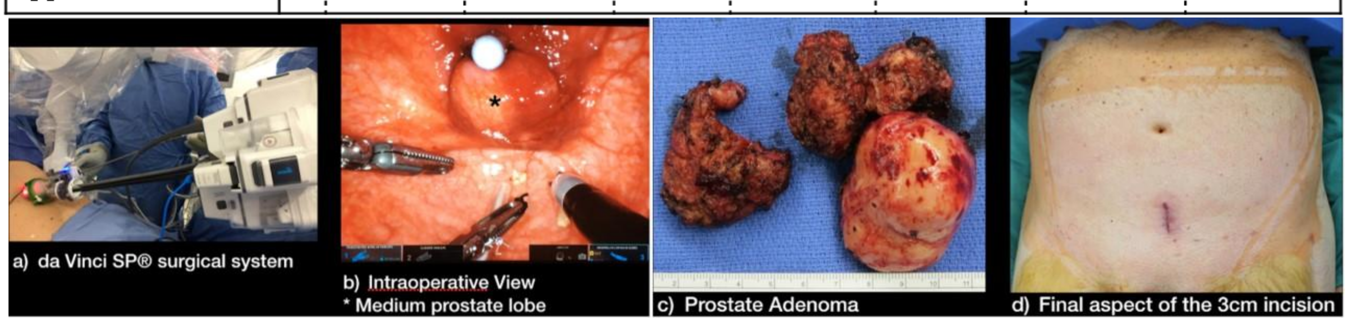

a) da Vinci SP® surgical system
b) Intraoperative View
* Medium prostate lobe
c) Prostate Adenoma
d) Final aspect of the 3cm incision

ABSTRACT 19

ADJUSTABLE LOOP FOR TRANSURETHRAL RESECTION

Steven Monda[1,2], Mike Glamore[2]

[1]School of Medicine, Saint Louis University, St. Louis MO
[2]Division of Urologic Surgery, Washington University in St. Louis, St. Louis MO

Introduction: Transurethral resection of prostate and bladder tissue is common. Traditional electrode loops used in monopolar and bipolar resection offer a restricted cutting area with which to remove tissue. We aimed to make an adjustable loop designed inline with the scope to allow cutting visualization with a fixed lens angle.

Methods: We attached an electrode wire co-axially within an outer sheath with a slit for wire exit and entrance. This allowed real-time analog adjustment of electrode loop *depth* by feeding additional wire into the system (Figures 1 and 2). A second sheath outside of the first allows for adjusting loop *length*. We tested an initial prototype of this design on an *ex vivo* avocado model using cold resection to determine variability in chip volume and precision in resection chip size.

Results: We created an inline resection loop that cuts with a twisting motion of the resectoscope. Resection chips at three different depth sizes showed different average chips sizes of 0.10, 0.45, and 0.75 grams in comparision to the typical chip size of 0.282 of a standard monopolar loop (Figures 3 and 4). Chip size could be adjusted to be smaller or larger than standard resection chips with more spherical than classical cylindrical chip shape (Figure 3).

Conclusion: An adjustable depth inline resection loop allowed for controllable variation in resection chip sizes. This could allow urologists to target specific depths of resection in either bladder tumors or resection of the prostate. The inline design seems ideal for lateral and dome bladder tumors but may have difficulty resecting the posterior wall. Future work will focus on optimizing adjustment design, specifically in insulation of an adjustable wire, possible incorporation of bipolar loops and testing in porcine models. Additionally, we hope to find a 'maximum' resection loop depth where the majority of chips would still fit through a standard resectoscope and be amenable to Ellik evacuation, not requiring morcellation.

Figure 1. Traditional monopolar loop electrode and proposed adjustable loop electrode.

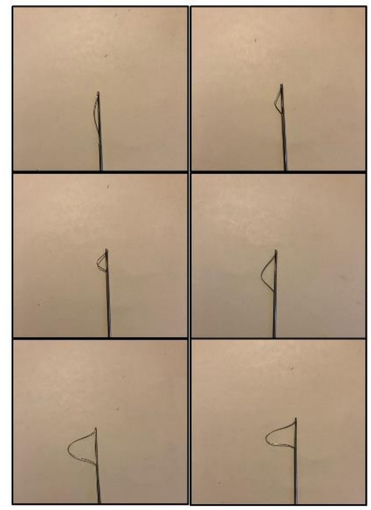

Figure 2. Various loop sizes adjusted to.

Figure 3. Left to right, chips from traditional loop and experimental loops at configurations 1, 2, and 3.

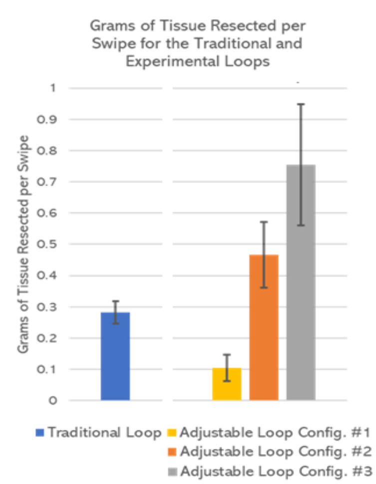

Figure 4. Testing results.

ABSTRACT 20

PRECISE FOCAL THERAPY OF THE PROSTATE USING PHOTODYNAMIC APPROACH

I. Skalkidis[1], D. Hüttenberger[2], J. Arnhold[3], G. Sakas[1,4], U. Tunn[5]
[1]MedCom GmbH, [2]Synverdis GmbH, [3]Medical Practice for Oncology Königstein, [4]Technical University of Darmstadt, [5]Urology Offenbach

Introduction: Patients with localized and low-grade prostate cancer (PCa) can be treated successfully oncologically with focal therapy (FT). Our approach for FT is photodynamic therapy (FDT) using a third generation photosensitizer Chlorin e6 (Ce6) Trisodiumsalt. The first mandatory step is to carefully localize the tumor, then planning takes place and light electrodes are placed around the CA-cite(s). The used Chlorin-derivative shows enrichment in tumour cells and can be excited with visible blue light to fluorescence. Under red light, however Chlorin interacts with the surrounding molecular oxygen, which is excited to its singlet state becoming thereby highly reactive and cell phototoxic. Due to the selective localization of the substance within tumour cells, the cells are destroyed within 24 to 48 hours.

Methods: The photosensitizer is applied intravenously three hours before treatment. Cancer localization, treatment planning, and electrodes placement are performed by means of BiopSee® (MedCom GmbH, Germany). Mp-MRI data and U/S fusion and specific algorithms are used for supporting these tasks. Using the template-grid and under ultrasound guidance, flexible needles (routinely used for prostate brachytherapy) are positioned in and/or around the tumour-area (Fig 1). Chlorin shows high enrichment in neoplastic tissue and fluorescence under blue light, the fluorescence signal level indicates the concentration of the photosensitizer in the tissue. During the validation stage, optical fibres are inserted through said needles and then blue light is applied, which creates a fluorescence signal measured with a spectrometer. Thus, on one hand, the concentration of Chlorin can be controlled, and on the other hand a fine-tuning of the electrodes positioning can be performed, if necessary. After the final adjustment of the needles, optical fibres with cylindrical light diffusors each with 4 cm length are positioned inside them. By means of a diode laser with an emission wavelength of 665nm, the tissue is illuminated with a power density of 200 mW/cm applicator length. As reference, the fluorescence was measured in a control biopsy hole. After ca. 12 minutes the treatment ends with a local energy dose of 150 J/cm applicator length.

Results: By BiopSee®'s stereotactic approach for localization of tumour, grid-guided needle implantation under live U/S control, as well as by the blue-light verification prior to treatment, we ensure the correct position of the fibres and confirm that the treatment is localized in the target area. 8 patients with highly localized PCa refusing standard therapies or active surveillance (AS) were treated with tissue-targeted PDT using Ce6 as photosensitizer. We observe practically no fluorescence in the normal prostatic tissue and a strong signal in the area of the tumour (Fig 2): the fluorescence lever ratio between normal and tumour tissue was about 1:16. Maximum treatment time under general anaesthesia was 1 hour. All patients were treated on an outpatient basis without complications. Within the present observation period of half a year, all patients maintained their levels of genito-urinary function compared to their pre-treatment status. During follow up, the PSA level and the tumour size is monitored according to the guidelines. First results show an increase of PSA directly after the treatment, followed by a decrease to normal. A concluding evaluation cannot be made yet due to a too small number of cases and an intermediate data status.

Conclusion: We regard our approach of Ce6 tumour-tissue-targeted PDT and stereotactic guided fibre implantation therapy under MRI-U/S fusion to be a feasible alternative for patients who refuse standard treatments or AS, for patients with low risk localized cancer or for patients with no other treatment options. It is planned to perform a clinical trial under this set-up.

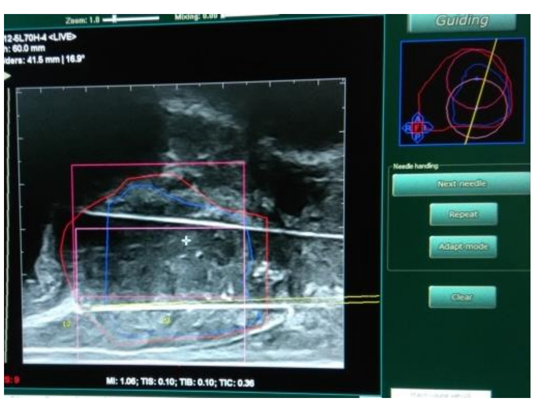

Figure 1: Photodynamic fibers with BiopSee®

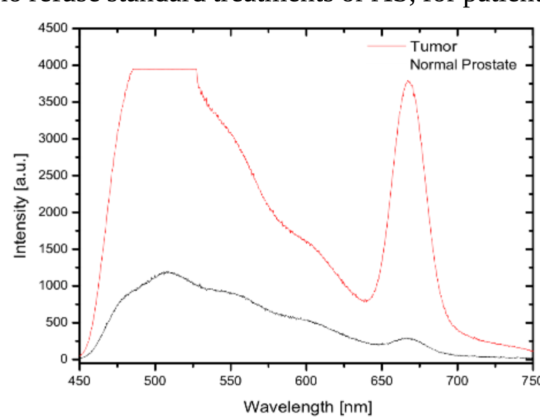

Figure2: Fluorescence signal in tumor and normal tissue

ABSTRACT 21

DYNAMICS OF FOLEY CATHETER INSERTION: A CADAVER STUDY

Xiaoyin Ling[1], Michael B. Tradewell[2], Amer Safdari[2], Robert M. Sweet[3], Timothy M. Kowalewski[1]

University of Minnesota, Department of Mechanical Engineering[1], Biomedical Engineering[2]
University of Washington, Department of Urology[3]

Introduction: Catheter associated urinary tract infection (CAUTI) is among the most common non-payment hospital acquired conditions. Foley catheter placement has been shown to impact CAUTI rates [PMID20156062]. Notably, inexperienced healthcare providers such as medical students are associated with a 4-fold higher CAUTI rate [PMID30145285]. Little is known about the mechanical dynamics of urinary catheter insertion. Our objective is to characterize the mechanics of Foley catheter insertion to aid the creation of accurate training modules and simulators.

Methods: The mechanics of Foley catheter insertion were characterized with n = 8 unfixed male cadavers (access through University of Minnesota Medical School Anatomy Bequest Program) and n = 4 simulators. 16f Foley catheters were attempted across all 8 donors. A 16f Coude catheter was used when the Foley was unsuccessful due to prostatic obstruction. Custom designed instrumentation, with a calibrated ± 2 mN accuracy, was used to measure the insertion force [Fig. 1]. OpenCV ArUco markers were used to capture the 3D insertion motion with a GoPro camera.

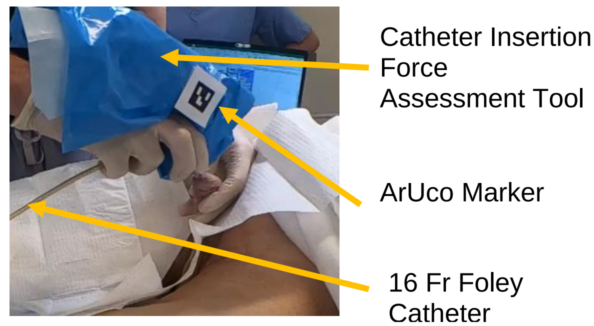

Figure 1: Device and motion tracking marker used during cadaveric procedure.

Results: Out of the 8 donors, only 5 yielded successful catheterizations; all simulator insertions were successful. Greater insertion forces were observed in the simulators. Insertions in the prostate region were also correlated with higher force compared to the distal urethra [Fig. 2]. Both results were statistically significant. Additionally, procedure times were found to be longer for simulator catheterizations (75s mean for simulators, 35s for donors) although this was not statistically significant.

Conclusion: The coupled force measurements and computer vision motion capture gives a first-of-its-kind full mechanic assessment of urinary catheter insertion. With future efforts, we plan to replicate this work in living patients to compare to these cadaveric results and to inform the creation of accurate training modules and simulators.

Acknowledgement: The authors wish to thank the individuals who donated their bodies to the University of Minnesota's Anatomy Bequest Program for the advancement of education and research.

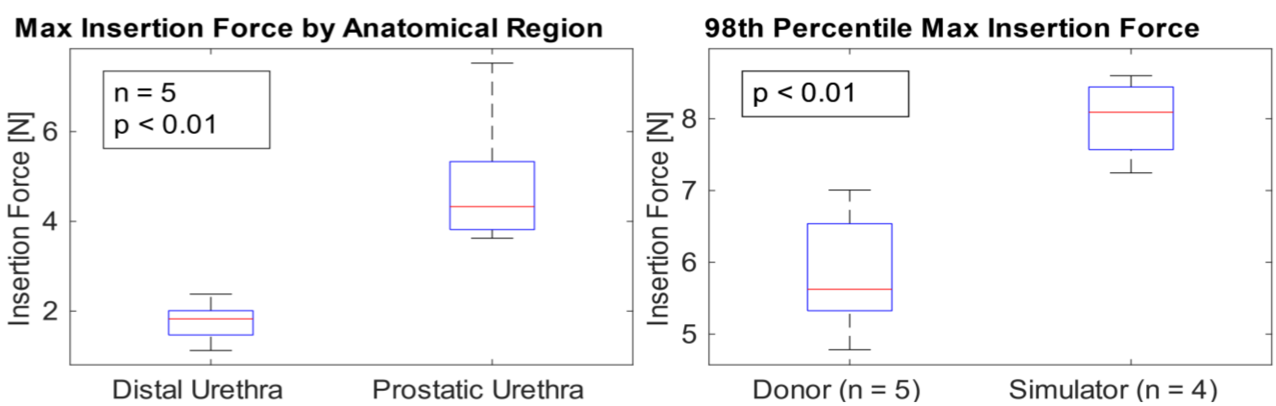

Figure 2: Summary statistics of donor and simulator experiments.

ABSTRACT 22

REAL-TIME WOUND AREA TRACKING AND 3D-MORPHOLOGICAL EDGE DETECTION

Y.M. Zhao[1], Edward H. Currie[1], S. Mohammadi Sedaghat[1], L. Kavoussi[2], Sina Y. Rabbany[1]

[1]DeMatteis School of Engineering and Applied Science, Hofstra University, Hempstead, New York
[2]Department of Urology, Long Island Jewish Medical Centre

Introduction: Great interest has arisen in using robotic technology to improve surgical outcomes. Robotic systems have the potential to overcome inherent limitations of humans and offer substantial advantages to patients including reduction in surgery time as well as decrease technical errors that lead to variability. Our group has undertaken the challenge of developing a wound closure system. One of the initial steps is to allow accurate assessment of wound surface geometry. Recently, non-contact wound measurement methods employing ultrasonic and optical technologies are under development. However, most of these methods require complicated hardware, high-speed processing capabilities and complex architecture, leading to high costs and low adaptability. We present a vision system employing a stereo camera shown in Figure 1(a) to detect a 3D wound edge and implement a topological calculation to define the wound area.

Methods: 2D wound edge detection was performed on an image from the stereo camera. To guide the robotic arm to perform the tasks associated with wound closure, the robotic control system required the 3D topology of the wound edge, i.e., position and orientation. This was obtained by mapping the 2D wound edge to the point cloud generated from the stereo camera. The estimated 3D wound edge was determined by the minimum signed distance of the points in the 3D point cloud space to the expectation surface. The process of finding the 3D edge is summarised in Figure 1 (b). To verify the proposed method, a circular area was tested. The circumference is referred to as ground truth of wound edge.

Results: The average error (AE) with standard deviation (σ) in X, Y and Z direction were 0.51 (1.16), 0.65 (0.52), and 1.95 (2.06), respectively. The maximum error of the normal direction (MEND) along the circumference was 1.2º. This result is important for wound closure applications because the closure fixture position relative to the wound edge on wound surface determines the quality of wound closure. The point clouds of different wound models were compared with scans using a Faro laser scanner.

Conclusion: A method for defining a 3D wound edge is proposed, which can accurately extract detailed information from a noisy environment. This allows tracking even in the presence of wound movement.

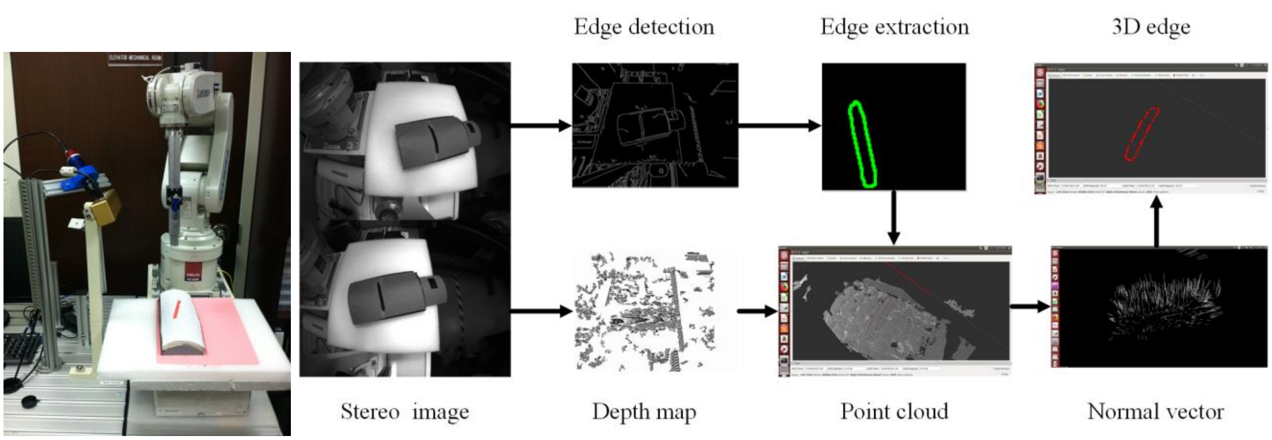

(a) (b)

Figure 1: (a) System configuration; (b) 3D edge and topological information, e.g., normal, of wound area can be obtained by mapping the 2D edge to the wound surface point cloud

ABSTRACT 23

EXTRAPERITONEAL SINGLE PORT ROBOTIC RADICAL PROSTATECTOMY: CLINICAL EXPERIENCE WITH THE FIRST 10 CASES

Rair Valero[1] , Guilherme V. Sawczyn[1], Juan Garisto[1] , Jihad Kaouk[1]

Glickman Urological and Kidney Institute, Cleveland Clinic, Cleveland, OH, USA

Introduction: Robotic surgery is increasingly used in Urology especially to treat prostate cancer. Robotic platforms have evolved and the recent introduction of the SP da Vinci Surgical System as a purpose-built device for single port surgery gave a new options for minimally invasive surgical approaches. After proving the feasibility of the SP platform for trans-peritoneal radical prostatectomy [1], we performed the extra-peritoneal approach to offer our patients potential additional value of a small single incision, no Trendelenburg positioning during surgery, no additional lateral ports, no drain and in most cases outpatient same day discharge). The aim of this presentation is to demonstrate the feasibility and evaluate peri-operative data of our first 10 cases experience**.**

Methods: Data from the first 10 consecutive cases (no selected patients) was collected during February 2019. Surgeries were performed by a single surgeon using the da Vinci SP Surgical System (Intuitive Surgical, Sunnyvale, CA); a 3 cm incision one fingerbreadth below the umbilicus was done, dissection of the extra-peritoneal space was achieved using a kidney shape space-maker balloon (Covidien, Dublin, Ireland) which was placed through the infraumbilical incision caudally reaching the retropubic space. Thereafter a GelPOINT Mini advanced access platform (Applied Medical, Rancho Santa Margarita, CA) was inserted and a dedicated 25-mm multichannel port and a 12-mm accessory laparoscopic port were placed through the gel cap, and the robot was docked. Robotics instruments were introduced and the procedure was done replicating the technique previously described for multi-arms platforms or trans-peritoneal single port prostatectomy[1].

Results: Surgeries were all completed without conversion. Mean age, BMI, was 62.3±6.4; 30.01±5.73 respectively. Six patients were classified preoperatively as high or very high risk according with the NCCN risk classification. Mean total operative time was 204.5±44.6 minutes with a mean console time 149.9±27.3. Average Blood loss was 143cc. No complications were recorded. Patients were discharged either the same day or the next day after surgery and report minimal pain. No drains were used.

Conclusion: Extra-peritoneal single port radical prostatectomy is feasible and represents a minimally invasive option to treat prostate cancer. Further investigations with larger sample size and comparative studies with multi-arm robotic platforms and standard techniques need to be done.

Demographics and Perioperative Outcomes of Patients that Underwent Exra-peritoneal Single Port Radical Prostatectomy

Case No	Age	BMI (Kg/m²)	Previous abdominal surgery	TOT (min)	EBL (ml)	Pain scale (0-10)*	Clavien Intraop	LOS (days)	pT	Margins	pProstate size
1	65	30.2	none	281	200	2.5	None	1	pT3bN0	Pos	81.4
2	48	23.5	none	198	50	2.7	None	0	pT2N0	Neg	19.7
3	63	31	none	208	100	3.4	None	0	pT3aN0	Neg	47.7
4	58	25.5	none	197	100	2.5	None	1	pT2N0	Pos	33.1
5	59	27.3	none	153	100	3.6	None	0	pT3bN1	Pos	35.3
6	62	29.1	Cholecystectomy Hemicolectomy	190	150	1.2	None	0	NYR	NYR	NYR
7	68	24.6	none	237	150	0	None	0	NYR	NYR	NYR
8	61	38.6	Cholecystectomy	184	100	4.6	None	0	NYR	NYR	NYR
9	69	41.0	Cholecystectomy	260	400	6.7	None	1	NYR	NYR	NYR
10	70	28.9	Laparoscopic liver biopsy	137	80	0	None	1	NYR	NYR	NYR

BMI= Body mass index; TOT= Total operative time; EBL= Estimated blood loss; LOS= Length of stay; pT= pathological report; *= mean, p= pathological

ABSTRACT 24 **TOP 10 ABSTRACT**

DEVELOPMENT OF AN OFFICE BASED LASER ABLATION SYSTEM FOR PROSTATE CANCER

Josh Shubert[1], Yash Kamothi[1], Alan Lee[1], Brittany Berry-Pusey[1], Alan Priester[1,2], Rory Geoghegan[2], Leonard Marks[1,2], Shyam Natarajan[1]

[1] Avenda Health, Inc., Santa Monica, CA
[2] Department of Urology, University of California, Los Angeles

Introduction: Focal therapy of prostate cancer (CaP) involves ablation or removal of an index lesion, while minimizing impact on healthy tissue. Existing laser-based CaP therapies require concurrent temperature measurement in a Magnetic Resonance Imaging (MRI) suite. These methods of treatment are expensive and impractical for routine urological use. We sought to develop an ultrasound-guided, office-based laser ablation system, previously tested in prototype form in 10 patients (PMID28396184), which monitored treatment with interstitial thermal sensors. We report on initial benchtop results using an integrated system with multiple thermal sensors integrated into a single needle.

Methods: An office-based laser ablation system was developed, consisting of a PC workstation, a 25W 980nm diode laser, peristaltic pump, and touchscreen monitor (Fig 1). Laser ablation was performed using a saline-cooled diffusing fiber integrated inside of a 14Ga stainless steel needle with optical window. Ablations were monitored using a sensor needle consisting of eight thermocouples, spaced 4mm apart. The laser delivery catheter and sensor probe were inserted in parallel into *ex vivo* bovine tissue with an 8mm offset, and saline actively cooled the tissue prior to laser activation. Four trials were conducted.

Table 1. Laser parameters and results

Trial	Parameters	Starting Temp	Max Temp	Treatment zone
1	10W/6min	29°C	58°C	17.9 x 19.7 mm
2	12W/3min	29.6°C	61.6°C	15 x 15 mm
3	12W/3min	35.4°C	64.7°C	12 x 10 mm
4	13.7W/3min	24.3°C	36.5°C	17.6 x 16.5 mm

Results: Sensor data were successfully collected during ablation tests (Table 1). The maximum ablation size was achieved using a 10W, 6-minute ablation, resulting in an ellipsoidal treated area of 17.9 x 19.7 mm (Fig 2), compared to a treatment zone of 16mm x 21mm in a clinical study (PMID28396184).

Conclusion: Multi-element thermocouple monitoring of laser hyperthermia is feasible, with treatment zones were similar to measured effect in a previous clinical study which used multiple, single element sensor needles . Future work includes optimization of laser parameters and clinical testing in an IDE study.

Acknowledgements: This work was supported by the NCI/NIH (R01CA218547) and Avenda Health Inc.

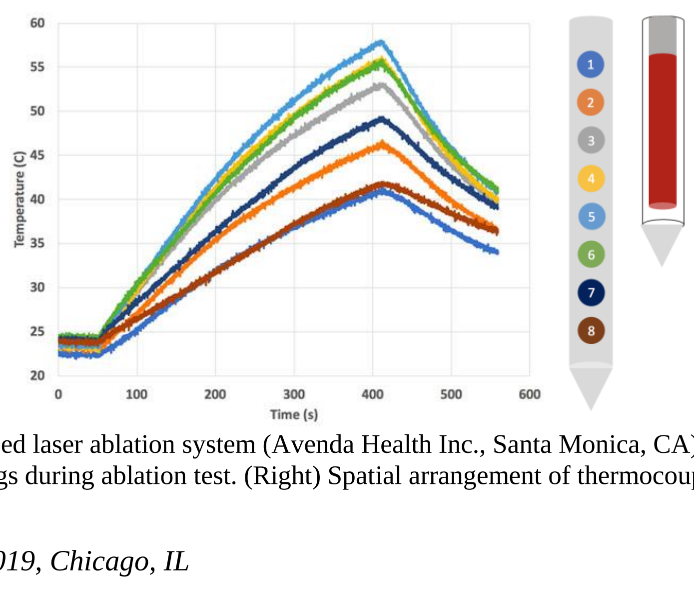

Figure 1: Office-based laser ablation system (Avenda Health Inc., Santa Monica, CA).
Figure 2: (Left) Thermal readings during ablation test. (Right) Spatial arrangement of thermocouple elements.

ABSTRACT 25

ROBOTIC RECTOVESICAL FISTULA REPAIR AFTER ROBOTIC ASSISTED RADICAL PROSTATECTOMY FOR PROSTATE CANCER

Surcel C[1,2] , Mirvald C[1,2], Najjar S[3], Mihai V[3], Dugan M[1], Vlaicu A[1], Dermengiu A[3], Labanaris A[4]

[1] Centre of Uronephrology and Renal Transplantation, Fundeni Clinical Institute, Bucharest, Romania.
[2] "Carol Davila" University of Medicine and Pharmacy, Bucharest, Romania.
[3] Robotic Urological Center, Monza Hospital, Bucharest, Romania
[4] Interbalkan Medical Center, Thessaloniki , Greece

Introduction: Rectovesical Fistula (RVF) represents a rare complication following radical prostatectomy for prostate cancer. Previous TUR-P and the use of Hem-o-Lock sutures are considered as risk factors. Despite different techniques described in the literature, there is still no standard treatment. We present the case of a 68-year-old patient with previous history of TUR-P for BPH, who underwent robotic radical prostatectomy for locally advanced prostate adenocarcinoma.

Methods: The non-nerve sparing robotic prostatectomy was uneventful. Hem-o-Lock suture were used during neurovascular dissection. At 30 days postoperative, the patient presented at the hospital with faecaluria. Cystoscopy revealed a 1.5 cm trigonal fistula near the left ureteric orifice with patent urethrovesical anastomosis. Rectoscopy confirmed the presence of the fistula at ~ 10 cm from the anal sphincter. Conservative management consisting of urinary diversion with a 20Ch bladder catheter, diversion ileostomy, broad-spectrum antibiotics and parenteral nutrition was initially attempted. Rectoscopy and cystoscopy 2 months postop revealed a persistent rectovesical fistula. Robotic assisted fistuloraphy was performed with closing of the rectal lesion with a running PDS 3-0 double-layer suture. A muscle flap from the left levator ani was put between bladder and rectum. Due to the proximity of the fistula to the urethrovesical anastomosis, we dissected the bladder anteriorly and performed a redo urethrovesical anastomosis after exsion of the bladder fistula.

Results: Operative time was 240 min and blood loss 160ml. Hospital stay was 7 days. Urethrovesical catheter was removed after 1 month following a normal cystography. Bowel continuity was restored 2 months later following normal cystoscopy and rectoscopy.

Conclusion: Rectovesical fistula following prostatectomy is a feared complication that requires a complex, multimodal approach. Robotic repair is feasible and represents an attractive alternative to the open approaches.

Fig.1 Intraoperative aspect of recto-vesical fistula

ABSTRACT 26

TECHNOLOGICAL ADVANCEMENTS IN LARGE PROSTATE ENDOSCOPIC SURGERY PUT TO THE TEST OF TIME – AN EVIDENCE-BASED, LONG-TERM, PROSPECTIVE, RANDOMIZED-CONTROLLED CLINICAL COMPARISON BETWEEN BIPOLAR PLASMA VAPORIZATION, RESECTION AND ENUCLEATION VERSUS OPEN PROSTATECTOMY

Bogdan Geavlete[1], Cristian Moldoveanu[1], Cosmin Ene[1], Catalin Bulai[1], Georgiana Balan[1], Andrei Ene[1], Marin Bloju[1], Petrisor Geavlete[1]

[1]"Saint John" Emergency Clinical Hospital, Department of Urology, Bucharest, Romania

Introduction: The study compared the transurethral resection in saline (TURis), transurethral vaporization in saline (TUVis), bipolar plasma enucleation of the prostate (BPEP), and open prostatectomy (OP) in a single-center, long-term, prospective, randomized-controlled clinical setting exclusively involving severe lower urinary tract symptoms' large prostate patients.

Methods: During a 4½ year enrollment period, a total of 320 cases of prostate volume over 80 mL, maximum flow rate (Q_{max}) below 10 mL/second, International Prostate Symptom Score (IPSS) over 19 or urinary retention were prospectively included in the trial and equally randomized in the four study arms. Patients were assessed preoperatively as well as every 6 months during a complete four years' period after surgery by using the IPSS, quality of life (QoL) score, Q_{max}, post-voiding residual urinary volume (PVR) and prostate-specific antigen (PSA) levels as relevant follow-up parameters.

Results: Similar preoperative parameters were established in the four series. The OP and BPEP procedures were characterized by resembling operating times, while TURis and TUVis displayed prolonged surgical durations. The TURis technique resulted in a substantially decreased mean resected tissue weight. The TUVis approach showed the lowest mean hemoglobin level drop, followed by TURis and BPEP (equivalent results) and finally OP (highest bleeding). The OP alternative described the longest mean catheterization period and hospital stay, followed by TURis and afterwards by TUVis and BPEP (similar data). During the 4 years' follow-up period, statistically equivalent IPSS, QoL, Q_{max} and PVR outcomes were established in the OP, BPEP and TURis study arms. The TUVis series displayed significantly smaller long-term Q_{max} improvements but otherwise statistically similar functional features. Significantly lower mean PSA levels were determined secondary to OP and BPEP when compared to bipolar resection and subsequently to vaporization up to the 48 months' postoperative assessment.

Conclusion: The OP and BPEP therapeutic alternatives emphasized the highest prostatic bulk ablation capacity (with prolonged postoperative recovery for open surgery), while the TUVis modality displayed the lowest hemorrhagic risks. On the medium and long term, generally resembling functional outcomes were determined for the four techniques, with significantly decreased mean PSA values secondary to the OP and bipolar enucleation procedures by comparison to transurethral resection/vaporization.

ABSTRACT 27

THE LONG-TERM IMPACT OF NBI TECHNOLOGICAL ADVANCEMENT IN NON-MUSCLE INVASIVE BLADDER CANCER ONCOLOGIC OUTCOME – A FIVE YEARS' PROSPECTIVE, RANDOMIZED-CONTROLLED CLINICAL ANALYSIS ASSESSING THE OPTICALLY ENHANCED DIAGNOSTIC ACCURACY BY COMPARISON TO STANDARD WHITE LIGHT VISUALIZATION

Bogdan Geavlete[1], Cristian Moldoveanu[1], Cosmin Ene[1], Catalin Bulai[1], Georgiana Balan[1], Andrei Ene[1], Marin Bloju[1], Petrisor Geavlete[1]

[1]"Saint John" Emergency Clinical Hospital, Department of Urology, Bucharest, Romania

Introduction: The trial was aimed to determine the impact of narrow band imaging (NBI) guided transurethral resection of bladder tumors (TURBT) in non-muscle invasive bladder cancer (NMIBC) long-term recurrence rates by comparison to the standard white light (WL) cystoscopy and resection.

Methods: During a two years' inclusion period, a total of 190 NMIBC cases were prospectively enrolled and equally randomized in the two series. The 95 patients of the study arm benefitted from both white light and NBI cystoscopy and TURBT, while solely the standard diagnostic and therapeutic approach was applied in the control arm. The inclusion criteria were represented by positive urinary cytology and/or abdominal ultrasound/contrast CT bladder tumors' diagnostic. Chemotherapeutic/BCG instillations were performed in accordance with the NMIBC recurrence and progression EORTC risk tables' classification. The follow-up protocol was extended for a period of five years and included WL and NBI cystoscopy in the study group and only conventional cystoscopy in the control series, also scheduled as resulting from the risk categories. Patients that failed to completely undergo all the follow-up check-ups and those diagnosed with muscle-invasive bladder cancer were excluded from the trial.

Results: In the study arm, the overall NMIBC (96.2% vs. 87.2%) and CIS (100% vs. 66.7%) patients' detection rates were significantly improved for NBI when compared to WL. On a tumors' related basis, NBI cystoscopy emphasized significantly superior detection rates concerning the CIS (95.2% vs. 61.9%), pTa (93.9% vs. 85.2%) and overall NMIBC (94.8% vs. 83.9%) lesions. Additional tumors were diagnosed by NBI in a significant proportion of CIS (55.5% vs. 11.1%), pTa (26.5% vs. 10.2%), pT1 (30% vs. 10%) and overall NMIBC (30.8% vs. 10.3%) patients. The postoperative intravesical instillation treatment was significantly improved due to NBI additional findings leading to risk category modifications (16.7% versus 5.1%). 74 patients in the NBI and 76 in the WL series completed the follow-up protocol. The NBI study arm was characterized by a statistically significant reduction in the cumulated recurrence rates at one (16.2% vs. 28.9%), two (22.9% vs. 39.5%), three (27% vs. 44.7%), four (29.7% vs. 47.4%) and five (30.3% vs. 49.8%) years by comparison to the WL-TURBT group.

Conclusion: The NBI assisted TURBT represents a feasible diagnostic and therapeutic approach in NMIBC patients, bringing a statistically significant improvement in terms of patients' and tumors' detection rates as well as additionally found lesions and superior postoperative instillation treatment. NBI resection and follow-up provided a significant advantage regarding the NMIBC long-term oncologic outcome, as proven by the evidence-based decreases in the one to five years' recurrence rates.

ABSTRACT 28

IN VITRO EVALUATION OF STONE FRAGMENT EVACUATION: URETEROSCOPY SUCKS

Garen Abedi, Douglas Schneider, Renai Yoon, Roshan Patel, Jaime Landman, and Ralph V. Clayman

University of California, Irvine Department of Urology

Introduction: Contemporary flexible stone baskets often are unable to extract sub-millimeter stone fragments at the time of ureteroscopy. Our aim of this in vitro study was to assess the feasibility of suctioning sub-millimeter fragments with a standard luer lock syringe through a flexible ureteroscope.

Methods: Phantom stones made from industrial plaster were mechanically fragmented and passed sequentially through 1mm and 0.5 mm metal sieves. Both sub-1 mm groups and sub-0.5 mm groups were divided in to five trial samples and dry weights were obtained. Each stone group was then mixed in a 400-ml beaker filled with 75 cc of normal saline on a stir plate. A standard 10cc luer lock syringe was connected to a fiber-optic ureteroscope with a 3.6Fr (1.2 mm) working channel. The luer lock syringe was then used to suction stone fragments from the beaker. This was repeated a total of five times for each trial group. The suctioned stone fragments and the stone fragments left behind in the beaker were separated, placed in centrifuge tubes and dried in an incubator set at 37° Celsius for 48 hours after the supernatant solution was removed. Dried weights were then measured and recorded. The percentage of stone fragments suctioned in each group were then compared.

Results: Mean fragment weight for sub-0.5mm and sub-1.0mm stone groups at baseline were 1.105 grams and 0.684 grams respectively. The mean percentage of stone fragments suctioned through the ureteroscope for the sub-0.5mm and sub-1.0mm groups were 86.8% and 88.8% respectively ($p=0.575$). In addition, the amount of stone fragments suctioned was linearly related to starting dry mass and was not related to stone fragment size ($R^2=0.95$). During suctioning, 58.5% of stones in the sub-0.5mm group were trapped in either the working channel of the ureteroscope or within the luer lock syringe compared to 84.4% of stones in the sub-1mm group ($p=0.001$).

Conclusion: It is feasible to suction sub-millimeter stone fragments by connecting a luer lock syringe to a flexible ureteroscope. The limiting factor for removing stone fragments appears to be the working channel of the flexible ureteroscopes, which can cause trapping of stone fragments during suctioning.

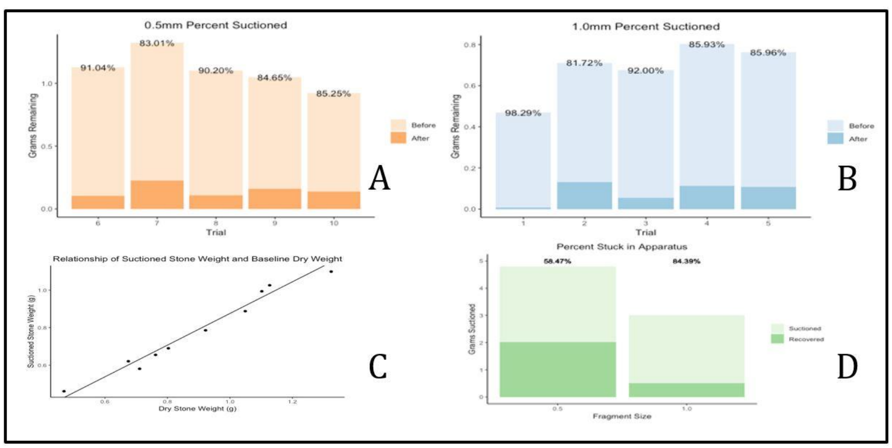

Figure 1: A and B demonstrate percent of stone fragments suctioned in sub-0.5mm and sub-1mm groups respectively. C demonstrates the relationship to stone mass suctioned compared to baseline dry weight. D demonstrates the percentage of stone fragments in each group trapped in either the ureteroscope or the luer lock syringe.

ABSTRACT 29 **TOP 10 ABSTRACT**

REAL-TIME HIGH RESOLUTION DIAGNOSTIC IMAGING FOR PROSTATIC TISSUE WITH EX VIVO FLUORESCENCE CONFOCAL MICROSCOPY: OUR PRELIMINARY EXPERIENCE

Eissa A.[1,2], Puliatti S. [1] , Bertoni L. [3], Bevilacqua L. [1] , Sighinolfi M.C. [1] , Reggiani Bonetti L [4] , Patel V. [5] , Bianchi G. [1] , Micali S. [1] , Rocco B. [1]

[1]Dept. of Urology, University of Modena and Reggio Emilia, Italy, [2]Dept. of Urology, Faculty of Medicine, Tanta University, Egypt, [3]Dept. of Surgical, Medical, Dental and Morphological Sciences with Interest transplant, Oncological and Regenerative Medicine, University of Modena and Reggio Emilia, Italy, [4]Dept. of Pathology, University of Modena and Reggio Emilia, Modena, Italy. [5]Dept. of Urology, Global Robotics Institute, Florida Hospital-Celebration Health Celebration, Florida, USA.

Introduction: Prostate cancer "real time" intra-operative pathological examination is the corner stone for ensuring cancer free surgical margin; however, it still utilizes frozen section, despite the many inherent limitations of this procedure [PMID27257084, PMID22591631]. The aim of this study is to determine the diagnostic accuracy of fluorescence confocal microscopy (FCM) for non-neoplastic and cancerous prostate tissue compared to the gold standard histopathological diagnoses. Moreover, we aimed to determine the level of agreement for the identification of typical malignancy features at fluorescence confocal microscopy and histopathological evaluation.

Methods: 89 specimens from 13 consecutive patients with clinically localized prostate cancer were evaluated. All patients underwent RARP with fresh prostatic tissue biopsies taken at the end of each intervention, using an 18 Gauge biopsy punch. The FCM VivaScope® 2500M-G4 (Mavig GmbH, Munich, Germany; Caliber I.D.; Rochester NY, USA) is an optical technology that depends on two different types of lasers (785 nm, and 488 nm) to provide optical microscopic images of freshly excised tissues based on two different modalities; the reflectance mode (different refractive indices of subcellular structures) and the fluorescence mode (using fluorescent agents to increase the contrast within the epithelium-stroma). The FCM is characterized by vertical resolution of 4 µm, maximum penetration depth of 200 µm, total scan area of 25 x 25 mm, and 550X magnification power. Furthermore, the microscope is equipped with a 38X water immersion objective with numerical aperture of 0.85 [http://www.vivascope.de].

Specimens were randomly assigned to 3 collaborating pathologists for evaluation using fluorescence confocal microscopy, as well as for histopathological examination.

Results: Overall agreement between FCM and histopathological diagnoses was substantial with 91% correct diagnosis ($\kappa = 0.75$) and an area under the curve (AUC) of 0.884 (95% CI 0.840 – 0.920), 83.33% sensitivity and 93.53% specificity. The level of agreement for the identification of typical malignancy features (i.e. infiltrative pattern of glandular growth, $\kappa = 0.83$ and AUC = 0.891) was accurate as well.

Conclusion: FCM seems to be a promising tool for enhanced specimens' reporting performance, given its simple application and very rapid microscopic image generation (less than 5 min per specimen).

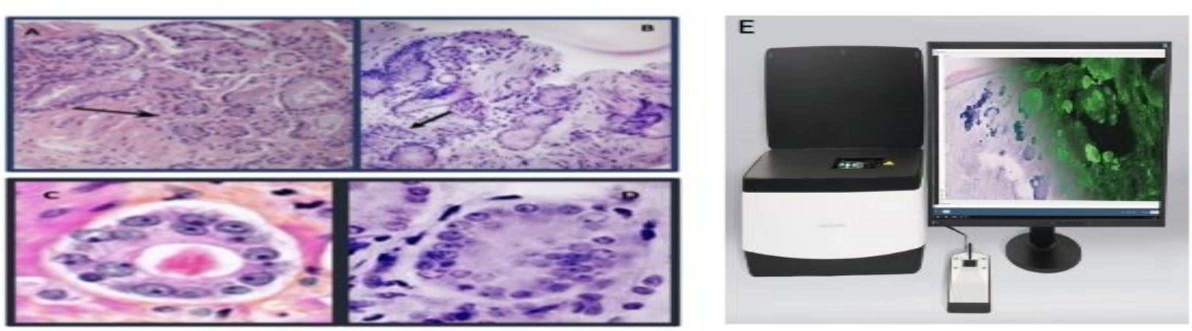

Figure: Atypical architecture in neoplastic glands. Comparison between traditional H&E staining (A) and confocal digital image technology (B). Nuclear atypia in neoplastic prostatic glands. Comparison between traditional H&E staining (C) and confocal digital image technology (D). The Ex-vivo Fluorescence confocal microscopr (E)

ABSTRACT 30

MULTI-TUMOR SILICONE PARTIAL NEPHRECTOMY MODELS FOR ROBOTIC-ASSISTED LAPAROSCOPIC PARTIAL NEPHRECTOMY TRAINING

Charles H. Schlaepfer[1], Steven M. Monda[1,2], James H. L. Thu[1], Michael Glamore[1], R. Sherburne Figenshau[1]

[1]Division of Urologic Surgery, Washington University in St. Louis, St. Louis MO
[2]Saint Louis University School of Medicine, St. Louis MO

Introduction: Robotic-assisted partial nephrectomy (RAPN) is technically challenging. The goal is to completely resect the renal mass and maximally preserve the function of the remaining kidney tissue. Training aids to help residents learn these skills have varied from *in vivo* animal models to computer simulations to synthetic models. We have previously demonstrated construct, conduct, and face validity in a one-tumor silicone partial nephrectomy model using a 4 cm hilar mass, nephrometry score of 7 [PMC5938177]. We now present a three-tumor model. By increasing the tumor diversity within our original silicone model, we increase the cost-efficiency of our model as well as varying difficulties for trainee surgeons.

Methods: We identified three candidate renal masses from patients that underwent partial nephrectomy at our institution. 3D rendering of CT data was created for prior intraoperative display [EUS 2018, pg. 61]. Tumors were combined into a single kidney and 3D printed blanks were printed to create silicone molds. Sequential molding was used to create kidney models with three tumors. The tumors varied in size, location, shape, and the degree of endophicity. R.E.N.A.L. nephrometry scores were calculated for each tumor in the model. The models are currently being incorporated into resident training sessions on the daVinci robotic surgery system.

Results: The models have 3 distinct tumors for that vary in color and texture from the model parenchyma tissue. Tumor diameters are 2.7, 3.6, and 5.6 centimeters. Nephrometry scores are 5, 7, and 7. A senior resident evaluated the models and is incorporating this model into resident training sessions on the da Vinci robotic surgical system.

Conclusion: We successfully created 3D renderings of three renal tumors and combined them into a single silicone model. To our knowledge, this is the first time a silicone model with more than one tumor will be used as a training model for RAPN and compliments prior work with a single-tumor model. We plan to perform a more comprehensive evaluation of this cost-effective model for simulation of RAPN for urological surgery resident training.

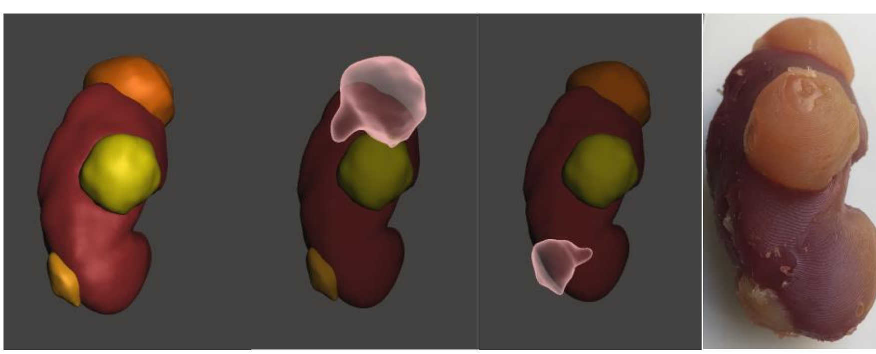

Figure 1: 3D model with three tumors, anterior-posterior view

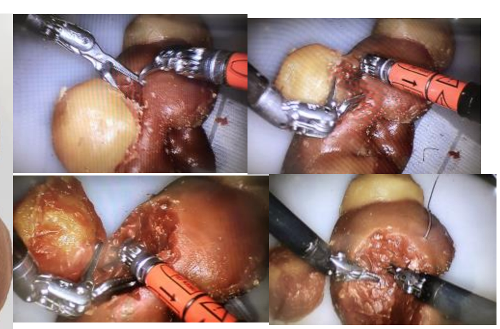

Figure 2: Example of robotic excision of medial, hilar tumor and suturing the silicone.

ABSTRACT 31

NOVEL RENAL COLLECTING SYSTEM MODEL FOR PROCEDURAL TRAINING UNDER ULTRASOUND GUIDANCE

Tareq Aro[1,2], Sunghwan Lim[1], Doru Petrisor[1], Kevin Koo[2], Brian Matlaga[2], Dan Stoianovici[1,2]

[1]Robotics Laboratory, [2]Department of Urology, Johns Hopkins University

Introduction: In recent years, there has been increasing interest in the use of ultrasound guidance for endoscopic and percutaneous procedures. Existing training models for renal collecting system imaging and percutaneous access are limited to other imaging modalities. Models are normally made of rubber-like materials that attenuate sound waves and cannot be imaged under ultrasound, or alternatively are crafted of fresh animal organs and tissues, which limits widespread utilization. We created a reproducible method for manufacturing an ultrasound-compatible collecting system model.

Methods: A computer tomography urography was used in 3DSlicer software [1] to segment the left kidney's collecting system and the overlying skin contour and stored in stereolithography (STL) format, CREO (PTC, Needham, MA) was used to create a containment box around the skin contour and a shaft connecting the collecting system while preserving the 3D orientation (Fig 1). MakerBot Replicator 2X (MakerBot Industries®) was used to 3D print the containment box (Fig 1), a special Makerbot dissolvable filament was used to print the collecting system connected to the designed shaft (Fig 1). Gelatin was made, using formula of blooming gel:glycerin:sorbitol:water (300:300:200:2500g) at 55°C, and poured into the box. Subsequently the mixture was cooled at room temperature overnight. D-Limonene solution was continuously irrigated using a Peristaltic Liquid Pump, resulting in complete dissolution of the collecting system filament in less than 2 days. The gelatin was extracted from the container and the collecting system was filled with water. The model was imaged with ultrasound to assess echogenicity and suitability for simulating ultrasound-guided procedures.

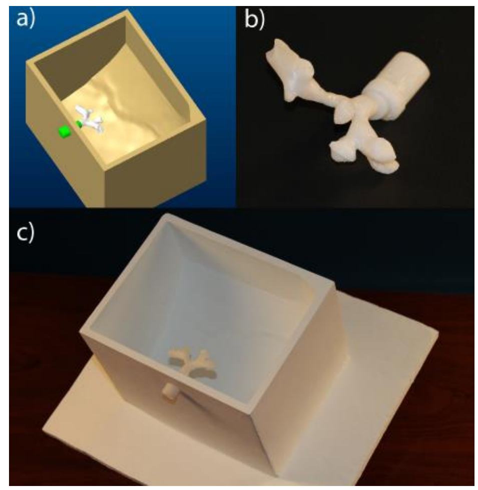

Figure 1: a) PTC-CREO containment box with collecting system shaft. B) collecting system printed with dissolvable filament. C) final printed collecting system and containment box

Results: The D-Limonene solution did not dissolve any of the gel elements, resulting in a clear shape of the collecting system observed inside the gel structure (Fig 2). Structural integrity was preserved, and there were no observable manufacturing marks or separation seams. Ultrasound images of the model demonstrated clear differentiation at the gelatin-water interface (Fig 2). A mock stone and needle were inserted into the collecting system to simulate percutaneous needle access, and both were visible under ultrasound.

Conclusion: We developed a novel method of creating a renal collecting system model suitable for ultrasound-guided percutaneous access. This model can enhance training and simulation under ultrasound guidance.

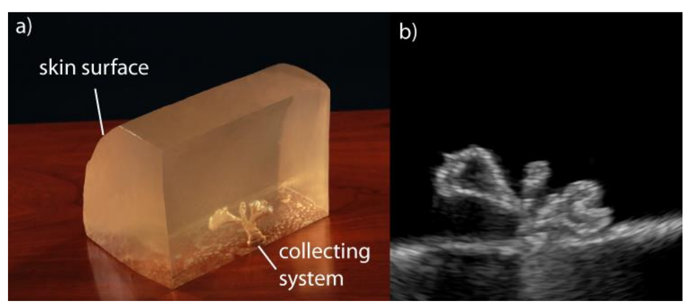

Figure 2: a) Gelatin based mockup, b) Ultrasound image of the water filled collecting system in the mockup

ABSTRACT 32

"OPERATOR DUTY-CYCLE": ANALYSIS OF LASER ACTIVATION PATTERNS DURING HOLMIUM LITHOTRIPSY

Ali H. Aldoukhi[1], Timothy L. Hall[2], Khurshid R. Ghani[1], John M. Hollingsworth[1], Sapan N. Ambani[1], Casey A. Dauw[1], William W. Roberts[1,2]

[1] Department of Urology, University of Michigan, Ann Arbor, MI, USA.
[2] Department of Biomedical Engineering, University of Michigan, Ann Arbor, MI, USA

Introduction: Use of higher power settings for laser lithotripsy incurs an increased risk of thermal injury. Previous work has shown that thermal toxicity can occur in as little as 10 seconds with continuous laser activation at 40 W settings with low irrigation rates. In previous studies temperature was measured during 1-minute of continuous laser activation. Although this is not representative of clinical treatment, patterns of laser activation during ureteroscopy have not been rigorously studied. Determining "operator duty-cycle" – the ratio of laser time to total time in a given period - is necessary to properly estimate thermal dose and develop mitigation strategies. In this current study, we sought to measure operator duty-cycle during clinical ureteroscopy cases.

Methods: Laser logs (pulse energy, pulse frequency, and timing of pedal activation) from de-identified ureteroscopic procedures performed by five endourologists at an ambulatory center (June-August 2018) were downloaded (pulse 120; Lumenis, CA) for evaluation. Cases with total lasing time > 3 minutes were included in this analysis. A customized Matlab algorithm was used to plot the rolling 1-minute average power for each case. From this data, the operator duty-cycle during the 1-minute period of greatest power was calculated.

Results: 31 cases met criteria with total lasing time between 3.2 and 23.9 minutes and 94% of cases < 8.2 minutes. Operator duty-cycle (during the 1-minute of greatest energy delivery for each case) averaged 72% (range 42-100%). The average laser power applied during this 1-minute was 24.7W (range 5.2-54.4W). A representative tracing of power applied over a rolling 1-minute average is shown in Figure 1.

Conclusion: In this study the operator duty-cycle during the 1 minute of greatest energy delivery was 72% - which is greater than anticipated. This data also indicates that in certain clinical cases very high 1-minute average power was applied, increasing the risk of thermal toxicity and reinforcing the rationale to develop robust measures to control thermal dose. Additional data is needed to confirm these findings and determine variability of operator duty cycle at other centers. Future research is planned to determine the necessary irrigation rate needed to manage heat produced from high power laser settings applied at high operator duty-cycle.

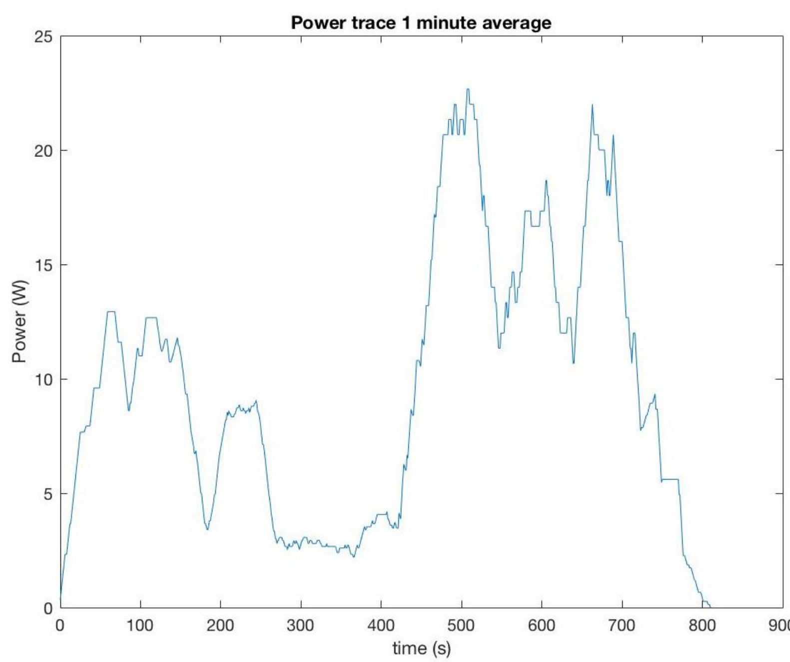

Figure 1: A representative plot of 1-minute interval average laser power applied during a clinical ureteroscopy case.

ABSTRACT 33

IMAGE CORRECTION FOR RIGID CYSTOSCOPY

Sunghwan Lim[1,2], Tareq Aro[1,2], Kevin Koo[2], Doru Petrisor[1,2], Brian R. Matlaga[2], Dan Stoianovici[1,2]

[1]Robotics Laboratory, [2]Department of Urology, Johns Hopkins University

Introduction: Despite the advancement in flexible cystoscopy, rigid scopes are still widely used for diagnoses and almost exclusively needed for treatments inside the bladder. An angled-scope is commonly used to provide a wide and oblique view, as shown in Fig. 1a. However, these introduce barrel image distortion (Fig. 1c) caused by the lens and a deflected optical axis (Fig. 1d), respectively. The resulting image is a distorted representation of the field of view. We present a software based image correction method.

Methods: A 25° cystoscope optic (Φ4mm, Panoview 8989.33, R. Wolf) was mounted to a linear slide and an 8-by-6 checker board (square size: 2.75mm) was placed in front of the angled-scope, as shown in Fig. 1b. In the first step, the lens image distortion is corrected using a fisheye lens calibration technique (Fig. 1d). In the second step, the deflected optical axis distortion is corrected by estimating and applying a homography matrix (Fig 1e).

Results: After image corrections, the two types of distortions in the scope image have been corrected, as shown in Fig 1d and Fig 1e, respectively.

Conclusion: The proposed image correction approach could avoid the barrel distortion and deflected optical axis problem of the angled-cystoscope. This technique could be applied not only to cystoscopes, but also to any angled-scope. This could potentially result in more accurate image interpretation for diagnosis and treatments. Further studies are required to validate the method.

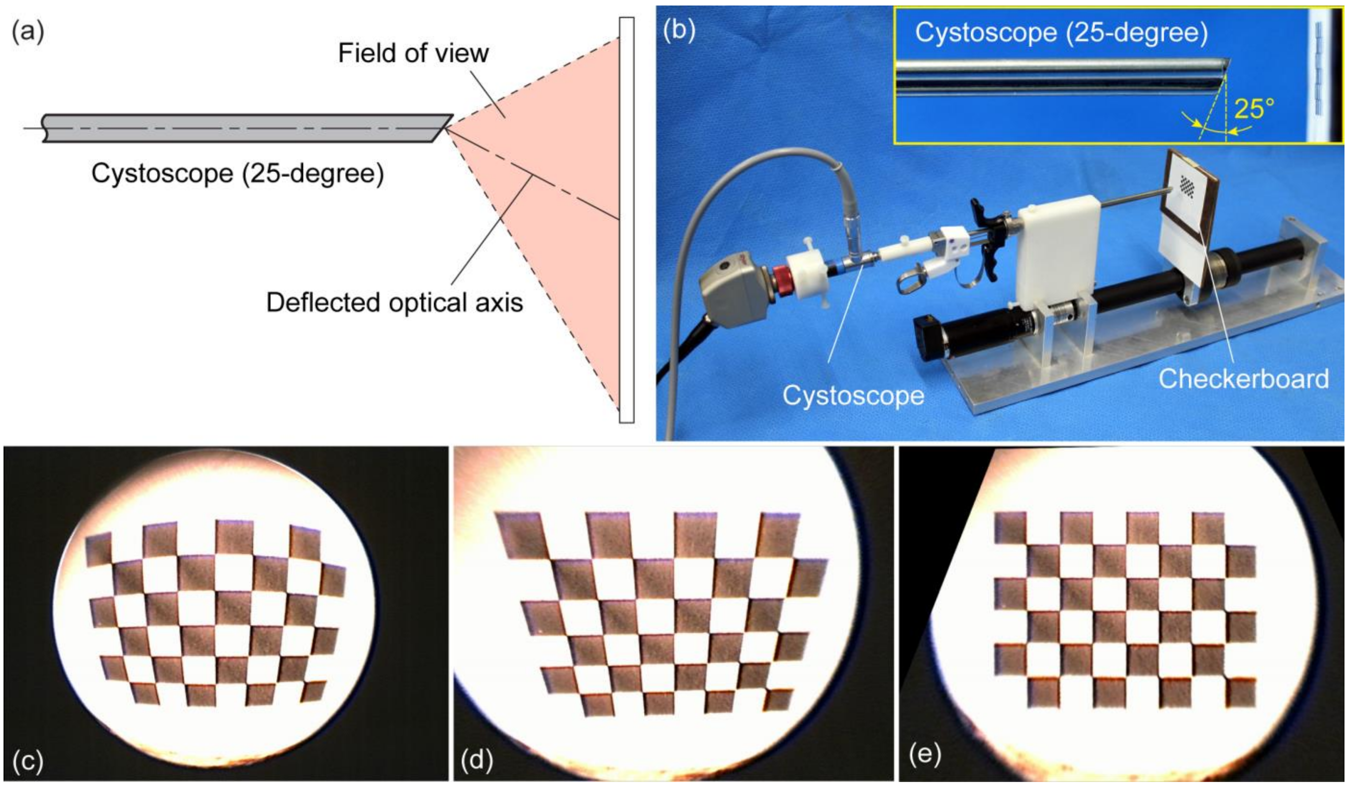

Figure 1: (a) 25° cystoscope image showing field of view and deflected optical axis, (b) Experimental setup, (c) Original image showing barrel distortion; (d) Intermediate image showing deflected optical axis distortion; (e) Corrected image

ABSTRACT 34

THE DEVELOPMENT OF AN AUTOMATED, SELF-SUSTAINING KIDNEY CANCER REGISTRY FROM ELECTRONIC HEALTH RECORDS

Niranjan J. Sathianathen[1], Vidhyalakshmi Ramesh[2], Shawn Grove[1], Makinna C. Oestreich[1], Christopher J. Weight[1]

[1] Department of Urology, University of Minnesota, Minneapolis, MN
[2] Clinical and Translational Science Institute, University of Minnesota, Minneapolis, MN

Introduction: Electronic health records (EHRs) are now mandated for all US healthcare systems. An alluring possibility of digitized health information is the ability to easily collect and analyse data. If data can be extracted in a structured way from episodes of care, we could learn from each patient in real time. We therefore aimed to develop an automated nephrectomy registry for kidney cancer using structured data from EHRs and enriching the dataset with chart review.

Methods: A cohort of patients was identified by using Common Procedural Terminology and International Classification of Diseases codes. A collaborative group of clinicians and Clinical Informatics experts integrated data from sources including EPIC, REDCap, CoPath, billing records, state death indexes, geo coding and natural language processing into a clinical data repository. The registry was built on a protected health information-compliant environment using best practice procedures. Regular manual validation of the data was performed by clinicians. These data were exported to a data shelter in a form which facilitates analysis. The data are refreshed weekly to ensure it is up-to-date.

Results: We created a cohort of 1,562 patients who had undergone a nephrectomy between 2011 and 2018. The registry creation required 80 hours of work from the Clinical Informatics team. We collected data on patient demographics, vital status, comorbidities, laboratory results and pathology. We were able to collect complete data for primary demographic points and vital status. Similarly, we were able to identify at least one comorbidity according to the Charlson Comorbidity Index in 1,245 (79.7%) of patients. Laboratory data extraction was also successful with 1,411 (90.3%) of patients returning a valid serum creatinine value prior to surgery. Pathology results were only obtainable for 1,035 (66.3%) of the cohort. The reliability of such a registry is limited by the coding of patients' surgery and disease indication, as it was apparent during data validation that non-cancer cases (e.g. renal transplant) were included in the cohort.

Conclusion: We have demonstrated the feasibility of creating an automated surgical database, that grows automatically with each episode of clinical care. This automated approach would improve accessibility to high quality, clinical data and facilitate both quality improvement initiatives and clinical research. The reliability of the data can be improved by accurate coding and standardizing clinical documents such as peri-operative notes, discharge summaries and pathology/radiology reports.

ABSTRACT 35

MOSES TECHNOLOGY IN MINIPERC: IN PURSUIT OF TOTAL STONE CLEARANCE.

Gopal Ramdas Tak, Mahesh Desai, Sudharsan S Balaji, Naveen Kumar Reddy M

Muljibhai Patel Urological Hospital, Gujarat, India.

Introduction: Reaching a total stone - free state in the kidney within one treatment episode remains a challenge for conventional miniperc procedures, especially for stones 1 to 2 cm in size. Even with all the newer advancements in PCNL, migration of small fragments produced with laser lithotripsy remains a concern, which may result in incomplete stone clearance. In the pursuit of finding a better method for total stone clearance, here we describe a new technology miniperc with 18Fr ClearPetra sheath and Moses ™(Lumenis INC, Israel) laser fiber technology which promises to disintegrate the stone into fragments and dust, thus helping in total stone clearance.

Methods: This was a prospective study involving 30 consecutive patients who underwent miniperc with ClearPetra 18Fr sheath and Moses laser fiber technology from July 2018 to December 2018. Surgery was performed using a 12Fr nephroscope (Storz/Apple) and the 18Fr sheath with suction and Moses 365 DFL laser fiber technology (Figure 1 & Figure 2). All patients underwent Plain CT KUB within 48 hours of the procedure to assess the stone free status. At 30 day follow up, Plain CT KUB was done only for those patients with residual stones in the immediate post operative period.

Results: The mean age of the group (n = 30; 21 males and 9 females) was 44.6 ± 18.15 years. Mean stone size and volume were 1.35 ± 0.68 cm and 1458.42 ± 322.64 mm^3 respectively. Mean stone density was 1244.54 ± 194.24 HU. 19 patients had middle calyceal puncture and 11 had lower calyceal punctures. The laser setting varied from 0.4-0.8J and 40Hz-80Hz (Mean Total energy: 39.54 ± 23.56KJ). The mean lasing time was 15.47 ± 10.76 min. Exit strategy was DJ stent in 9 patients (30%), tubeless with ureteric catheter in 16 patients (54%) and nephrostomy with ureteric catheter in 5 patients (16%). The mean operative time was 38.55 ± 15.64 min. The mean haemoglobin drop was 0.95 ± 0.20g/dl with no blood transfusion. Postoperatively, two patients had a fever, managed with IV antibiotics. The mean post operative hospital stay was 26.35 ± 2.43 hours. The immediate total stone clearance rate was 80% (24/30) and 30 day stone clearance rate was 100%.

Conclusion: Miniperc with Moses laser fiber technology is an improvised technique of minimally-invasive PCNL with the potential advantage of total stone clearance.

Limitation:
Comparison between traditional mini-PCNL and Moses with Clear Petra sheath; to assess, whether the Moses laser is truly superior or at least non-equivalent, is needed.

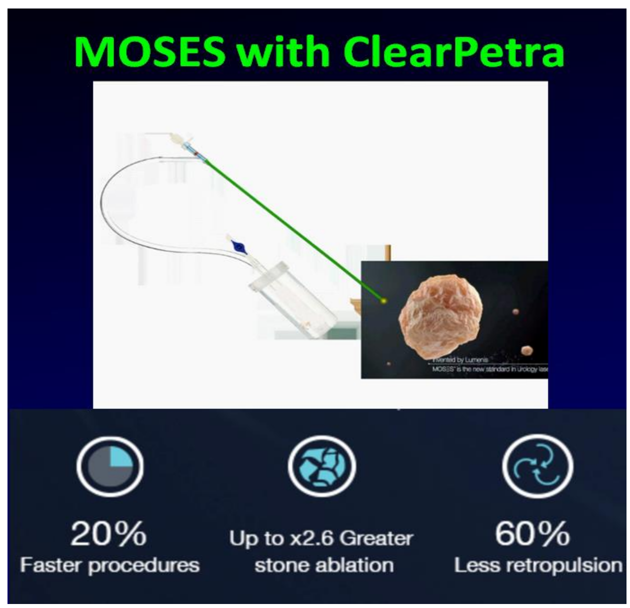

Figure 1

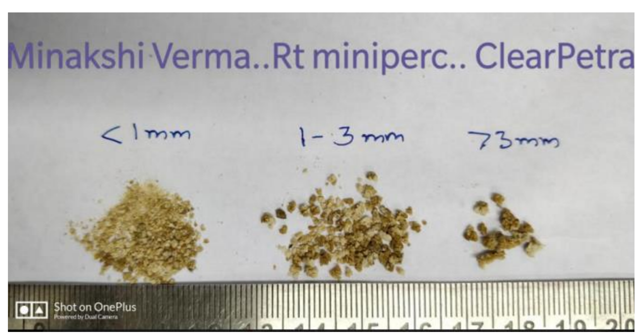

Figure 2

ABSTRACT 36 **BEST ABSTRACT AWARD**

IMPROVING PROSTATE CANCER MARGIN PREDICTION WITH MACHINE LEARNING

Alan Priester[1], Steve Zhou[1,2], Yash Kamothi[1], Joshua Shubert[1], Shyam Natarajan[1]

[1]Avenda Health, Inc., Santa Monica CA
[2]David Geffen School of Medicine, UCLA, Los Angeles CA

Introduction: Magnetic resonance imaging (MRI) underestimates the size and extent of prostate cancer (CaP), necessitating treatment margins during focal therapy (PMC4726648). Uniform margins around the MRI region of interest (ROI) are commonly employed, but even a 10 mm margin may fail in up to 50% of cases (PMC27484386). Targeted prostate biopsy could help improve the accuracy of margin generation. To this end, we simulated biopsies in 113 whole-mount prostatectomy cases, generated biopsy- and MRI- based features, and then trained a machine learning classifier (MLC) to predict areas containing CaP.

Methods: 113 whole mount prostatectomy cases were identified with Gleason Sum ≤ 8 and tumor volumes < 10 CC. Tumors from these cases were modeled in 3D and registered to preoperative MRI. For each case, 50 biopsy procedures were simulated with 12 systematic cores and 3-5 targeted cores for each ROI. Each virtual biopsy core was randomized with respect to 1) location, 2) tracking/registration accuracy, 3) tissue length, and 4) tissue position within the needle's throw. Then, for each simulated biopsy, 1x1x1mm voxels were randomly sampled from the patient's MRI volume, and features were generated relative to the virtual cores (e.g. distance to nearest positive or negative core), the ROI, and T2 MRI intensity/texture. Features were generated for 565,000 voxels (50% CaP, 50% healthy tissue), representing 5650 simulated biopsy procedures. Lastly, various MLCs were trained to predict whether each voxel contained CaP. Five-fold cross validation and L1 regularization were used to generate the MLCs, which were compared against uniform margins and quadrant-based treatment strategies.

Results: Table 1 and Figure 1 summarize MLC performance for CaP detection, and Figure 2 shows an exemplary case. Quadrant-based treatment strategies performed worst, and areas under the curve (AUC) for all MLCs significantly improved upon uniform margins ($p \leq 0.01$, Wilcoxon signed-rank tests). The most predictive features were those associated with negative core location, the proximity/length of positive cores, and Haralick correlation.

	AUC	ACCURACY
Linear Regressor (LR)	0.85 ± 0.05	0.78 ± 0.04
Decision Tree (DT)	0.86 ± 0.04	0.79 ± 0.04
Support Vector Machine (SVM)	0.87 ± 0.05	0.79 ± 0.04
Uniform Margins (UM)	0.79 ± 0.03	0.72 ± 0.01

Table 1: Mean performance of MLCs and uniform margins.

Conclusion: Machine learning classifiers, incorporating MRI and biopsy-derived features, can greatly improve focal treatment margins relative to uniform margins or quadrant-based treatment strategies.

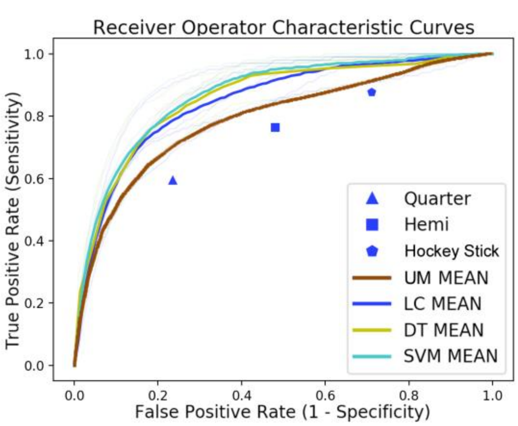

Fig 1: Predictive accuracy of MLCs, uniform margins (UM), and quadrant-based treatments

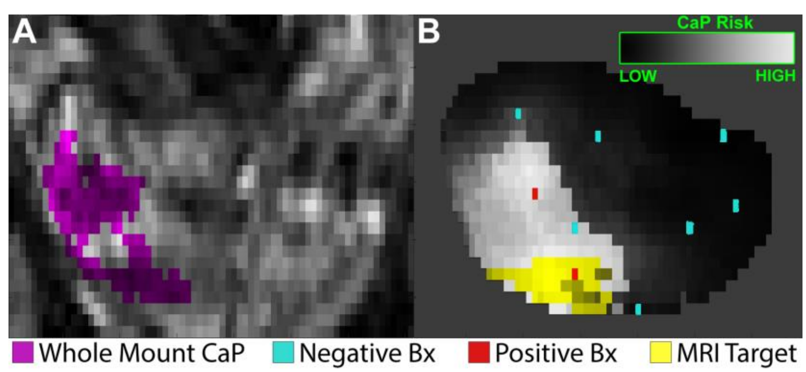

Fig 2: (A) Coronal T2 MRI, and (B) cancer probability map for LC model.

ABSTRACT 37 **TOP 10 ABSTRACT**

A PRECLINICAL TRANSRECTAL BOILING HISTOTRIPSY SYSTEM FOR PROSTATE ABLATION

George R. Schade[1], Tatiana D. Khokhlova[2], Christopher Hunter[3], Wayne Kreider[3], Pavel B. Rosnitskiy[4], Petr V. Yuldashev[4], Oleg A. Sapozhnikov[3,4], Vera A. Khokhlova[3,4]

[1]Department of Urology, [2]Department of Medicine, [3]Center for Industrial and Medical Ultrasound, University of Washington, Seattle, USA
[4]Physics Faculty, M.V. Lomonosov Moscow State University, Moscow, Russia

Introduction: Current clinical transrectal high intensity focused ultrasound (HIFU) systems for prostate ablation have limitations related to their relatively slow heating (100s of ms) and limited real-time monitoring. Boiling histotripsy (BH) is a HIFU method that produces precise mechanical tissue ablation using milliseconds duration (<20 ms) pulses containing shocks delivered at low-duty factor. Owing to the rapidity of tissue bioeffe c ts and the mechanical mechanism of action, BH minimizes heat-sinking and thermal spread that limit thermal treatment, while allowing for real-time ultrasound feedback due to generation of bubbles. Here we present a new preclinical transrectal BH system for prostate ablation.

Methods: A transrectal BH system was designed and constructed comprising a 2 MHz FUS transducer (5.0 x 3.5 cm, focus 4.0 cm) with inline B-mode imaging (Figure A), 1000 W amplifier, function generator, and clinical imaging system. Acoustic output of the system was characterized in water. The ability to produce BH was assessed in polyacrylamide gel (PAC) and agar-embedded chicken breast. BH thresholds were established for 1-10 ms pulses. BH lesions were generated in PAC (1-10 ms pulses) and CB (10 ms pulses) by administering 30 pulses at 1% duty factor.

Results: The system's outputs are presented in Figure B. The system produced peak+ and peak- pressures of 115 MPa and -21 MPa at 413 W acoustic power. Observed BH thresholds required shock amplitudes of 76, 76, 86, and 112 MPa for 10, 5, 2, and 1 ms pulses in PAC and 112 MPa for 10 ms pulses in chicken breast. For all pulse durations, sharply demarcated lesions consistent with BH mechanical ablation were observed in PAC (Figure C) and chicken breast.

Conclusion: We custom-built and acoustically characterized a transrectal BH system for prostate ablation. The system generates outputs capable of BH and produces lesions in PAC and *ex vivo* tissue. Pending experiments will evaluate *ex vivo* and *in vivo* prostate ablation in a canine animal model.

Acknowledgements: **S**upported by NIH R01EB007643, R01EB025187, R21CA219793, and RFBR 17-54-33034.

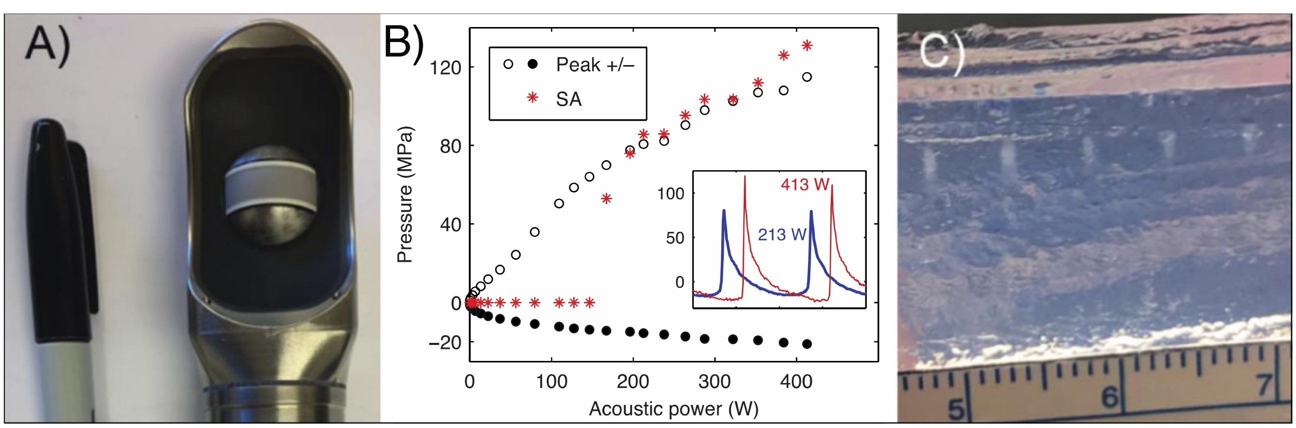

Figure: A) Transrectal FUS transducer, B) Plot of peak pressure values and shock amplitudes (SA), with inset showing waveforms at 213 W and 413 W, and C) appearance of lesions in PAC gel.

ABSTRACT 38 **TOP 10 ABSTRACT**

IMAGE GRADIENT AT KIDNEY-TUMOR BOUNDARIES AS A PREDICTOR OF COMPLEXITY IN NEPHRON SPARING SURGERY

Nicholas Heller[1], Arveen Kalapara[1], Niranjan Sathianathen[1], Edward Walczak[1], Keenan Moore[3], Heather Kaluzniak[2], Joel Rosenberg[1], Paul Blake[1], Zachary Rengel[1], Zachary Edgerton[1], Matthew Peterson[1], Makinna Oestreich[1], Shaneabbas Raza[2], Nikolaos Papanikolopoulos[1], Christopher Weight[1]

[1] University of Minnesota, [2] University of North Dakota, [3] Carleton College

Introduction: The use of cross-sectional imaging to inform the decision between partial and radical nephrectomy for kidney tumors has received considerable attention over the last decade. Notably, the R.E.N.A.L. [1, Pg.844], PADUA [2, Pg.786], and Centrality-Index [3, Pg.1708] scoring systems aim to quantify complexity with evaluations based on tumor size, endophycity, and location. We propose the *boundary hardness* between the kidney and the tumor as a new predictor of partial nephrectomy complexity.

Methods: Retrospective review of 544 patients undergoing nephrectomy for suspected kidney cancer between 2010 and 2018 yielded 326 patients with available CT imaging in the late-arterial phase. We randomly selected 126 who underwent partial nephrectomies and manually segmented the kidneys and tumor. In order to quantify *boundary hardness (S)*, we computed the average absolute Sobel directional derivative orthogonal to the boundary everywhere along the interface between the tumor and kidney tissue.

$$S(I;B) = \frac{\sum_{(i,j,k)\in B}|\nabla I_{i,j,k} \cdot \hat{N}_{i,j,k}|}{|B|} \quad (1)$$

where B is a collection of tuples defining voxel locations lying on the kidney-tumor boundary, $I_{i,j,k}$ is the Hounsfield Unit intensity of the ijkth voxel of the late-arterial phase CT image, and $\hat{N}_{i,j,k}$ is the unit vector normal to the kidney-tumor boundary found by normalizing the gradient of the boundary surface. We compare this metric with the well-established metric of radiographic size as a predictor of readmission following surgery, estimated blood loss, and high-grade complications.

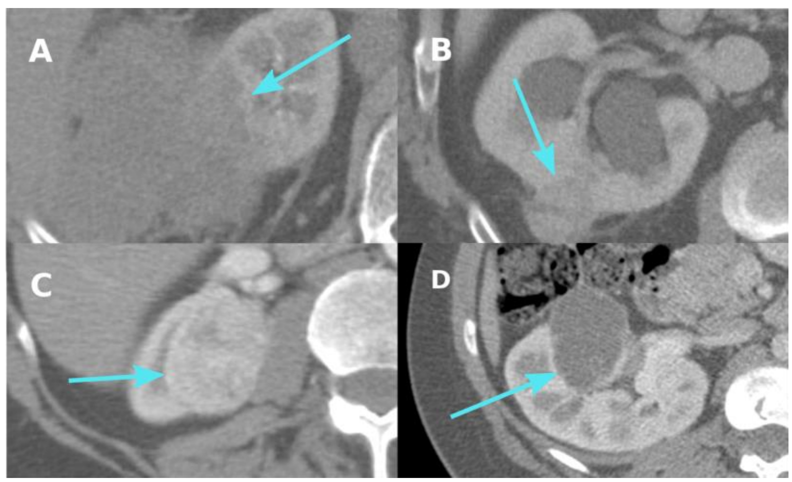

Fig. 1: Four examples of kidneys with varying boundary hardnesses. **A**: *S*=30.77, **B**: *S*=64.38, **C**: *S*=88.49, **D**: *S*=103.8.

Results: ROC analysis and ANOVA showed a significant negative association between boundary hardness (*S*) and high-grade complications (AUC 0.77, $p < 0.01$), much stronger than the positive association with size (AUC 0.48, $p > 0.15$). Univariate regression showed a significant negative association between S and estimated blood loss ($p < 0.01$), but less significant than size ($p < 0.001$). Neither *S* nor size was significantly predictive of readmission (p-values of 0.11 and 0.66 respectively).

Conclusion: Our data suggests that boundary hardness quantified by Eq. (1) is linked to blood loss and complications in nephron sparing surgery, indicating that this marker could play an important role in clinical decision making concerning kidney tumor treatment. This data will be made publicly available mid-March 2019 at kits19.grand-challenge.org as part of the KiTS19 kidney tumor segmentation challenge held in conjunction with the 2019 International Conference on Medical Image Computing and Computer Assisted Intervention (MICCAI). Research reported in this publication was supported by the National Cancer Institute of the National Institutes of Health under Award Number R01CA225435.

ABSTRACT 39

EFFICIENCY OF HOLMIUM LASER LITHOTRIPSY USING A STONE STABILIZATION SUCTION DEVICE

Matthew S Lee[1], Ali H Aldoukhi[1], Timothy L Hall[2], Khurshid R. Ghani[1], William W. Roberts[1,2]

[1] Department of Urology, University of Michigan, Ann Arbor, MI, USA.
[2] Department of Biomedical Engineering, University of Michigan, Ann Arbor, MI, USA

Introduction: Ureteroscopy with laser lithotripsy is one of the most commonly performed procedures for treatment of stones. However, laser lithotripsy efficiency is improved by minimizing the distance between laser fiber and stone. We hypothesize that a prototype to contain and stabilize stones with suction will improve efficiency of laser lithotripsy.

Methods: Surgeons treated a 5mm Begostone (composition 15:5) using preset laser settings of 0.3 J x 50 Hz (120W Holmium laser - P120; Lumenis, Israel). in three experimental conditions for 3.5 min trials. Condition 1: suction stabilization device **with** suction; Condition 2: suction stabilization device **without** suction; Condition 3: calyx model without suction. The suction stabilization prototype measures 1 cm deep and wide, with a 1mm hole at the base that provides 50 ml/min of suction (Figure 1a). The calyx model is in the shape of a round bottom flask with a diameter of 20 mm (Figure 1b). Experiments were carried out in a water tank using a flexible ureteroscope (LithoVue; Boston Scientific, MA) containing a 242 um core laser fiber (Flexiva; Boston Scientific). Surgeons were given three 3.5 min practice runs, one for each condition. Surgeons then completed five trials for each condition. Stone fragments that bounced out of the containment device during trials were counted as untreated fragments. Stone dry weights were compared before and 24 hours after each trial. Fragments were separated using serial sieves (1 mm to 0.25 mm opening). The laser fiber was stripped between each trial run. Two surgeons participated in the study thus far and we aim to accrue data from six surgeons. Statistical comparison was performed using Student T-tests.

Results: Stone mass lost was 80.3%,71.3%, and 64.4% for condition 1-,2,and 3 respectively. Percentage of residual stone fragments that were > 1.0 mm were 17.8%, 25.6%, and 30.6% for conditions 1,2 and 3 respectively (Figure 1b). The differences between conditions 1 and 2 and conditions 1 and 3 were statistically significant for stone mass lost and percentage of residual fragments > 1.0 mm.

Conclusions: Improvement in laser lithotripsy efficiency is seen with stone containment alone and stone containment with suction using a prototype device. Additional data is needed to verify these results and inform additional refinements of the prototype to further enhance improved laser lithotripsy efficiency.

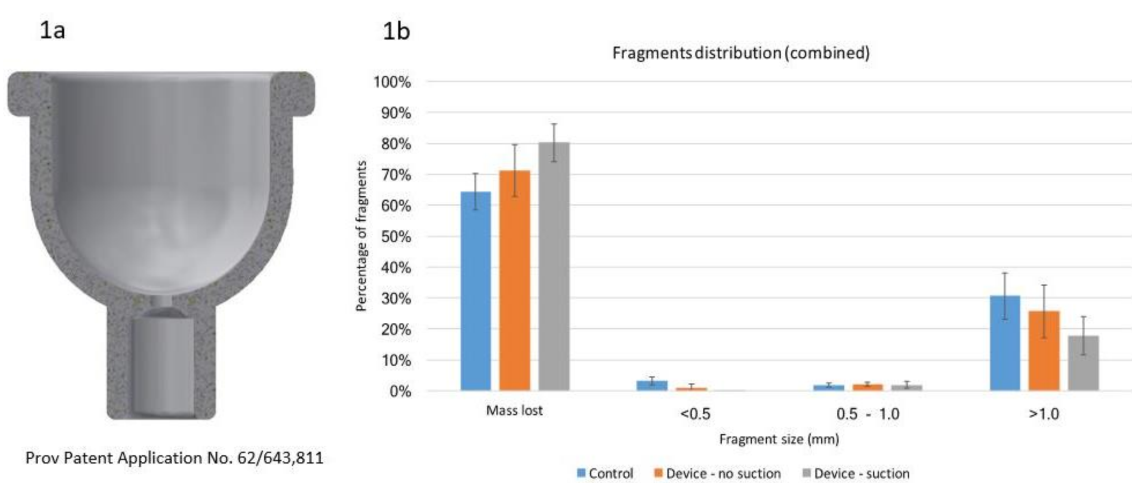

Figure 1a. prototype suction device. Figure 1b. Comparison of lithotripsy efficiency using suction stabilization device with a control condition.

ABSTRACT 40

NEURAL-NETWORK BASED ACOUSTIC MONITORING OF CAVITATION IN LITHOTRIPSY

Kazuki Maeda[1*], Adam D. Maxwell[2, 3]
[1] Department of Mechanical Engineering, University of Washington
[2] Department of Urology, University of Washington School of Medicine
[3] Center for Industrial and Medical Ultrasound, Applied Physics Laboratory, University of Washington

Introduction: Cavitation bubbles that are nucleated in the urinary tract during Burst Wave Lithotripsy (BWL) [PMC6258362] can cause shielding of the incoming wave energy and potentially lead to loss of efficacy of stone comminution. Toward real-time monitoring of cavitation *in situ*, we promote an artificial neural-network to process numerical data, and correlate the energy transmitted into the stone against the scattered acoustic waves. Using the model, we demonstrate acoustic monitoring of cavitation *in vitro*.

Methods: We used an in-house, compressible flow solver [PMC6364854] to simulate interactions among the focused wave with an amplitude of approximately 5 MPa and a frequency of 340 kHz, cavitation bubbles, and the epoxy and glass stones *in vitro* to model the process of Burst Wave Lithotripsy (BWL). We varied the size and initial void fraction of bubble clouds over ranges of 0 – 2.0 mm and 0 - 10^{-4}, respectively, with a stone size of 6 mm. We used an artificial neural-network algorithm to process the numerical data, and model the nonlinear correlations among the transmitted energy, scattered acoustics, and aforementioned parameters. In the experiment, we sent pulses of a focused ultrasound wave from a multi-element array medical transducer to the kidney stone model with various values of PRF between 10-200 Hz. We captured the bubble distribution using a high-speed camera and concurrently measured the back-scattered acoustic signal. Given the signal as an input, we used the model to compute the energy.

Results: The neural network-based algorithm was able to construct a model that can predict the energy transmitted into the stone, given the scattered acoustic signal. For the range of parameters addressed in the present study, the model was found to outperform a linear regression model. In the experiment, we observed a layer of cavitation bubbles on the proximal side of the stone in each pulse (figure 1). The obtained correlation between the transmitted energy and the scattered acoustic intensity for representative parameters are shown in figure 2. The energy shielding was found to have a monotonic, negative correlation with the PRF. For a specific stone, with a high PRF of 200 Hz, the magnitude of the energy shielding that was outputted by the new model can exceed 90%, while with a low PRF of 10 Hz, the magnitude was ~1-10%.

Conclusion: We constructed a neural-network based strategy to quantitatively monitor the energy shielding of kidney stones that is caused by cavitation bubble clouds during lithotripsy. The strategy may be of use to control cavitation and the energy shielding *in situ* for better therapy outcomes. This work was supported by NIH P01 DK043881 and K01 DK104854.

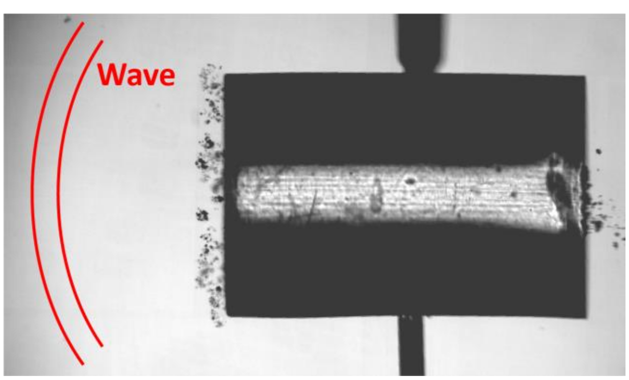

Figure 1: High-speed image of cavitation bubbles excited on the proximal surface of a cylindrical stone model during the passage of the focused ultrasound wave. The length of the stone is 10 mm.

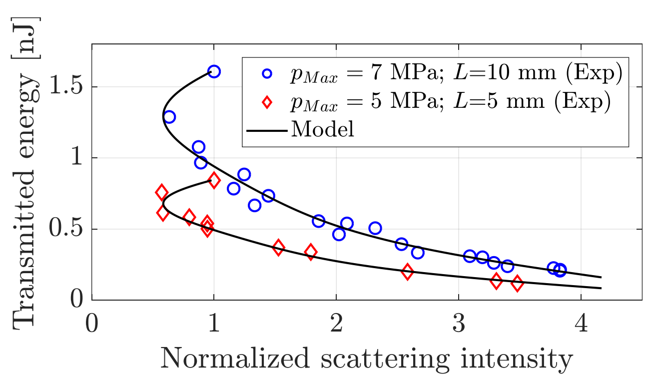

Figure 2: Correlations between the acoustic energy transmitted into epoxy stones against the scattering intensity for various values of wave amplitude, p_{Max}, and stone length, L. The intensity is normalized by that obtained without bubbles.

ABSTRACT 41

COMPUTER GENERATED TUMOR VOLUME, SURFACE AREA AND IRREGULARITY AS PREDICTORS OF PATHOLOGICAL OUTCOMES IN RENAL CELL CARCINOMA

Arveen Kalapara[1], Nicholas Heller[2], Niranjan Sathianathen[1], Edward Walczak[1], Paul Blake[1], Keenan Moore[3], Heather Kaluzniak[4], Joel Rosenberg[1], Zachary Rengel[1], Makinna Oestreich[1], Zachary Edgerton[1], Matthew Peterson[1], Shaneabbas Raza[4], Nikolaos Papanikolopoulos[2], Christopher Weight[1]

[1] Department of Urology, University of Minnesota
[2] Department of Computer Science & Engineering, University of Minnesota
[3]Carleton College
[4]University of North Dakota

Introduction: With greater use of cross-sectional computed tomography (CT) imaging and the rising incidence of renal cell carcinoma (RCC), decision making between surgical management and active surveillance has relied primarily on tumor size as a predictor of pathological and long-term oncological outcomes. Other morphological factors which may help predict these outcomes include tumor volume (V), surface area (S) and tumor irregularity. We have defined the latter as an 'irregularity index', calculated as tumor radius (R) multiplied by the surface area to tumor volume ratio (ie. R x S/V). We aimed to assess the ability of computer generated (CG) tumor volume, tumor surface area and irregularity index to predict presence of RCC, high grade tumor (Fuhrman 3-4), high stage tumor (pT3-4) and tumor necrosis, compared to manually generated (HG) tumor diameter alone.

Methods: Retrospective review of 544 patients who underwent nephrectomy following late arterial phase CT imaging for suspected RCC at a single institution between 2010 and 2018. Patients with angiomyolipoma, tumor thrombus, non-oncological indications for nephrectomy and incomplete or missing imaging were excluded. After manually delineating tumors on CT, we developed an algorithm to calculate CG tumor volume and surface area. Irregularity index was subsequently calculated using these measured parameters. Tumor diameter was also measured manually (HG) by five medical professionals, independently. We used Wilcoxon rank test to compare HG and CG tumor diameter, and receiver operating characteristic (ROC) curve analysis to quantify discriminative ability of each parameter.

Results: CT imaging was available for computer processing in 195 patients who underwent nephrectomy. 183 (94%) had malignant tumors, including 74% clear cell RCC, and 60 (31%) had high stage (T3 or greater) disease. Median CG tumor diameter (4.5cm, IQR 3.0–7.0) was greater than HG diameter (4.2cm, IQR 2.6–6.5) ($p<0.001$). CG volume (AUC 0.68) and CG surface area (AUC 0.67) showed moderate discrimination for cancer, compared to HG diameter (AUC 0.71). CG volume (AUC 0.79) and CG surface area (AUC 0.79) were good predictors of high stage disease, along with HG diameter (AUC 0.82). CG volume (AUC 0.74) and CG surface area (AUC 0.73) were also good predictors of high grade tumor, comparable with HG diameter (AUC 0.75). Irregularity index showed inferior discrimination for cancer (AUC 0.60), high stage (AUC 0.59), high grade (AUC 0.55) and tumor necrosis (AUC 0.55).

Conclusion: Computer generated tumor volume and surface area, but not tumor irregularity, accurately discriminated RCC and pathological outcomes, when compared with tumor diameter alone. Deep learning automatically segments tumor and kidney, calculating these parameters without human capital. These are promising findings which may improve with refinement of our algorithm.

ABSTRACT 42

EFFECTS OF HUMAN URINE AND ARTIFICIAL URINE ON URETERAL STENT MECHANICAL PROPERTIES

Bradley C Hansen, PhD[1], Andrew P. Breidenbach, PhD[2], Jonathan Sheets, MS[2], Ray Boudreaux, PhD[1], Ben H. Chew, MD[3], Dirk Lange, PhD[3]

[1] Cook Research Incorporated, West Lafayette, IN
[2]Cook Medical, Bloomington, IN
[3] University of British Columbia, Vancouver, BC, CA

Introduction: ASTM F1828:2017 specifies ureteral stents shall be immersed in human urine for 30 days to induce mechanical changes prior to testing, claiming human urine is more aggressive than artificial urine formulations. The effects of human and artificial urine on polyurethane stents are similar, but unclear [PMC9363338]. This study evaluated tensile properties of ureteral stents following immersion in human or artificial urine. Due to the design of artificial urine, it is hypothesized that human urine does not reduce the break strength of ureteral stents more than artificial urine.

Methods: Normal human urine from n=11 donors (age: 19-57, M/F: 6/5) was obtained (Lee Biosolutions Inc., Maryland Heights, MO). Stents made of polyether polyurethane (PtPU), polycarbonate-based polyurethane (PcPU), and silicone (Si) (n=30 for each immersion medium) were immersed in human urine, artificial urine (ASTM F1828:2014, Formulation 2), or normal saline for 30 days. Immersion media were maintained at 37°C and pH of 5.5-6.5 and changed every 7 days. Non-immersed stents were used as controls (n=30 of each device). Break strength tests were performed per ASTM F1828 on the curled end and the shaft of the stents. Immersed stent data were normalized by non-immersed stent data to account for variance among devices, and a two-way ANOVA was performed with factors of device and immersion condition. One-way ANOVA and a Tukey post-hoc analysis was performed on the devices separately.

Results: The interaction effect of device and immersion medium on curl break strength was significant ($p=0.0049$), with devices immersed in artificial urine having lower break strength than devices immersed in human urine (Fig. 1.A). This interaction effect on shaft break strength was also significant ($p<0.0001$), however only shaft break strength for Si immersed in artificial urine was lower than Si immersed in human urine (Fig. 1.B). In the one-way ANOVA, immersion medium was a significant factor for each device in curl and shaft break strength ($p<0.0001$, individual differences displayed in Fig. 1).

Conclusion: The results demonstrate that human urine is not more aggressive than artificial urine in degrading ureteral stent mechanical properties. Artificial urine provides a wider safety margin and is a more controlled environment for testing. This control allows for repeated testing, compared with the high variability in human urine. The effects of immersion media on retention strength, evaluated in ASTM F1828, should also be investigated, although a different artificial urine formulation may be more appropriate. Further directions of this work could be to investigate longer immersion times to validate the use of artificial urine solutions to simulate long term indwell times.

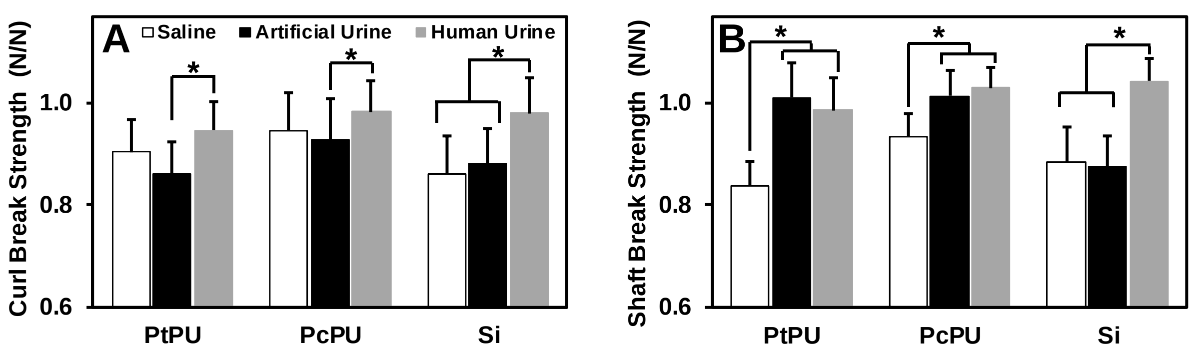

Figure 1: Normalized (A) curl and (B) shaft break strength of PtPU, PcPU, and Si stents. Mean ± SD, *=p<0.0001.

ABSTRACT 43

ROBOTIC-ASSISTED EXTRAPERITONEAL DUAL KIDNEY TRANSPLANTATION USING THE SP® SURGICAL SYSTEM IN A PRE-CLINICAL MODEL

Mohamed Eltemamy, Juan Garisto, Eric Miller, Alvin Wee, Jihad Kaouk

Glickman Urological and Kidney Institute, Cleveland Clinic, Cleveland, OH, USA

Introduction: Robotic kidney transplantation has been described as a novel minimally invasive approach. We aimed to assess the feasibility of dual kidney transplantation using the novel Da Vinci SP® surgical system in a pre-clinical model.

Methods: In 1 male cadaver the da Vinci SP® Surgical system (Intuitive Surgical, Sunnyvale, CA, USA) was used to perform an extraperitoneal dual kidney transplantation. Two kidney grafts were obtained from the local organ procurement organization after declined by all transplant centers. Kidneys were benched in a usual fashion and wrapped in cold sponges (Figure A). A peri-umbilical midline incision was performed. A kidney-shaped laparoscopic balloon was inserted through the incision to create the extraperitoneal space (Figure B). SP robot was docked (Figure C) followed by dissection of iliac vessels bilaterally. The robot was undocked and the first graft was inserted through the Alexis® wound retractor. The robot was re-docked and the renal vein anastomosis to external iliac vein was performed (Figure D) followed by renal artery anastomosis to external iliac artery using 5-0 Gore-Tex® (W.L. Gore& Associated) sutures. Ureteroneocystostomy was performed using the Lich-Gregoir technique over a transplant stent. Same steps were replicated for the left kidney transplant. Once procedures were done, kidneys were then harvested with the iliac vessels to examine the quality of the anastomosis.

Results: Using the da Vinci SP® Robotic Platform, we successfully designed and performed a bilateral extra-peritoneal dual kidney transplantation in a fresh human cadaver. There was no need for conversion to the standard multiport technique or placement of additional assistant ports. No accidental intraoperative punctures or obvious organ damage was identified during the procedure. Total operative time was 270 minutes. Vascular and ureteric anastomosis times are reported in table 1.

Conclusions: In this first pre-clinical experience, dual kidney transplantation was feasible using the SP surgical platform. The multi-quadrant versatility of the SP system may prove benefic with the expected increase in dual kidney transplants in the face of national organ shortage and prolonged waiting list time. Further clinical investigations are needed.

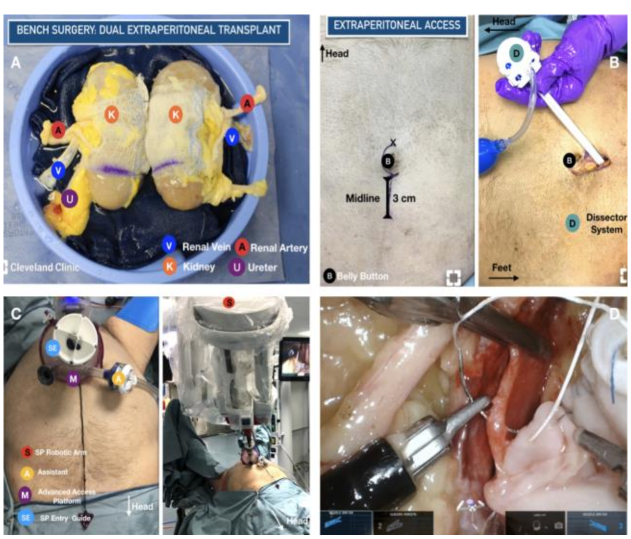

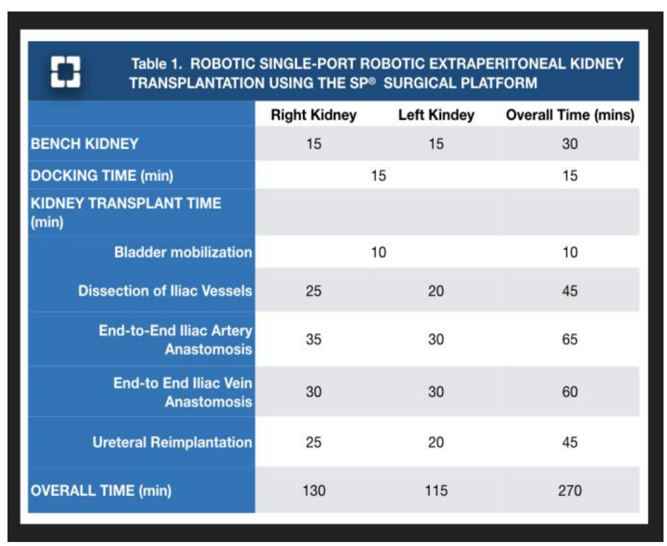

Table 1. ROBOTIC SINGLE-PORT ROBOTIC EXTRAPERITONEAL KIDNEY TRANSPLANTATION USING THE SP® SURGICAL PLATFORM

	Right Kidney	Left Kindey	Overall Time (mins)
BENCH KIDNEY	15	15	30
DOCKING TIME (min)	15		15
KIDNEY TRANSPLANT TIME (min)			
Bladder mobilization	10		10
Dissection of Iliac Vessels	25	20	45
End-to-End Iliac Artery Anastomosis	35	30	65
End-to End Iliac Vein Anastomosis	30	30	60
Ureteral Reimplantation	25	20	45
OVERALL TIME (min)	130	115	270

ABSTRACT 44

URINE CONDUCTIVITY FOR USE IN AMBULATORY URODYNAMICS

Benjamin Abelson[1], Ian McAdams[3], Robert Butler[2], Steve Majerus[3], Margot Damaser[2]

[1] Cleveland Clinic Glickman Urological and Kidney Institute
[2] Cleveland Clinic Lerner Research Institute
[3]Advanced Platform Technology Center, Louis Stokes Cleveland VA Medical Center

Introduction: Urodynamic studies (UDS) provide a crucial tool for urologists to evaluate the health of the bladder and to diagnose a variety of disease states and symptoms, including neurologic disease, overactive bladder, obstructed voiding, and incontinence [1]. Efforts to develop ambulatory, catheter-free UDS to improve patient experience, expand diagnostic capabilities, and integrate with neuroprostheses have been hampered by several pitfalls, including failure to incorporate volume alongside pressure sensing [2, 3]. The relationship between volume of a fluid and conductivity has been used in the field of cardiovascular monitoring to accurately and continuously measure right atrial volume to evaluate cardiac output [4, 5]. We have demonstrated that this technology can be applied to detecting bladder volume *in vitro*. [6] However, little is known about normal values and ranges of conductivity in human urine as well as the impact of urologic and kidney diseases on urine conductivity.

Methods: We recruited forty healthy volunteers and 100 urology and nephrology patients to provide single, random urine samples. Five volunteers provided samples from each void over a 24-hour period. Samples were tested for conductivity then sent to our institution laboratory for urinalysis and urine electrolyte testing (sodium, chloride, potassium and calcium).

Results: Mean ages of patients and volunteers were 56.4 years and 39.9 years respectively, with approximately half of both groups being male. The 100 patients represented multiple disease categories including incontinence (25), renal disease (26), and stones/infection/pain (21). Mean urine conductivity for patients and volunteers was 26.3±12.8 mS and 38.0±14.4 mS respectively ($p<0.001$). Urine conductivity in both groups correlated strongly with urine electrolyte concentration with r-squared values of 0.90, 0.83, 0.58, an 0.11 for chloride, sodium, potassium, and calcium, respectively (all $p<0.05$). Urine conductivity did not differ significantly between various urologic and kidney disease. Furthermore, individual's urine conductivity changed significantly throughout a 24-hour period, primarily based on fluid intake.

Conclusion: This study serves to establish normal values and ranges of urine conductivity and correlates changes in urine conductivity with urine electrolyte concentration. We demonstrate that this correlation is consistent both in healthy volunteers as well as the target population that serves to benefit from in-development ambulatory urodynamics devices. This is a crucial step in development of ambulatory urodynamic monitoring systems that use fluid conductance to measure volume.

ABSTRACT 45

PROSPECTIVE COHORT STUDY COMPARING THE DIAGNOSTIC YIELD AND SAFETY OF OFFICE-BASED TRANSPERINEAL VS. TRANSRECTAL PROSTATE BIOPSY

Alexa R. Meyer, Gregory A. Joice, Zeyad R. Schwen, Michael Zimmerman, Rana Harb, H. Ballentine Carter, Misop Han, Alan W. Partin, Mohamad E. Allaf, Michael A. Gorin

The James Buchanan Brady Urological Institute and Department of Urology, Johns Hopkins University School of Medicine, Baltimore, MD. USA

Introduction: Prostate cancer (PCa) is most commonly diagnosed with use of ultrasound-guided transrectal prostate biopsy (TR-Bx). The risk of infectious complications with this procedure remains high due to the need for needles to pass through the rectal mucosa. Recent technological advancements have allowed for performance of transperineal prostate biopsy (TP-Bx) in the office setting. This technique minimizes the risk of infectious complications and offers the advantage of superior sampling of the anterior prostate. We present interim results from a prospective cohort study comparing these two methods of prostate biopsy.

Methods: Enrolled patients underwent a TR-Bx or TP-Bx with or without MRI guidance based on patient and surgeon preference. Patients were compared between groups for differences in overall cancer detection, clinically-significant (CS) cancer detection (≥grade group 2), and adverse events. Patients were assessed for adverse events by follow-up telephone calls at 4-6 and 25-31 days post biopsy.

Results: Between August 2017 and October 2018, a total of 143 men were enrolled in this study. 55 (38.5%) underwent a TR-Bx and 88 (61.5%) underwent a TP-Bx. There were no significant differences in baseline characteristics including patient age, race, PSA level, and indication for biopsy (all p>0.2). Additionally, there was no difference in the rate of prior MRI use (p=0.9) or MRI guidance at the time of biopsy (p=0.2). Patients were sampled with a median of 12 (range 12-18) and 13 (range 12-23, p=0.2) cores in the TR-Bx and TP-Bx groups, respectively. Among patients who underwent a TR-Bx, the overall PCa detection rate was 60.0% and the CS PCa detection rate was 29.1%. Patients in the TP-Bx had similar rates of overall (71.6%) and CS PCa (42.3%) detection (overall PCa p=0.2 and CS PCa p=0.1). No differences were observed between groups in the frequency and severity of adverse events (both p>0.5).

Conclusion: TP-Bx can be safely performed in the office setting. Early data from our clinical trial suggest that the rate of PCa detection is similar between TR-Bx and TP-Bx. Given that TP-Bx does not require antibiotic prophylaxis, this technique may ultimately be preferred. With continued enrollment in this trial, additional comparisons between groups can be made allowing for further discernment of differences in the cancer yield and safety of these procedures.

ABSTRACT 46

EARLY CLINICAL OUTCOMES IN THE USE OF THE DA VINCI SINGLE PORT SURGICAL SYSTEM IN PROSTATECTOMY PATIENTS

Michael Zhang, MD[1], Samuel Aly, MD[2], Gregory Lovallo, MD[3], Mutahar Ahmed, MD[3]

[1] New York Medical College Dept Urology
[2]Rutgers New Jersey Medical School Dept Urology
[3]Hackensack Univeristy Medical Center Dept Urology

Introduction: The da Vinci Single Port Surgical System (SP) represents the next evolutionary step in robotic systems. In this study we aim to evaluate the initial clinical experience in our series of single port prostatectomy patients and compare our outcomes to a series of patients undergoing standard multiport (MP) robotic prostatectomy.

Methods: Over a two-month period, five patients with localized prostate cancer underwent robot assisted radical prostatectomy with bilateral pelvic lymph node dissection using the SP. An additional patient underwent robot assisted suprapubic simple prostatectomy for BPH. All cases were performed by the same surgeon and approached through a 3cm skin incision around the umbilicus. The first four cases were done through a transperitoneal approach and latest two were done through an extraperitoneal approach. In each case, a 12mm assistant port was placed in the lower left quadrant and converted to the final drain site. The operative time, EBL, length of stay, and narcotic use was reviewed for each patient. The outcomes were compared with a series of six patients undergoing MP prostatectomy in the same time frame, performed by the same surgeon.

Results: The mean operative time was 111 minutes using the SP robot compared to 83 minutes using the MP robot. As surgical technique and device familiarity improved, the mean operative time improved from 133 minutes from the first three cases to 88 minutes for the last three. EBL did not differ between the two groups. All patients in both groups were discharged the next day, with no significant difference in length of stay. The SP patients required less overall narcotic use: 16.3 morphine milligram equivalents (MME) vs 21.3 MME in MP patients, although this did not reach statistical significance (p=0.48).

Conclusion: Even during the initial learning curve of using the SP, clinical outcomes were similar between SP and MP prostatectomy. This shows the safety and feasibility of using the SP system for prostatectomies. In particular, the single port allows for an easy extraperitoneal approach because the peritoneum does not have to be mobilized laterally. This avoids the complications associated with intraperitoneal surgery, including ileus, bowel obstruction, and increased pain. This also allows for potential same day discharges. As we gain increased experience and refinement of surgical technique, other advantages may emerge in the future.

	SinglePort	MultiPort	p
OR time (min)	110 ± 31	82.7 ± 10.9	0.11
LOS (hours)	23.0 ± 2.3	23.7 ± 3.1	0.73
EBL (mL)	63 ± 52	58 ± 34	0.85
Narcotic use (MME)	16.3 ± 7.4	21.3 ± 22	0.48

ABSTRACT 47

MRI CHANGES AFTER IN-OFFICE FOCAL CRYOABLATION OF PROSTATE CANCER: A PILOT STUDY

Steve R Zhou[1,2], Bashir AH Al Awamlh[3], Daniel Margolis[4], Alan Priester[1], Joshua Shubert[1], Yash Kamothi[1], Shyam Natarajan[1], Jim Hu[3]

[1]Avenda Health, Inc., Santa Monica, CA
[2]David Geffen School of Medicine, University of California, Los Angeles, CA
[3]Department of Urology, Weill Cornell Medicine–New York Presbyterian Hospital, NY
[4]Department of Radiology, Weill Cornell Medicine–New York Presbyterian Hospital, NY

Introduction: Focal cryoablation (FCA) of prostate cancer (PCa) —enabled by advanced image-guidance and disease localization—has become a more viable option for select patients (PMID30659903). However, little work has been done to explore the applicability of the standard PI-RADS v2 protocol to post-FCA magnetic resonance imaging (MRI) (PMID 28799121). The objective of this analysis is to explore image-based assessments of FCA efficacy.

Methods: Analysis was based on results of an ongoing IRB-approved prospective observational study on in-office FCA to treat patients with focal clinically significant PCa (csPCa)—defined as presence of Grade Group (GG) ≥ 2—under local anesthesia. Patients were selected based on csPCa focality demonstrated by MRI and targeted biopsy of any suspicious PI-RADSv2 lesions (grade ≥ 3), in addition to whole-gland systematic biopsy. The procedure was guided by MRI-ultrasound (MRI/US) fusion, consisting of 2-3 transperineally-placed cryotherapy probes to ablate between 1 and 2 lesions. All patients received 6-month repeat MRI with targeted and systematic biopsy cores. Spatially-tracked biopsy coordinates were used to perform direct resampling of in-field histologic changes in cases for which the original target disappeared following ablation (Fig. 1).

Results: From August 2018 to February 2019, 10 patients were treated at a single institution. Mean age was 68.6 years. Median (IQR) baseline PSA and PSAD were 7.0 ng/mL (5.7 – 9.3) and 0.12 ng/mL/cc (0.11 – 0.15) respectively. The cohort consisted of seven patients with GG2 disease, two with GG3, and one with GG5. FCA was completed successfully in all without significant complications. Median (IQR) decreases in PSA and PSAD were 4.3 ng/mL (2.8 – 5.1, p = 0.004) and 0.06 ng/mL/cc (0.04 – 0.08, p = 0.002). Smaller PSAD decrease was associated with presence of post-procedure csPCa (p = 0.04), but PSA and prostate volume (PV) were not (p = 0.55 and 0.79, respectively).

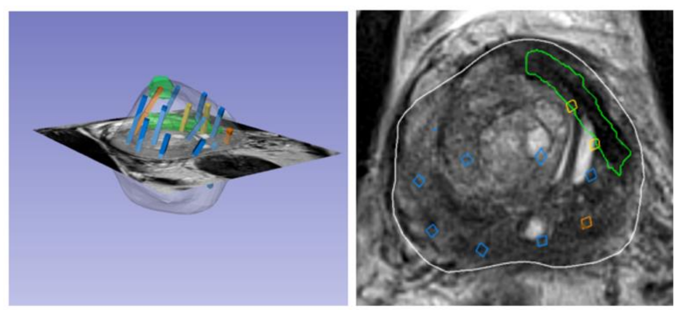

Figure 1. 3D (left) and axial (right) image of post-FCA MRI and biopsy. Persistent apical PI-RADSv2 grade 5 lesion (green) was found with residual GG1 disease on biopsy (orange). New grade 4 left anterior lesion (green) was benign on biopsy (yellow).

Targeted biopsy of all baseline suspicious PI-RADSv2 lesions revealed PCa, although two were clinically-insignificant. Initial PI-RADSv2 lesion grade did not predict treatment failure (p = 0.79). Disappearance of a suspicious primary PI-RADSv2 lesion after FCA was seen in 4/10 cases (40%), and post-procedure systematic biopsy revealed no csPCa. Of the remaining 6 cases with persistent lesions, three harbored residual GG2 disease and three contained GG1 disease. Four cases also revealed additional MRI-negative csPCa on systematic follow-up biopsy. 5/10 cases exhibited new suspicious lesions on repeat MRI, of which only 1 harbored csPCa on targeted sampling.

Conclusion: Although PI-RADSv2 reliably identifies csPCa, value of the protocol may decrease in the post-FCA setting due to tissue response to injury. PSAD decrease may aid prediction of treatment failure. Our findings demonstrate opportunities to improve PCa surveillance imaging following FCA.

ABSTRACT 48 **TOP 10 ABSTRACT**

OUT OF THE RECTUM: FREE-HAND FULLY TRANSPERINEAL FUSION-GUIDED PROSTATE BIOPSY

Reza Seifabadi*, Amir H. Lebastchi, Sheng Xu, Victoria Anderson, Peter L. Choyke, Baris Turkbey, Peter A. Pinto, Bradford J. Wood

National Institutes of Health, Clinical Center, Bethesda, MD

Introduction: Currently, a standard of care prostate biopsy is performed by placing biopsy needles transrectally under transrectal ultrasound (TRUS) guidance in an office setting. Unfortunately, the transrectal approach is associated with a high risk for infection in up to 4% of patients. Previous studies have demonstrated prostate biopsies via a transperineal route reduces the risks for infection significantly. However, this method has some major burdens, as it requires bulky equipment as well as the perceived need in the past for general anesthesia or sedation. Recent improvements include free-hand transperineal (TP) biopsies using a grid-less TP coaxial guide attached to the ultrasound, under TRUS guidance. Two coaxial puncture sites are taken through which, after adequate local anesthesia, all needles are passed with redirecting of coaxial needle via peri-prostatic redirection. However, this technique still requires placement of an US probe into the rectum. It is also not compatible for patients without a rectum. Here, we report a free-hand fully transperineal (FFTP) fusion biopsy, where both the US probe and the needle insertion are performed transperineally, i.e. entirely "out-of-the rectum". This was performed in addition to standard targeted fusion biopsy of the MRI-defined targets using a TP grid template and standard TP fusion TRUS guidance.

Methods: Patients with MRI-suspicious prostate targets underwent fusion biopsy with a conventional TP access with fusion based on TRUS. During the same session, patients also underwent TP biopsy following a free-hand US technique performed to enhance diagnostic potential. On an IRB-approved retrospective reporting protocol, we compared the clinical accuracy of two techniques. The standard technique was TP fusion biopsy using an EM-tracked grid template, a tracked stepper, and a commercially available MRI/US fusion platform (Uronav, Invivo) under anesthesia. The FFTP fusion biopsy technique used MRI/US fusion with a TPUS 2D sweep to build a 3D model which was fused to MRI. This technique avoided placement of a transrectal ultrasound transducer. A C9-5 endocavity tracked probe (Philips) with disposable needle guide (Civco) were used for TP needle placement. A freehand, fan 2D sweep, (e.g. left-right sagittal or up-down coronal) was done over the perineum to generate the 3D US volume which was then fused with MRI. Semi-manual registration was performed using anatomy as reference using a custom fusion platform. Targeted TP biopsies were performed using both techniques: 1) Standard TP fusion with TRUS approach: using the tracked grid template needle guide, stepper grid template, 2) FFTP: totally free hand technique, entirely out of rectum and semi-manual registration.

Results: Eight targets were biopsied using both TP approaches. For each target, the pathology results were compared between the two methods. Using the FFTP approach, six of the eight ROI targets correlated with the standard pathology result. 2 cases were positive for cancer, but under-graded by Gleason score. Table 1 summarizes the pathology results of both approaches.

Table 1. Comparison of transperineal biopsy techniques

Target # (ROI)	Standard (Gleason score)	FFTP (Gleason score)
1	3+4=7	HGPIN*
2	benign	benign
3	4+4=8	3+4=7*
4	benign	benign
5	3+4=7	3+4=7
6	3+3=6	Benign*
7	benign	benign
8	4+5=9	4+4=8*

HGPIN: High grade prostatic intraepithelial neoplasia;
TP transperineal, ROI: region of interest
* Underestimated grading

Conclusions: A FFTP fusion biopsy is feasible and avoids instrumentation via the rectum. This technique may have advantages such as avoidance of transrectal US probe placement, no need for anesthesia, and may carry cost efficacy in terms of the office setting. However the approach cannot be recommended as an alternative to standard TRUS fusion at this time, without major refinements in technique, given uncertainties in registration accuracy and in under-estimation or under-diagnosis of cancer in 4 of 8 cases.

ABSTRACT 49

A NOVEL MICROFLUIDIC DEVICE FOR ISOLATION OF EXTRACELLULAR VESICLES

Richard C. Zieren[1, 2], Liang Dong[1], Theo M. de Reijke[2], Kenneth J. Pienta[1]
[1]The James Buchanan Brady Urological Institute, Johns Hopkins School of Medicine, Baltimore, MD, USA
[2]Amsterdam UMC, University of Amsterdam, Amsterdam, The Netherlands

Introduction: Extracellular vesicles (EVs) are membranous nanoparticles of variable size, secreted by all cells. EVs are considered a promising biomarker resource for kidney, bladder and prostate cancer. A caveat of EV research is the lack of standardized isolation methods, resulting in heterogeneity of EV studies [1]. In this study, we compared yield, purity, and workflow of a novel microfluidic EV isolation device, the Exodisc (disc), with ultracentrifugation (UC), considered the golden standard, and a commercial precipitation kit. The Exodisc is uses low-speed centrifugation to create a tangential flow. Small EVs (~20-600 nm), including exosomes, are isolated using nanofilters [2].

Methods: EVs were isolated from various samples (healthy donor urine, healthy donor plasma or LNCAP-conditioned media) by three different isolation methods: (1) UC: EVs were pelleted twice in 2-hour centrifugation on 100.000 G; (2) Kit: samples were incubated with Total Exosome Isolation Reagent (Invitrogen) corresponding to the manufacturer's manual, followed by centrifugation at 10.000 G; (3) Disc: samples were sequentially loaded into the sampling chamber, followed by low speed (500 G) centrifugation for 10-30 minutes. After isolation, EVs were resuspended or eluted in 100μL PBS. Total particle count (yield) and size distribution were measured by Nanoparticle Tracking Analysis (NTA). EV quality control of isolated samples was performed corresponding to Minimal Information for Studies of Extracellular Vesicles 2018 [3]. Additionally, we did a recovery experiment using UC-purified plasma EVs as sample input for the three methods.

Results: EVs were successfully isolated by all methods. Total particle yield (Figure 1) of the kit and disc isolation plasma EVs were 100x and 50x higher than UC, respectively. For urine, kit and disc isolated 2x and 50x as many EVs as UC. For conditioned media, the kit's and disc's yield were 10x and 40x higher than UC, respectively. Size distribution differed per sample, but the range was comparable between the different isolation methods. In the recovery experiment, 2.6 x 10^9 UC-isolated EVs were divided into equal parts, of which the disk, kit and UC recovered 18%, 9% and 4%, respectively (Figure 2).

Conclusion: The Exodisc demonstrates several advantages in the isolation of EVs over UC and the isolation kit. The disc protocol is relatively fast, and was superior in isolation yield of diluted samples (urine and media). For plasma, the disc had a higher yield than UC. The difference in recovery rate of 'pure' EVs, i.e. after reduction of contaminants, by the Exodisc and UC demonstrates a promising capability of EV isolation. The Exodisc may increase the reproducibility and sample throughput, necessary for clinical validation of biomarkers. However, additional analysis of remaining contaminants is required. Furthermore, compatibility with non-EV-enriched samples, such as tissue-conditioned media, should be evaluated to aid the discovery of cancer biomarkers.

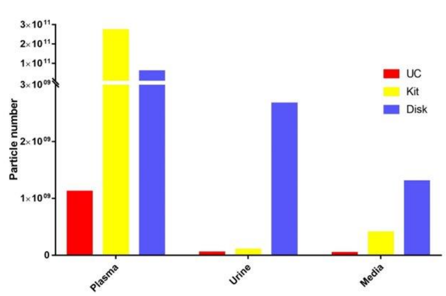

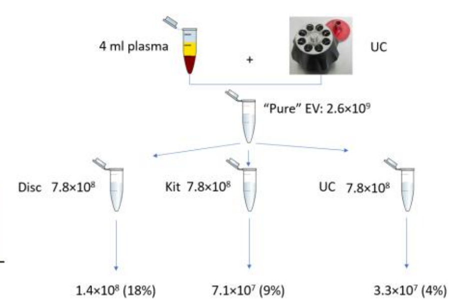

Figure 1 (left): Normalized particle count measured by NTA of isolation by UC, kit and disc, for various samples (plasma, urine, media). Figure 2 (right): Recovery rates of ¨purified¨ EVs by disc, kit or UC

SOCIETY OFFICERS:

PRESIDENTS
Robert Sweet
Tim Kowalewski

SECRETARY
Margaret Pearle

TREASURER
Chandru Sundaram

COUNCILOR
Louis Kavoussi

EXECUTIVE DIRECTOR
Dan Stoianovici

ADVISORY BOARD
Jeffrey Cadeddu

Ralph Clayman

Jean de la Rosette

Misop Han

Pilar Laguna

Thomas Lawson

Manoj Monga

Pierre Mozer

Stephen Nakada

Jens Rassweiler

Koon Ho Rha

William Roberts

Arthur Smith

Li-Ming Su

Gerald Timm

Hessel Wijkstra

Kevin Zorn

AWARDS:

BEST ABSTRACT AWARDS:

INTRAOPERATIVE GUIDANCE FOR ROBOTIC PARTIAL NEPHRECTOMY USING SURFACE-BASED REGISTRATION: INITIAL MODEL ASSESSMENT. E. B. Pitt[1], J. M. Ferguson[1], N. L. Kavoussi[2], E. J. Barth[1], R. J. Webster III[1], S. D. Herrell[2]. [1]Department of Mechanical Engineering, Vanderbilt University, Nashville, TN [2]Department of Urologic Surgery, Vanderbilt University Medical Center, Nashville, TN

IMPROVING PROSTATE CANCER MARGIN PREDICTION WITH MACHINE LEARNING. Alan Priester[1], Steve Zhou[1,2], Yash Kamothi[1], Joshua Shubert[1], Shyam Natarajan[1]. [1]Avenda Health, Inc., Santa Monica CA. [2] David Geffen School of Medicine, UCLA, Los Angeles CA

AWARDS:

TOP 10 ABSTRACTS:

IMAGING THE DEVELOPING HUMAN UROGENITAL SYSTEM WITH LIGHT SHEET FLUORESCENCE MICROSCOPY. Dylan Isaacson*[1], MD, MPH; Dylan McCreedy[2,], PhD; Meredith Calvert[3], PhD; Joel Shen[4], BS; Adriane Sinclair[5], PhD ; Mei Cao[5], BA; Yi Li[5], MD; Todd McDevitt[6,8], PhD; Gerald Cunha[5], PhD; and Laurence Baskin[5,7], MD. [1]Department of Urology, Northwestern University Feinberg School of Medicine, Chicago, IL. [2]Department of Biology, Texas A&M University, College Station, TX. [3]Histology and Light Microscopy Core, J. David Gladstone Institutes, San Francisco, CA. [4]CytomX Therapeutics, Inc. South San Francisco, CA. [5]Department of Urology, University of California, San Francisco, San Francisco, CA. [6]Department of Bioengineering and Therapeutic Sciences, J. David Gladstone Institutes, San Francisco, CA. [7]Division of Pediatric Urology, University of California San Francisco Benioff Children's Hospital, San Francisco, California. [8]Institute of Cardiovascular Disease, J. David Gladstone Institutes, San Francisco, CA

ROBOTIC 3D ULTRASOUND-GUIDED TARGETING FOR PERCUTANEOUS RENAL ACCESS. Tareq Aro[1,2], Sunghwan Lim[1], Doru Petrisor[1], Dan Stoianovici[1,2]. [1]Robotics Laboratory, [2]Department of Urology, Johns Hopkins University

DIGITAL STONE MEASUREMENT IN URETEROSCOPIC STONE PROCEDURES: A WORKFLOW FEASIBILITY STUDY. Kevin Koo[2], Tareq Aro[1,2], Sunghwan Lim[1,2], Doru Petrisor[1,2], Dan Stoianovici[1,2], Brian R. Matlaga[2]. [1]Robotics Laboratory, [2]Department of Urology, Johns Hopkins University

DEVELOPMENT OF AN OFFICE BASED LASER ABLATION SYSTEM FOR PROSTATE CANCER. Josh Shubert[1], Yash Kamothi[1], Alan Lee[1], Brittany Berry-Pusey[1], Alan Priester[1,2], Rory Geoghegan[2], Leonard Marks[1,2], Shyam Natarajan[1]. [1] Avenda Health, Inc., Santa Monica, CA. [2] Department of Urology, University of California, Los Angeles

REAL-TIME HIGH RESOLUTION DIAGNOSTIC IMAGING FOR PROSTATIC TISSUE WITH EX VIVO FLUORESCENCE CONFOCAL MICROSCOPY: OUR PRELIMINARY EXPERIENCE. Eissa A.[1,2], Puliatti S. [1] , Bertoni L. [3], Bevilacqua L. [1] , Sighinolfi M.C. [1] , Reggiani Bonetti L [4] , Patel V. [5] , Bianchi G. [1] , Micali S. [1] , Rocco B. [1]. [1]Dept. of Urology, University of Modena and Reggio Emilia, Italy, [2]Dept. of Urology, Faculty of Medicine, Tanta University, Egypt, [3]Dept. of Surgical, Medical, Dental and Morphological Sciences with Interest transplant, Oncological and Regenerative Medicine, University of Modena and Reggio Emilia, Italy, [4]Dept. of Pathology, University of Modena and Reggio Emilia, Modena, Italy. [5]Dept. of Urology, Global Robotics Institute, Florida Hospital-Celebration Health Celebration, Florida, USA.

A PRECLINICAL TRANSRECTAL BOILING HISTOTRIPSY SYSTEM FOR PROSTATE ABLATION. George R. Schade[1], Tatiana D. Khokhlova[2], Christopher Hunter[3], Wayne Kreider[3], Pavel B. Rosnitskiy[4], Petr V. Yuldashev[4], Oleg A. Sapozhnikov[3,4], Vera A. Khokhlova[3,4]. [1]Department of Urology, [2]Department of Medicine, [3]Center for Industrial and Medical Ultrasound, University of Washington, Seattle, USA. [4]Physics Faculty, M.V. Lomonosov Moscow State University, Moscow, Russia

IMAGE GRADIENT AT KIDNEY-TUMOR BOUNDARIES AS A PREDICTOR OF COMPLEXITY IN NEPHRON SPARING SURGERY. Nicholas Heller[1], Arveen Kalapara[1], Niranjan Sathianathen[1], Edward Walczak[1], Keenan Moore[3], Heather Kaluzniak[2], Joel Rosenberg[1], Paul Blake[1], Zachary Rengel[1], Zachary Edgerton[1], Matthew Peterson[1], Makinna Oestreich[1], Shaneabbas Raza[2], Nikolaos Papanikolopoulos[1], Christopher Weight[1]. [1] University of Minnesota, [2] University of North Dakota, [3] Carleton College

OUT OF THE RECTUM: FREE-HAND FULLY TRANSPERINEAL FUSION-GUIDED PROSTATE BIOPSY. Reza Seifabadi*, Amir H. Lebastchi, Sheng Xu, Victoria Anderson, Peter L. Choyke, Baris Turkbey, Peter A. Pinto, Bradford J. Wood. National Institutes of Health, Clinical Center, Bethesda, MD

AWARDS:

BEST REVIEWER AWARDS (LAST 5 YEARS):

		2015	2016	2017	2018	2019
Ernesto III	Arada		☼			
Tareq	Aro					☼
Ben H.	Chew		☼			
Isaacson	Dylan				☼	☼
Cosmin	Ene	☼				
Arvind	Ganpule	☼		☼		
Bogdan	Geavlete					☼
Michael	Gorin		☼	☼		
Ryan	Hsi			☼		
Ryan	Hutchinson			☼		
Louis	Kavoussi	☼				☼
Thomas	Lawson	☼	☼			
Evangelos	Liatsikos				☼	
Wesley	Ludwig	☼	☼	☼		
Salvatore	Micali				☼	
Cristian	Mirvald		☼			
Steven	Monda				☼	☼
Razvan	Multescu	☼				
Sutchin	Patel	☼	☼	☼		
Arnoud	Postema	☼				
Alan	Priester		☼			
Koon Ho	Rha				☼	☼
Ioanel	Sinescu	☼	☼			
Cristian	Surcel	☼	☼	☼		
Michael	Tradewell				☼	

AWARDS:

The active review committee comprises 34 reviewers. We gratefully acknowledge their contribution to the success of the meeting and thank them for taking the time to promote the best science.

Andrei Ene	Joshua Shubert	Sherif Mehralivand
Balan Georgiana	Kevin Koo	Shyam Natarajan
Bogdan Geavlete	Koon Ho Rha	Stefano Puliatti
Brittany Berry-Pusey	Kymora Scotland	Steve Zhou
Catalin Andrei Bulai	Louis Kavoussi	Steven Monda
Cosmin Ene	Michael Glamore	Tareq Aro
Dan Stoianovici	Nelson Stone	Theo D Reijke
Dylan Isaacson	Nicholas Heller	Thomas Polascik
Ilias Skalkidis	Oscar Fugita	Vipul Patel
Jeffrey Cadeddu	Petrisor Geavlete	William Roberts
Joseph Ditrolio	Reza Seifabadi	Yasuhito Takeuchi
	Richard Zieren	

THANKS:

Dr. George Nagamatsu, Engineering and Urology Society Founder (1985)

Dr. Jack Vitenson, Society Treasurer (1985)

Special thanks to **Tareq Aro,** MD for his help formatting this program.

We thank **Michelle Paoli** and **Debra Caridi** for organizing the Annual Meeting.